SENCKENBERG
world of biodiversity

Universität Bremen

Hydro-acoustic characterization of trawl marks in the German Exclusive Economic Zone (North Sea) as a function of sediment properties

Dissertation zur Erlangung des Doktorgrades der Naturwissenschaften /
Dissertation to obtain the academic degree

Dr. rer. nat.

vorgelegt am Fachbereich Geowissenschaften der Universität Bremen /
submitted to the Faculty of Geosciences, University of Bremen

von/*by*

Ines Bruns

Bremen, Germany

Juli 2023

Diese Promotionsarbeit wurde in der Arbeitsgruppe Marine Sedimentologie am Forschungsinstitut Senckenberg am Meer, Wilhelmshaven, und am Fachbereich 05 Geowissenschaften der Universität Bremen angefertigt.

This doctoral thesis was written in the working group Marine Sedimentology at the research institute Senckenberg am Meer, Wilhelmshaven, and Faculty 05 of Geosciences of the University of Bremen.

Reviewer

Prof. Dr. André Freiwald

Senckenberg am Meer, Wilhelmshaven, Germany

University of Bremen, Bremen, Germany

Prof. Dr. Ingrid Kröncke

Senckenberg am Meer, Wilhelmshaven, Germany

Carl von Ossietzky Universität Oldenburg

Datum des Promotionskolloquiums / Date of the doctoral colloqium

11. September 2023

Abstract

Marine habitats are increasingly affected by human activities, such as oil and gas extraction and shipping. Fishing, and bottom trawling in particular, is also a contributing factor. Not only because populations of target species (e.g., flatfish) and organisms that typically enter nets as bycatch (e.g., juvenile fish or vegetation) can decrease in areas of high fishing activity, but also because bottom trawling causes sediment re-suspension and re-deposition that can disturb the benthic habitat. An indicator of fishing activity and associated alteration of the seabed sediment can be so-called trawl marks. These are elongated furrows left in the sediment by the heavy trawl nets and can be detected in underwater video footage or hydro-acoustic data (e.g., side-scan sonar images). These trawl marks are known from different marine habitats and their significance for the respective sedimentation environment, e.g., as an indication of increased erosion, is already the subject of many studies. However, for the North Sea part of the German Exclusive Economic Zone (EEZ), which is extensively used for economic purposes, there have been rarely any detailed investigations of trawl marks regarding their frequency, geometry and effects on the physical sediment properties. This dissertation therefore includes a comprehensive mapping of trawl marks based on approximately 4800 km^2 of side-scan sonar (SSS) backscatter data collected in the North Sea part of the German EEZ. Based on this mapping, a detailed description of the trawl marks (appearance in the backscatter data, geometry, spatial density and estimation of persistence) and the assignment of the marks to the different fishing gears (beam trawls and otter trawls) was performed. The trawl marks of individual beam trawls were on average about 11 m wide and could be identified more frequently than those of otter trawls (average width 126 m). In addition, seasonal changes in the spatial density of trawl marks could be identified: Their overall density was highest in late summer and autumn (up to 20 marks per km^2). An estimate of the minimum persistence of trawl marks revealed a few days to months. To relate these findings on the characteristics of trawl marks directly to changes in the physical properties of the seabed sediment, backscatter data were combined with sediment strength data. In areas with a high density of trawl marks (20 per km^2), a reduced sediment strength (approx. 20 kPa lower) was found than in areas without trawl marks. This reflects the re-suspension and re-deposition of surface sediment on the seabed related to bottom trawling. In addition, the extensive SSS dataset enabled the development of an approach for automated trawl mark detection. An unsupervised image classification of the SSS backscatter mosaics was performed using QGIS and GRASS GIS software. The automated detection is limited by artifacts in the SSS mosaic; however, an estimate of the area that was trawled was possible. This area estimate was compared with

that derived from manual trawl mapping. The automated detection underestimated the trawled area in one case (by 6.5 %) and overestimated it in the other case (by roughly 65 %). A comparison of the manually mapped trawl marks with fishing activity data based on position and logbook data was not possible because these datasets were only available for the German fishing fleet with positional and temporal accuracy, but a significant part of the fishing activity and thus trawl tracks is also caused by other European fishing fleets. This dissertation provides important insights into habitat mapping with a focus on anthropogenic impact on the seabed. It shows the complex physical effects of bottom trawling on marine sediments of the German EEZ (North Sea) and offers the possibility to combine the present results with biological datasets (e.g., population data) to shed light on the impact of bottom trawling on marine habitats in a holistic way. In particular, the approach for automated trawl mark detection presented here can serve as a support or extension to fisheries monitoring approaches. A detailed knowledge of the impact of bottom trawling on the marine environment is of great importance, as the high global resource demand requires a careful and sustainable planning of resource extraction.

Zusammenfassung

Marine Habitate werden zunehmend durch menschliche Aktivitäten, wie beispielweise Öl- und Erdgasgewinnung und Schifffahrt beeinflusst. Auch die Fischerei und insbesondere die grundberührende Schleppnetzfischerei tragen dazu bei. Nicht nur, weil die Population der Zielarten (z.B. Plattfische) und Organismen, die typischerweise als Beifang in die Netze geraten (z.B. Jungfische oder Vegetation), in Gebieten mit hoher Fischereiaktivität stark zurück gehen kann, sondern auch, weil die grundberührende Schleppnetzfischerei Sedimentumlagerungen verursacht, die den Lebensraum benthischer Arten stören kann. Ein Indikator für Fischereiaktivität und damit einhergehende Veränderungen des Sediments am Meeresboden können sogenannte Schleppnetzspuren oder Trawl Marks sein. Dabei handelt es sich um längliche Furchen, die von den schweren Schleppnetzen im Sediment hinterlassen werden und in Unterwasservideoaufnahmen oder hydro-akustischen Daten (z.B. Side-Scan Sonarbildern) zu sehen sind. Diese Schleppnetzspuren sind aus unterschiedlichen marinen Lebensräumen bekannt und ihre Bedeutung für den jeweiligen Sedimentationsraum, z.B. als Hinweis auf verstärkte Erosion, ist bereits Gegenstand vieler Untersuchungen. Für den Nordsee-Teil der deutschen Ausschließlichen Wirtschaftszone (AWZ), der wirtschaftlich stark genutzt ist, gab es bisher jedoch kaum detaillierte Untersuchungen von Schleppnetzspuren bezüglich ihrer Häufigkeit, Geometrie und Auswirkungen auf die physikalischen Sedimenteigenschaften. Die vorliegende Dissertation beinhaltet daher eine umfassende Kartierung von Schleppnetzspuren auf Grundlage von ca. 4800 km^2 Side-Scan Sonar (SSS) Rückstreudaten, die im Nordsee-Teil der deutschen AWZ erhoben wurden. Anhand dieser Kartierung wurde eine detaillierte Beschreibungen der Schleppnetzspuren (Erscheinungsbild in den Rückstreudaten, Geometrie, räumliche Dichte und Abschätzung der Persistenz) und die Zuordnung der Spuren zu den verschiedene Fanggeräten (Baumkurren und Scherbrettnetze) durchgeführt. Die Schleppnetzspuren von einzelnen Baumkurren waren durchschnittlich rund 11 m breit konnten häufiger identifiziert werden als solche von Scherbrettnetzen (durchschnittliche Breite 126 m). Außerdem konnten saisonale Veränderungen in der räumlichen Dichte der Schleppnetzspuren sichtbar gemacht werden: Ihre Gesamtdichte war im Spätsommer und Herbst am höchsten (bis zu 20 Spuren pro km^2). Eine Abschätzung der minimalen Persistenz der Schleppnetzspuren ergab wenige Tage bis Monate. Um diese Erkenntnisse über die Ausprägung der Schleppnetzspuren in direkten Zusammenhang mit den physikalischen Veränderungen des Oberflächensediments zu bringen, wurden die Rückstreudaten mit Daten zur Sedimentfestigkeit kombiniert. In Bereichen mit einer hohen Dichte von Schleppnetzspuren (20 pro km^2) konnten geringere

Sedimentfestigkeiten (um ca. 20 kPa) festgestellt werden, als in Bereichen ohne Schleppnetzspuren. Dies spiegelt die Umlagerung des Oberflächensediments am Meeresboden wider, die durch die grundberührende Schleppnetzfischerei verursacht wird. Außerdem ermöglichte der umfangreiche SSS-Datensatz die Entwicklung eines Ansatzes zur automatisierten Erkennung von Schleppnetzspuren. Mit Hilfe der Softwares QGIS und GRASS GIS wurde eine unüberwachte Bildklassifizierung der SSS-Rückstreumosaike durchgeführt. Die automatische Klassifizierung ist durch Artefakte in den SSS-Mosaiken limitiert, jedoch konnte eine Abschätzung der befischten Fläche durchgeführt werden. Diese Flächenschätzung wurde mit der auf den manuell kartierten Schlappnetzspuren verglichen. Die automatische Klassifizierung hat die befischte Fläche in einem Fall um 6,5 % unterschätzt und in dem anderen Fall um 65 % überschätzt. Der Vergleich von manuell kartierten Schleppnetzspuren mit Fischereiaktivitätsdaten, die auf Positions- und Logbuchdaten basieren, war nicht möglich, da diese Daten nur für die deutsche Fischereiflotte lage- und zeitgenau verfügbar waren und ein erheblicher Teil der Fischereiaktivität und somit der Schleppnetzspuren aber auch von anderen europäischen Fischereiflotten verursacht wird. Diese Dissertation liefert wichtige Erkenntnisse zur Habitatkartierung mit Schwerpunkt auf den anthropogenen Einfluss auf den Meeresboden. Sie zeigt die komplexen physikalischen Auswirkungen der grundberührenden Schleppnetzfischerei auf die marinen Sedimente der deutschen AWZ (Nordsee) und bietet die Möglichkeit, die vorliegenden Ergebnisse mit biologischen Datensätzen (z.B. Populationsdaten) zu kombinieren, um den Einfluss der Schleppnetzfischerei auf das Habitat ganzheitlich zu beleuchten. Insbesondere der hier vorgestellte Ansatz zur automatisierten Erkennung von Schleppnetzspuren kann als Unterstützung oder Erweiterung von Konzepten zum Fischerei-Monitoring dienen. Eine detaillierte Kenntnis des Einflusses der grundberührenden Schleppnetzfischerei auf die marine Umwelt ist insofern von großer Bedeutung, als das der hohe, globale Ressourcenbedarf eine sorgfältige und nachhaltige Planung der Ressourcenentnahme nötig macht.

Abbreviations

AIS	Automatic Identification System
dB	decibel
EEZ	Exclusive Economic Zone
GLCM	grey level co-occurrence matrices
Hz	Hertz
kHz	Kilohertz
kW	Kilowatt
LOA	length over all
MBES	multibeam echo sounder
MHz	Megahertz
MPA	marine protected areas
MSP	marine spatial planning
ms	millisecond
NM	nautical miles
OTB	bottom otter trawl
OTT	otter twin trawl
SA	swept area
SAR	swept area ratio
SSS	side-scan sonar
SOG	(vessel) speed over ground
TBB	beam trawl
TM	trawl marks
UW-video	under-water video
VMS	Vessel Monitoring System

Content

Abstract **5**

Zusammenfassung **7**

Abbreviations **9**

Content **11**

Thesis outline and author contributions **14**

1 Introduction **17**

1.1 Anthropogenic impact on the marine environment 17

1.2 Seabed mapping 18

1.3 Bottom trawling 20

1.4 Motivation and scientific questions 27

2 Materials and methods **29**

2.1 Hydro-acoustics systems 30

2.2 Sediment sampling 42

3 Identifying trawl marks in North Sea sediments **46**

3.1 Abstract 46

3.2 Introduction 47

3.3 Materials and Methods 51

3.4 Results 63

3.5 Discussion 74

3.6 Conclusions and Outlook 83

3.7 Author Contributions 85

3.8 Funding 85

3.9 Acknowledgments 86

3.10 Conflicts of Interest 86

3.11 References 86

4 Physical impact of bottom trawling on seafloor sediments in the German North Sea 87

4.1 Abstract ... 87

4.2 Introduction ... 88

4.3 Material and Methods ... 90

4.4 Results ... 97

4.5 Discussion ... 101

4.6 Conclusion ... 105

4.7 Acknowledgements ... 106

4.8 References ... 106

5 Automated mapping of bottom trawling impact ... 107

5.1 Abstract ... 107

5.2 Introduction ... 107

5.3 Materials and Methods ... 110

5.4 Results ... 119

5.5 Discussion and conclusion ... 124

5.6 Acknowledgements ... 127

5.7 References ... 128

6 Synthesis ... 129

6.1 Spatial extend of trawl marks ... 129

6.2 Seasonal variability and trawl mark persistence ... 130

6.3 Altered sediment properties due to bottom trawling ... 131

6.4 Developments in automated seabed mapping ... 133

6.5 Application to other shelf seas ... 134

7 Outlook ... 137

8 References ... 139

Appendix ... 155

Acknowledgements **165**

Versicherung an Eides Statt / Affirmation in lieu of an oath **167**

Thesis outline and author contributions

This cumulative doctoral thesis contains 7 main chapters. The scientific objectives are addressed with three manuscripts (chapter 3 to 5) that are published (chapter 3), submitted (chapter 4), or in preparation (chapter 5) to international peer-review journals. The manuscripts are arranged in chronological order of submission.

Chapter 1 ("Introduction") provides an introduction to the general topic of seabed mapping with focus on anthropogenic impact. Moreover, a description of how bottom trawling can affect marine habitats and the generation of trawl marks as well as their relevance for estimating the impact of fishery on marine flora and fauna is explained.

Chapter 2 ("Materials and Methods"), gives an overview of the data sets and methods (hydro-acoustic systems and sediment sampling) that were used in the scope of this thesis.

Chapter 3: Identifying trawl marks in North Sea sediments

Ines Bruns (IB), Peter Holler (PH), Ruggero M. Capperucci (RMC), Svenja Papenmeier (SP) and Alexander Bartholomä (AB)

Published in Geosciences on 25. October 2020 (Geosciences 2020, 10, 422; doi:10.3390/geosciences10110422).

Content: The study presents a comprehensive mapping of trawl marks in the German North Sea, including an analysis of their spatial and seasonal variations, their appearance in backscatter data and an estimation of their persistence.

Author contributions and funding: The funding for this study was acquired by AB, who was also the lead of the ASKAWZ project, which is a research and development cooperation between Senckenberg am Meer and the German Federal Maritime and Hydrographic Agency (BSH, Bundesamt für Seeschifffahrt und Hydrographie, ASKAWZ III Contract-No. 10038520). ASKAWZ is part of the *SedAWZ* project, which is coordinated by BSH and funded by German Federal Agency for Nature Conservation (BfN, Bundesamt für Naturschutz). The study design was created by IB, PH and AB. All data sets were collected within the framework of the *SedAWZ* project aboard R/V Heincke, R/V Alkor and R/V Senckenberg by the following authors: PH (chief scientist on surveys HE456, HE500, AL520_2, HE544 and all surveys with R/V Senckenberg), IB (scientist on surveys Senckenberg25_2018, Senckenberg32_2018, AL520_2, Senckenberg18_2019, Senckenberg21_2019, HE544) and SP (chief scientist on surveys HE474, HE478, HE502). The post-processing of the side-scan sonar (SSS) raw data sets was performed by IB with support by PH, who also checked the resulting interpretations

for integrity. IB performed the manual mapping and analysis of the trawl marks from the processed SSS-data sets. The post-processing of the multibeam echo sounder (MBES) was done by RMC and SP; RCM delivered the interpretation of the MBES-data. The results of the grain size analysis were interpreted by SP, PH and IB and the under-water videos were analyzed by IB. The original draft of the manuscript was prepared by IB with contributions by RMC, AB, PH, and SP. The figures and tables were designed by IB, with helpful advices by the co-authors. During the review process, IB was supported by RMC, SP and AB. The final manuscript was discussed and commented by all authors.

Chapter 4: Physical impact of bottom trawling on seafloor sediments in the German North Sea

Ines Bruns (IB), Alexander Bartholomä (AB), Francine Menjua (FM), Achim Kopf (AK).

The manuscript was submitted to the journal Frontiers in Earth Science (section Marine Geoscience) on 01.06.2023 and published on 09.11.2023. doi: 10.3389/feart.2023.1233163

Content: The study deals with physical impact of bottom trawling on sediments in the German North Sea and provides in-situ sediment strength data, which could show the reworking of the sediment after trawling activity.

Author contributions and funding: The funding for this study was acquired by AB, who was also the lead of the ASKAWZ project, which is a research and development cooperation between Senckenberg am Meer and the German Federal Maritime and Hydrographic Agency (BSH, Bundesamt für Seeschifffahrt und Hydrographie, ASKAWZ III Contract-No. 10038520). ASKAWZ is part of the *SedAWZ* project, which is coordinated by BSH and funded by German Federal Agency for Nature Conservation (BfN, Bundesamt für Naturschutz). The study design was created by IB and AB with support by AK. All data sets were collected within the framework of the *SedAWZ* project aboard R/V Heincke during expedition HE544. Chief scientist was our deceased colleague Dr. Peter Holler. IB was contributing as scientist, FM as student assistant to this expedition. The post-processing of the side-scan sonar (SSS) raw data sets was performed by IB and the processing of the penetrometer data by FM. The analysis of the SSS data was done by IB with support by AB and the analysis of the penetrometer data was done by FM and IB, supported by AK and AB. The statistical analysis of the grain size distribution was performed by IB and the results were interpreted by IB and AB. The original draft of the manuscript was prepared by IB. During the editing of the manuscript, IB had strong support by AB. AK and FM gave fruitful feedback towards the discussion. The figures and tables were designed by IB, with helpful advices by the co-authors. The submitted manuscript was discussed, commented and approved by all authors.

Chapter 5: Automated trawl mark mapping

Ines Bruns (IB) and Alexander Bartholomä (AB)

In preparation for the submission to the journal *remote sensing*.

Content: The third study provides an unsupervised image classification approach for the automated mapping of trawl marks and discusses limitations and advantages of the presented procedure.

Author contributions and funding: The funding for this study was acquired by AB, who was also the lead of the ASKAWZ project, which is a research and development cooperation between Senckenberg am Meer and the German Federal Maritime and Hydrographic Agency (BSH, Bundesamt für Seeschifffahrt und Hydrographie, ASKAWZ III Contract-No. 10038520). ASKAWZ is part of the *SedAWZ* project, which is coordinated by BSH and funded by German Federal Agency for Nature Conservation (BfN, Bundesamt für Naturschutz). The study design was created by IB and AB. The datasets were collected within the framework of the *SedAWZ* project aboard R/V Heincke (expedition HE544) and R/V Senckenberg (expedition Senckenberg32_2018). On both surveys, our deceased colleague Dr. Peter Holler was the chief scientist and IB contributed to obtaining the SSS dataset and performed the post-processing. IB evaluated the methods for this manuscript, developed the workflow within the GIS software and analyzed the SSS images according to this workflow. The results were checked for integrity by IB and AB. The original draft of the manuscript was prepared by IB. During the editing of the manuscript, IB had strong support by AB.

In **chapter 6 ("Synthesis")**, the interlinking between the three studies is stressed and they are put in a broader perspective within the research field of seabed mapping and bottom trawling impact. It is followed by an outlook **(chapter 7)**.

All references are listed at the end of the thesis **(chapter 8)** and in the appendix, supplementary material, namely the Python script of the GRASS GIS workflow from the study in chapter 5, can be found.

1 Introduction

1.1 Anthropogenic impact on the marine environment

Roughly 70% of the earth's surface is covered with oceans but only a small proportion of the seabed is already mapped; with different resolutions from centimeters for up to several meters. Shelf seas make up approx. 7 % of the world's oceans and since roughly 40 % of the global human population lives near to the coast, shelf seas are the area where the most human impact on the sea happens: Oil and gas platforms, offshore cables, wind farms and other constructions are build. Moreover, global shipping traffic and fishery have to share not only the high seas but especially coastal areas where these multiple use cases are prone to come into conflict as space is limited.

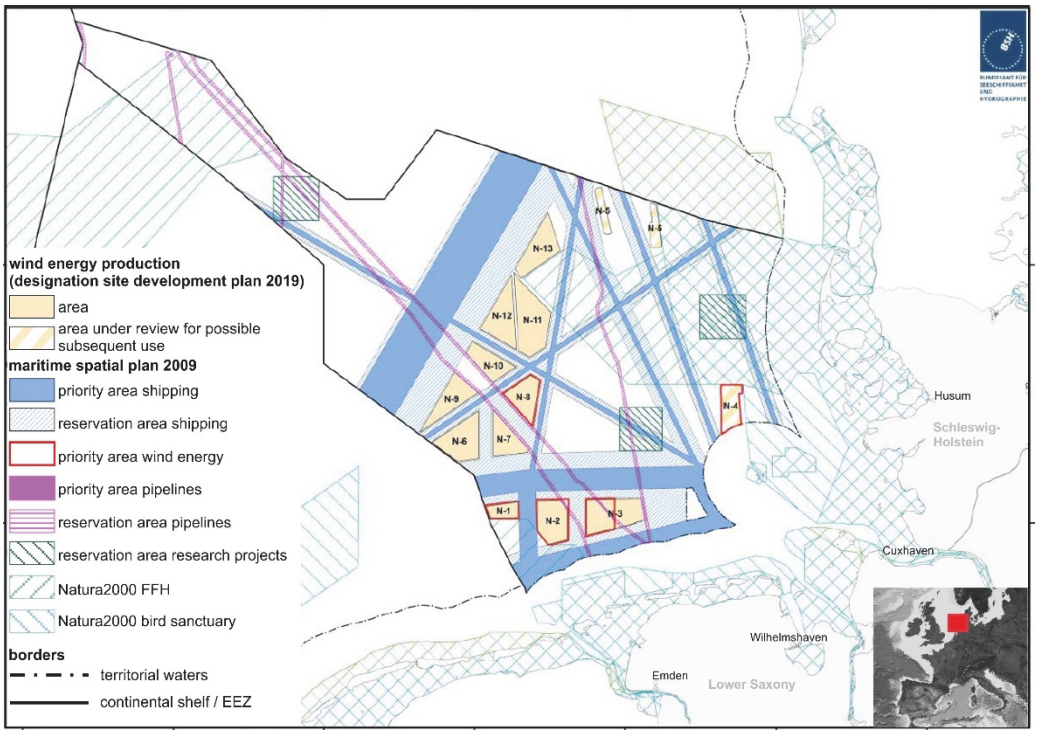

Figure 1: The site development plan of the German Exclusive Economic Zone (EEZ) in the North Sea (modified after BSH, 2019). It is an example of a part of a shelf sea where nature conservation as well as a variety of industries have to share a limited space. Overview of Europe: Imagery reproduced from the GEBCO grid (GEBCO-Compilation-Group, 2020).

To preserve natural structures and habitats from this human impact, different approaches are pursued e.g., quota in resource extraction or marine protected areas (MPA). The North Sea part of the German Exclusive Economic Zone (EEZ) is extensively used for different purposes

such as wind energy, pipelines and shipping (Figure 1). Thus, the space for resource extraction, e.g., fishery, is limited and fishery has to move to the remaining un-used areas given that target fish population is sufficiently abundant (Stelzenmüller et al., 2015, Emeis et al., 2019). Marine spatial planning (MSP) therefore is an important and highly complex task. To ensure optimal decisions, manifold information is consulted such as shipping density, fishing pressure as well as environmental information about biodiversity and the seabed surface (e.g., Campbell et al., 2014, Stelzenmüller et al., 2015, Fliessbach et al., 2019, Manea et al., 2020). Habitats are highly clustered and their sensitivity to human impacts is difficult to estimate and it is necessary to gather reliable and up-to-date data sets. For instance, the seabed sediment distribution is of major interest, as it reflects the hydro-dynamic regime and is related to the predominant marine habitat type (Populus et al., 2017). Thus, seabed mapping is an important requirement for habitat assessment and subsequent MSP and nature conservation.

1.2 Seabed mapping

In former times, marine habitat mapping was conducted on a relatively low resolution; e.g., a sediment sampling with roughly 1 km spacing (Figge, 1981). However, today a more detailed description of the seabed conditions is necessary to meet the requirements of the different stakeholders. Besides direct sampling of seabed sediments or fauna and flora (e.g., sediment cores, grab samples, experimental trawls) the seabed can be mapped with hydro-acoustic techniques such as side-scan sonars (SSS) or multibeam echo sounders (MBES). The general progress in computing power and storage capacity allowed mapping large areas with resolutions in the cm-range. In this way it is possible to study the bathymetry using MBES and the seabed in terms of sediment cover using the backscatter signal of SSS or MBES. Usually, the backscatter data is classified according to specific characteristics e.g., a high intensity backscatter signature indicates a gravelly seabed area and a low intensity signature a rather fine grained or “smooth” seabed. Such different areas can be mapped by means of their spatial extend and subsequently processed to a sediment distribution map (e.g., Markert, 2013, Holler et al., 2017, Amiri-Simkooei et al., 2019). Moreover, single objects on the seabed, e.g., boulders or anthropogenic structures, can be visualized and mapped (Papenmeier, 2018, Kampmeier et al., 2020) as well as indications of benthic communities such as populations of Bryozoa (Bartholomä et al., 2019) or seagrass, e.g., *Posidonia oceania* (Fakiris et al., 2019). Thus, these hydro-acoustic systems became extremely important in the marine habitat mapping realm (e.g., Holler et al., 2017, Lamarche, 2018, Fakiris et al., 2019).

On an international level, there is made a lot of effort to collect marine habitat data sets in order to make them available in large-scale maps (Populus et al., 2017) and other information systems (e.g., EUNIS, 2019). International experts are working together under the umbrella of *ICES* (International Council for the Exploration of the Sea) in different groups; e.g., the working group on marine habitat mapping (WGMHM, ICES, 2020) or the working group on spatial fisheries data (WGSFD, ICES, 2019). These groups also support advice regarding EU (European Union) strategies. These exemplified projects highlight the importance of marine habitat mapping in different kinds of environments such as soft seabed sediment as well as hard grounds. Regarding the diverse use of sea territory and its complex crosslinking among the disciplines (see chapter 1.1) it is essential to ensure a high resolution in habitat mapping in order to create a detailed database, which allows a profound estimate of the seabed characteristics, e.g., sediment types, sessile fauna and flora or human impact. If this is achieved, the advancement of scientific models and decision making in MSP is significantly enhanced (e.g., Buhl-Mortensen et al., 2016, Populus et al., 2017).

1.2.1 Mapping the seabed of the German North Sea

The first comprehensive sediment distribution map of the German EEZ (North Sea) was published in a 1:250,000 scale by Figge (1981). It is based on surface sediment samples that were taken in intervals of ≥1km and a few hydro-acoustic datasets (Figge, 1982). This map was updated with a new substantial data set of sediment grab samples and borehole data by Laurer et al. (2014). Due to the increased need for detailed data sets, versatile mapping projects were brought to life in recent years. The findings by Figge (1981) and Laurer et al. (2014) were incorporated into the project *SedAWZ* (BSH, 2016), which aimed on the high-resolution hydro-acoustic mapping of the German EEZ (North Sea and Baltic Sea) and the subsequent classification of the sediment-types in order to serve as a base for further investigations in marine biology and habitat assessment. Besides hydro-acoustic data sets, sediment grab samples and under-water video recordings were obtained in the scope of *SedAWZ* (BSH, 2016). As a result, new maps of the sediment distribution of the German North Sea were recently published (Holler et al., 2020, Papenmeier et al., 2019). Other projects that developed maps of the German EEZ focused on e.g., modeled data sets of the bathymetry and bead shear stress (by waves and currents) or the abundance of marine biodiversity and related parameters (e.g., Heyer and Schrottke, 2013, Emeis et al., 2019).

Such mapping projects lead to an extensive knowledge about the seabed characteristics of the German North Sea: The water depth is increasing slightly from 0 to 2.5 m at the coast up to 66 m at the northernmost part of the German North Sea sector, approx. 200 nautical miles (NM)

off the mainland (EMODnet-Bathymetry-Consortium, 2018). The hydro-dynamic regime is tide-driven in coastal areas and mostly wave-driven in the northern areas (Aldridge et al., 2015). Thus, the highest mean kinetic energy at the seabed due to currents is reached in coastal areas (approx. 100 N/m^2 to >250 N/m^2) and it decreases northwards to < 20 N/m^2 (Joint-Nature-Conservation-Committee). The mean kinetic energy at the seabed due to waves follows the bathymetric contours: In areas with < 35 m water depth, it ranges between 20 N/m^2 and 50 N/m^2 and can reach up to 100 N/m^2 in coastal areas. In deeper parts (> 35 m) it is < 10 N/m^2 (Joint-Nature-Conservation-Committee). The direction of sediment transport is west to east in the southern German North Sea sector and northerly directed in the northern part (Zeiler et al., 2014). The Holocene seabed sediments consist of reworked Pleistocene glacial deposits (Schwarzer et al., 2008). They can mostly be described as fine to medium sand; muddy as well as gravely sediments are only regionally distributed (Laurer et al., 2014, Holler et al., 2020, Papenmeier et al., 2019). These Holocene deposits form mobile sand covers, which can reach up to 10 m thickness (Zeiler et al., 2014).

However, in the seabed mapping realm, not only natural seabed characteristics are of interest. Anthropogenic features such as trawl marks are investigated as well in order to assess the human impact on the marine environment (e.g., Lucchetti and Sala, 2012, Buhl-Mortensen and Buhl-Mortensen, 2018, Schönke et al., 2022). In the German North Sea, bottom trawling adds to the different use cases that are shown in Figure 1 and is of major interest in MSP (Stelzenmüller et al., 2015).

1.3 Bottom trawling

Bottom trawling is a wide spread human impact on the marine environment throughout the globe (Oberle et al., 2016a, Amoroso et al., 2018) and is concentrated in shelf seas (Guiet et al., 2019) such as the German North Sea. In European waters different categories of bottom fishing gear are used for catching marine fauna: bottom otter trawls, beam trawls, demersal seines and dredges. In the offshore waters (outside the 12-nautical-mile-zone) of the German EEZ (North Sea part) mostly bottom otter trawls (OTB) and beam trawls (TBB) are used (Eigaard et al., 2017, Schulze, 2018). OTB have no rigid beam to open the net but two otter boards that are towed with varying distances to each other according to hydrodynamic forces depending on the towing speed and, in this way, controlling the opening of the net (Figure 2). TBB have a rigid beam to hold the net open and the ground gear has tickler chains to startle the fish. Gear widths of TBB can range between 4 and 20 m and door spreads of OTB between several tens of meters and 250 m (Eigaard et al., 2016). Both gear types (TBB and OTB) can

be towed in pairs, which is rather uncommon for OTB but a standard practice for TBB in the German EEZ. If towed in pairs, OTB are known as OTT (otter twin trawls).

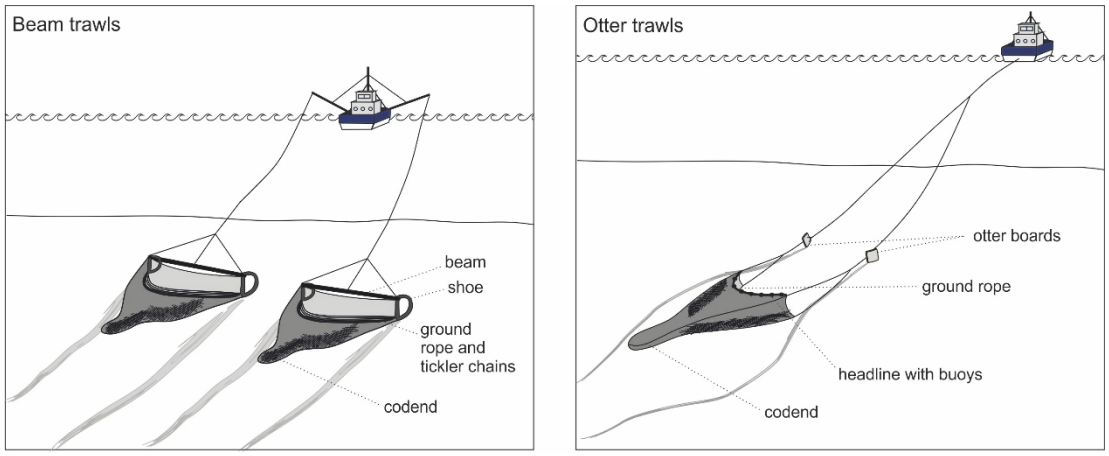

Figure 2: Schematic representation of beam trawls (left panel) and bottom otter trawls (right panel) with their main components (modified after Bruns et al., 2020).

In the German North Sea, small trawlers (<221 kW engine power and <24 m LOA) are common in coastal waters, i.e., within the 12-nautical-mile-zone, and large trawlers (>221 kW engine power and >24 m LOA) are operating mostly in the EEZ, in offshore waters (Schulze, 2018). Small trawlers equipped with TBB gears are targeting e.g., brown shrimp (*Cragnon cragnon*) or they use dredges (comparable to TBB but with a chain bag instead of a net) to catch bivalves (Eigaard et al., 2016, Schulze, 2018). Large trawlers using TBB or OTB often target on e.g., demersal flatfish like plaice (*Pleuronectes platessa*) ore sole (*Solea solea*) (ICES, 2019).

1.3.1 Spatial distribution of bottom trawling

In order to monitor bottom trawling and to evaluate fishing pressure in European waters, VMS (vessel monitoring system) data are analyzed (ICES, 2019). Since 2012, fishing vessels with a length over all (LOA) >12 m are legally bound to transmit their positioning data (EC, 2009). The positioning data is combined with information from the European Fleet register such as engine power, vessel length and the trawl gear type, in order to estimate the fishing activity (ICES, 2019). Fishing activity maps often depict the indices swept area (SA) and swept area ratio (SAR) in total (Figure 3) and per gear type (ICES, 2018d). Usually, their spatial resolution is roughly 0.05°*0.05° and the data are aggregated for one year (ICES, 2019). The index SA describes the area that is touched by the fishing gear. Then, SA is divided by the area of the grid cell in order to derive SAR. Thus, SAR describes how often an area equivalent to the grid cell was swept: SAR = 2 indicates that an area equivalent to the grid cell was swept

two times during the given time period, i.e., one year (ICES, 2019). As trawling overlaps, this does not mean that the whole grid cell was swept (ICES, 2020). The SAR assumes that trawling is distributed evenly across the grid cell but in fact, this is often not the case and therefore, SA and SAR are only an estimation of the bottom trawling impact on the seabed (Ellis et al., 2014). Moreover, VMS raw data is highly confidential and may not be available to non-governmental scientists or the public: Usually, only highly aggregated VMS data are available (Hinz et al., 2013), which leads to a coarse resolution and thus to uncertainties in the estimation of fishing effort and impact (Lambert et al., 2012).

According to VMS data-based estimations for the year 2017, the fishing activity concentrates in the coastal areas of the German North Sea (Figure 3). Almost along the whole coast, SAR is up to 15 and, in rare cases, > 20. Another highly impacted area can be found in the northern part at the border to the Danish sector (SAR up to 17). In the western German EEZ, SAR is smaller (up to 3) compared to the other two areas but still increased with regard to the remaining German EEZ (North Sea). A slightly increased SAR (up to 2.5) can be observed in the north-western most part, which belongs to the Dogger Bank.

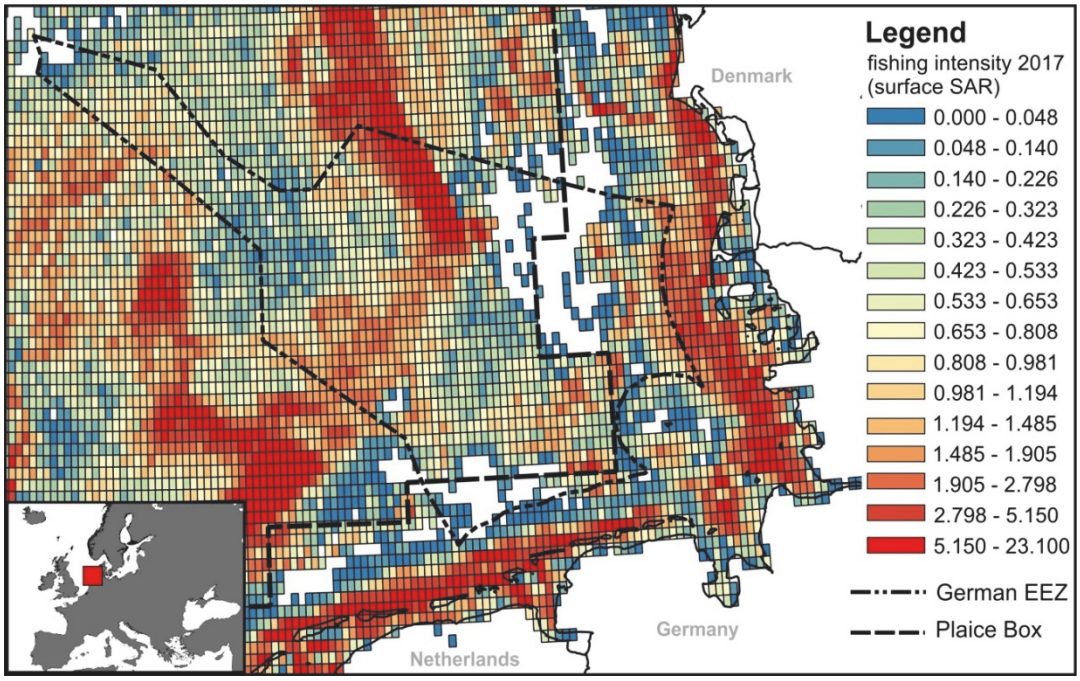

Figure 3: Exemplarily for the year 2017, a map of the total fishing intensity (all gear types) cumulated over the year for the southern North Sea is shown. The fishing intensity is presented in SAR (swept area ratio), which represents how often an area equivalent to the grid cell of 0.05°*0.05° was trawled over the year (ICES, 2018a). The image was produced after the ICES spatial data layers of fishing intensity (ICES, 2018e). The Plaice Box is a protection zone where bottom trawling is partly banned in order to support the recovery of the plaice (*Pleuronectes platessa*) population.

Seasonal changes in fishing activity can be observed as well: It is highest in summer and autumn in the German North Sea, which can also be derived from VMS-data if the temporal resolution is increased (Emeis et al., 2019). These inter-annual changes in fishing activity are likely related to weather conditions, economic reasons, e.g., fuel prices, and of course the abundance of target species (ICES, 2018d). Soles (*Solea solea*), for example, migrate to their coastal spawning areas in spring and move back to offshore waters in autumn (de Veen, 1976).

1.3.2 Implications for marine fauna and flora

Bottom trawling can increase the mortality of target species as well as non-target species due to injuries caused by the heavy trawl gear (e.g., Kaiser and Spencer, 1996, Lindeboom and de Groot, 1998, Buhl-Mortensen et al., 2016). However, it depends on the species and the particular habitat how intense the disturbance by bottom trawling is. Large-bodied fauna with a long life cycle such as sponges are more vulnerable to it compared to fauna with smaller bodies and shorter life cycles (Sciberras et al., 2018, Tiano et al., 2020). Species that inhabit areas affected by regular, natural disturbances (e.g., storm surges) may adapt to the additional effects of bottom trawling. Species of rather stable habitats are strongly affected by bottom trawling (Jennings and Kaiser, 1998). Furthermore, bottom trawling can remove biogenic structures such as tubes and mounds (Schwinghammer et al., 1998) or small bedforms such as ripples, which are used as a shelter by juvenile fish (Depestele et al., 2016).

Several studies were published that investigated the effects of bottom trawling on the geo- and biochemical integrity of the seabed. It was found that the percentage of chlorophyll and organic carbon significantly decreases in trawled areas (Morys et al., 2021) and that extensive bottom trawling can affect the nitrogen cycle (Ferguson et al., 2020, De Borger et al., 2021). The impacts mentioned above contribute to the condition of the benthic habitat and need to be considered in management strategies for MSP or nature conservation. The problem of endangered target species in the North Sea was already addressed in the 1990s, which resulted in the implementation of a protected area for plaice (*Pleuronectes platessa*). Since 1995, the Plaice Box (Figure 3) is closed for large trawlers (>221 kW engine power and >24 m LOA) with higher catch rates compared to small trawlers, which is expected to allow the recovery of the plaice population (Commission of the European Communities, 2005). In order to evaluate the condition of the European seas, further management strategies and measures were implemented that also include the assessment of bottom trawling impact such as EMPAS (ICES, 2008), EU Marine Strategy Framework Directive (MSFD) (Commission of the European Communities, 2008) or the European Water Framework Directive (WFD) (Commission of the

European Communities, 2000). However, some of these measures may lack sensitivity for the effects of bottom trawling (McLaverty et al., 2023), which stresses the need for in-depth investigations of bottom trawling.

If the impact of bottom trawling on the benthic habitat is well understood, it is possible to estimate eventual hazards to the species (e.g., Lindeboom and de Groot, 1998, Buhl-Mortensen et al., 2016, Mérillet et al., 2017, Tiano et al., 2020) or effects on the sediment budget (e.g., Palanques et al., 2014, Coughlan et al., 2015, Paradis et al., 2021), which may also affect the benthic species. The investigation of the environmental impact of fishery in general is necessary because fishing effort is distributed across the whole globe; however, it is concentrated in coastal areas (Guiet et al., 2019) where the space is limited due to other uses as exemplarily shown in Figure 1 for the German EEZ (North Sea).

1.3.3 Physical impact of bottom trawling

The mechanical interaction of the bottom trawl gear with the seabed results in displacement and compression of the sediment (e.g., Ivanović et al., 2011, O'Neill and Ivanović, 2015) as well as re-suspension (e.g., Palanques et al., 2001, Palanques et al., 2014, Paradis et al., 2021). Thus, furrows are created on the seabed, which are often called trawl marks and are a directly visible representation of the physical impact of bottom trawling (Figure 4b,d). As early as in the 1970s descriptions of trawl marks were published as they appeared in SSS data that were obtained in the scope of seabed mapping for e.g., pipeline installation (Caddy, 1973, Manley, 1977, Hovland and Indreeide, 1980). In the following decades hydro-acoustic techniques were developed further and became a standard tool for seabed mapping. Consequently, this led to numerous studies considering trawl marks that were detected in SSS data and MBES data of different sea regions (e.g Krost et al., 1990, Friedlander et al., 1999, Smith et al., 2007, Bruns et al., 2020, Lüdmann et al., 2021) as well as in under-water video recordings (e.g., Gilkinson et al., 2015, Buhl-Mortensen and Buhl-Mortensen, 2018, Mérillet et al., 2018).

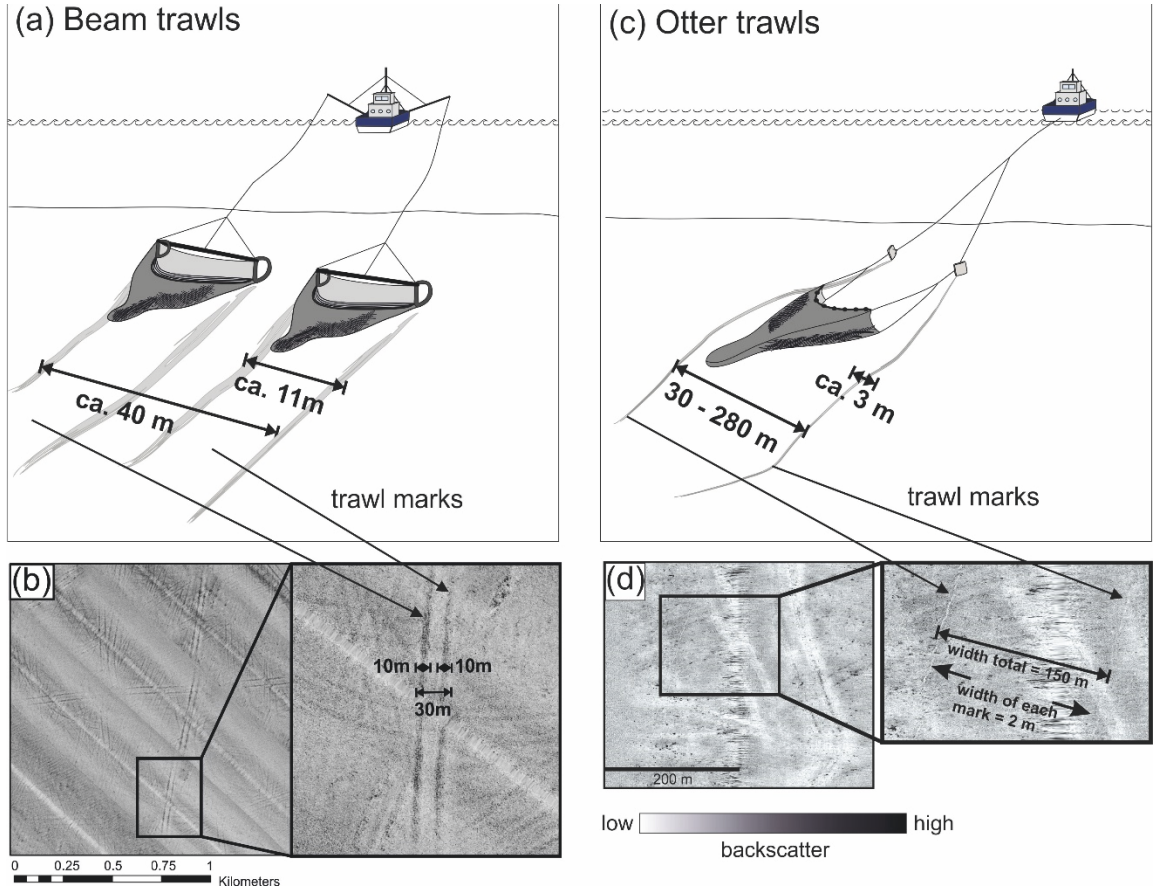

Figure 4: (a) Sketch of pair towed beam trawls and the resulting trawl marks on the seabed with the corresponding dimensions. Each beam trawl creates a mark of ca. 11 m width and the total width of the pair is approx. 40 m. (b) Example of trawl marks from pair towed beam trawls in a SSS image. The dimensions of the marks reflect the width of the trawl gear. (c) Sketch of an otter trawl and the trawl marks created by it on the seabed. The otter boards leave marks with approx. 3 m width and the distance between them can range between 30 m and 280 m. (d) Otter board marks in a SSS image with the corresponding dimensions of the gear (modified after Bruns et al., 2020).

From the observation of trawl marks, the question of the intensity of the physical disturbance of the seabed has arisen. Important indicators are the extent of the area that was touched by the trawl gear, the penetration depth of the trawl gear and the persistence of trawl marks. The dimensions of trawl marks and therefore the area of the seabed that was disturbed reflect the geometry of the gear (Figure 4). Otter board marks can have widths of a few 10s of centimeters to a few meters (e.g., Krost et al., 1990, Lucchetti and Sala, 2012) and beam trawl marks have widths of ca. 4 m to 20 m (e.g., Eigaard et al., 2016, Bruns et al., 2020).

The weight of the trawling gear controls the penetration into the seabed and the persistence of trawl marks: The heavier the gear, the higher the penetration depth and therefore the persistence of related trawl marks (Krost et al., 1990, Eigaard et al., 2016). For example, the

penetration depth of beam trawls is less, if compared to otter trawl doors (Table 1) as the latter are rather narrow and consequently, the weight is concentrated on a smaller area (Rijnsdorp et al., 2020).

	Penetration depth [cm]			
Gear type	**Coarse sediment**	**Sand**	**Mud**	**Mixed sediments**
Otter trawls	≤ 10	≤ 15	≤ 35	≤ 10
Beam trawls	≤3 - 10	≤3 - 10	≤ 10	≤ 10

Table 1: Penetration depths (in cm) of otter and beam trawls depending on the sediment type (after Eigaard et al., 2016).

As the distribution of trawl marks is quite diverse by means of sea regions with different environmental settings (e.g., hydro-dynamic regime and sediment-type), information concerning their persistence strongly differ. In general, it is assumed that the persistence of trawl marks increases, if they are located in fine and cohesive sediments (Palanques et al., 2001, Mérillet et al., 2018) and in greater water depths, where sediment transport is relatively small (Schwinghammer et al., 1998). It can range between several years in muddy sediments and/or areas with low sediment transport (Werner et al., 1990, Gilkinson et al., 2015) and a few days in fine to coarse sand in rather dynamic environments (Lindeboom and de Groot, 1998, Depestele et al., 2016).

Bottom trawling cannot be considered as occasional event. As shown in Figure 3, some areas of the German North Sea sector can be trawled up to 23 times a year. Thus, the disturbance of the seabed is rather chronic and can have broader implications on the sediment distribution. The re-suspension of seabed sediment may cause selective transport and thus a relative increase of the fine fraction (Trimmer et al., 2005) or the coarse fraction (Mengual et al., 2016, Palanques et al., 2014) depending on the hydrodynamic regime. Moreover, chronic bottom trawling can lead to the erosion of the upper tens of centimeters of the seabed (Coughlan et al., 2015). The eroded material is transported away and deposited elsewhere, which can significantly increase the sedimentation rate in that area (Paradis et al., 2021). Due to the erosion of the surface sediment it is likely that deeper layers are mobilized (O'Neill and Ivanović, 2015) as well as nutrients or pollutants (e.g., heavy metals) they might contain, which would then affect the geochemical properties of the benthic habitat (van der Molen et

al., 2013, Coughlan et al., 2015, Bunke et al., 2019) and thus the benthic community as described in chapter 1.3.2.

1.4 Motivation and scientific questions

The main motivation of this thesis was to gain new insights into the persistence of commercial trawl marks and, thus, to fill the gap of underrepresentation of studies in this context. A detailed description of trawl marks connected to commercial fisheries in German EEZ and information about their persistence was missing as well. Several existing studies focus on modeled data and experimental trawls (e.g., Ivanović et al., 2011, Depestele et al., 2016, Depestele et al., 2019). The persistence of trawl marks is directly linked to the impact on the habitat as it may indicate the recovery time. As the persistence of trawl marks strongly depends on the specific environment and time series are needed to estimate it, most of the existing data are based experimental trawls. However, commercial trawl gears often have bigger dimensions and thus a higher weight, which increases the penetration depth (Eigaard et al., 2016). For example Depestele et al. (2016), used a beam trawl with 4.4 m width for their study but the beam trawl fleets in the southern North Sea often operate with ≥ 10 m wide gear (Eigaard et al., 2016). Another lack of information is the impact of bottom trawling on the internal in-situ structure of the sediment. It may disturb the integrity of the sediment and thus making it prone to re-suspension by currents and waves and increased sediment reworking would affect the benthic communities (Queirós et al., 2006). Existing studies that investigated the change of the physical sediment properties due to bottom trawling are based on lab experiments, experimental trawling or modelling approaches (e.g., Paschen et al., 2000, O'Neill and Ivanović, 2015, Ivanović and O'Neill, 2015). The physical impact of bottom trawling is of major interest in MSP and nature conservation. However, the monitoring of fishing activities is a complex task due to heterogeneous data sets and large sea territories that have to be monitored. As VMS-data may not deliver a sufficient resolution, mapping trawl marks may be a more desirable approach in order to estimate small-scale fishing activity in certain areas. In order to speed up this time consuming process, the automated detection of trawl marks may be favorable. However, existing approaches are sparse and often use machine learning algorithms that require in-depth skills in programming and image analysis (Gournia et al., 2019, Michaelis et al., 2019). Thus, another motivation for this thesis was to find a convenient way for automated trawl mark mapping.

This dissertation therefore aimed to answer the following research questions:

1) Can trawl marks from commercial fishing fleets be classified in hydro-acoustic data by means of backscatter signature, persistence and spatial extend in the German EEZ (North Sea)? (chapter 3)

2) Does commercial bottom trawling alter the physical properties of the seabed sediment and if yes, in which order of magnitude? (chapter 4)

3) Can trawl marks be mapped by means of a user-friendly machine learning approach? (chapter 5)

2 Materials and methods

The manuscripts of this dissertation were written in the framework of the ASKAWZ project, which was part of the *SedAWZ* mapping project (see e.g., chapter 3.8) and thus multiple data sets from different surveys were integrated in the research for this thesis. The following table gives an overview of the surveys, the data sets that were used in the scope of this thesis (hydro-acoustics and samples) and whether I participated in the survey or not. Further details on the respective survey, i.e., exact locations, dates, specification of the instruments as well as data and sample processing, can be found in the corresponding manuscripts and in published cruise details.

Table 2: This table lists the surveys from which subsets of the overall data sets were used in the scope of this thesis. It is specified if side scan sonar (SSS) or multibeam echo sounder (MBES) data were used and which kind of samples from the seabed. Moreover, it is stated whether I participated in the survey or not (survey participant: yes or no) and where further details concerning the surveys and data processing can be found (this thesis and published cruise details).

survey name	hydro-acoustic data sets	samples	survey participant	further details	expedition details
Senckenberg 30_2015	SSS	Sediment	No	see chapter 3	Not published
HE456	SSS	Sediment	No	see chapter 3	Holler (2016)
HE474	SSS & MBES	Sediment, UW-Video	No	see chapter 3	Hass (2016)
HE478	SSS	Sediment, UW-Video	No	see chapter 3	Papenmeier (2017)
HE500	SSS	-	No	see chapter 3	Holler (2018)
HE502	SSS	-	No	see chapter 3	Hass (2018)
Senckenberg 25_2018	SSS	-	Yes	see chapter 3	Not published

Senckenberg 32_2018	SSS	Sediment	Yes	see chapter 3 and 5	Not published
AL520_02	SSS	Sediment, UW-Video	Yes	see chapter 3	Holler et al. (2019b)
Senckenberg 14_2019	SSS	-	Yes	see chapter 3	Not published
Senckenberg 18_2019	SSS	-	Yes	see chapter 3	Not published
Senckenberg 21_2019	SSS	-	Yes	see chapter 3	Not published
HE544	SSS	Sediment, dynamic free-fall penetrometer	Yes	see chapter 3 and 4	Holler and Bruns (2020)

The general hydro-acoustic survey set up can be described as follows: SSS and MBES systems were operated parallel and the vessel speed was approx. 5 kn (~ 2.5 m/s). In most of the surveys a 100 % coverage of the area was achieved (see chapter 3 for details). The sampling locations were selected according to particular seabed features, i.e., the verification of certain sediment types and the investigation of trawl marks (see chapter 3 and 4 for details).

In the following chapters, the general principles of the methods that were used in the scope of this thesis are briefly explained.

2.1 Hydro-acoustics systems

Hydro-acoustic techniques are commonly used in marine science for investigating the seabed, e.g., habitat mapping, in order to identify and classify natural seabed features such as different sediment types, hard grounds or the bathymetry. Man-made structures may be a target for seabed or habitat mapping as well: For instance, pipelines, mines, dumping and dredging grounds or the impact of bottom trawling (i.e., trawl marks) can be subject of the investigation.

There are different types of devices: Single beam echo sounders (SBES) and swath systems (SSS and MBES). They deliver a visualization of an area in top view (Figure 5) and also depth

information (does not apply to SSS). They are based on the principle of emitting acoustic waves from the source, which are scattered back from the target (i.e., seabed) and then recorded by the transducer unit attached to the source.

For seabed mapping, swath systems (SSS and MBES) are often used (e.g., Lucieer, 2012, Capperucci, 2013, Holler et al., 2017, Fakiris et al., 2019). SSS-systems have the advantage, that they can cover a larger area due to their beam geometry and reducing the time needed to map a certain amount of seabed, compared to MBES. However, in recent years MBES-systems have become more and more important, because MBES data yield the potential to provide additional information for sediment classification as they deliver more variables compared to SSS such as bathymetry, slope and curvature, which are also beneficial for automated sediment classification (e.g., Feldens et al., 2018, Amiri-Simkooei et al., 2019).

This thesis focuses on data sets obtained by SSS and MBES systems.

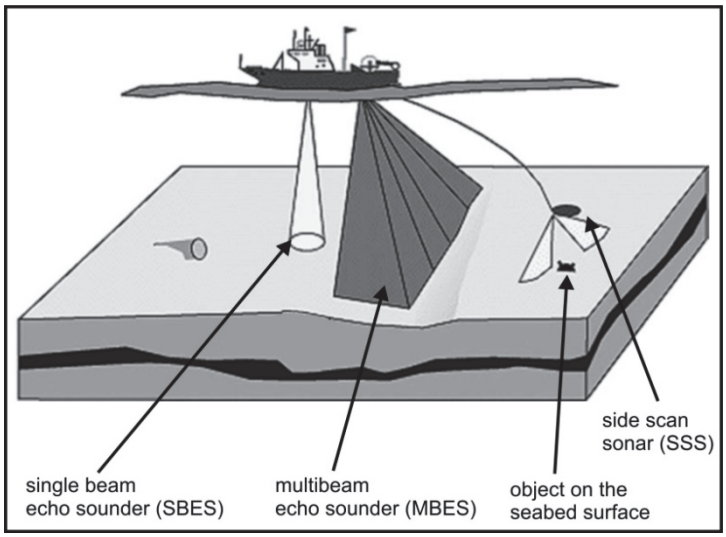

Figure 5: Schematic representation of different hydro-acoustic systems (modified after Blondel, 2009). All systems are based on the principles of acoustic wave propagation. The multibeam echo sounder (MBES) and the towed side-scan sonar (SSS) deliver a representation of the seabed surface and the objects on it. MBES also provides depth information. The operating principle of the sediment echo sounder (SES) or parametric echo sounder allows investigating the seabed subsurface as well.

2.1.1 Hydro-acoustic theory

An acoustic wave is defined as a pressure wave propagating through the water column and the target material (seabed in this case). It is send out by the source (e.g., sonar system), reflected or scattered back from the target and the change in acoustic pressure is then measured by hydrophones or the transducer of the sonar system. The wave has a certain

intensity of acoustic pressure, which is often expressed in a logarithmic scaling, i.e., in decibels (dB), as the change in intensity often covers several orders of magnitude (Blondel, 2009). Moreover, the wave is characterized by its frequency and the pulse length. The frequency *f* is defined by the wavelength λ and the velocity of sound in the medium *c:*

$$f = \frac{c}{\lambda}$$ Equation 1

In seawater, the sound velocity *c* is usually between 1,450 m/s and 1,550 m/s and approx. between 1,500 m/s and 2,000 m/s in saturated seabed sediment (Blondel, 2009, Lurton, 2002). The sound velocity in the water column depends on salinity, pressure and temperature and therefore it is of advantage to cast a sound velocity profile before starting the measurement with sonar systems (especially important for MBES as they deliver also depth information). Using a constant sound velocity would cause inaccuracies, as the acoustic waves follow Snell's law: In a stratified water column, the interface between the layers (n_1 and n_2 in this example) causes reflection and refraction of the acoustic wave (Figure 6a). Due to the different properties of the layers (e.g., differences in density), the sound velocity changes with depth (Figure 6b). Thus, the actual arrival of the wave would be further away from the source than expected when assuming a constant sound velocity (Figure 6c). Disturbances in the water column such as gas bubbles, waves or the wake of a vessels propeller can influence the recording of the acoustic wave as it may be scattered back from the interface of the two media.

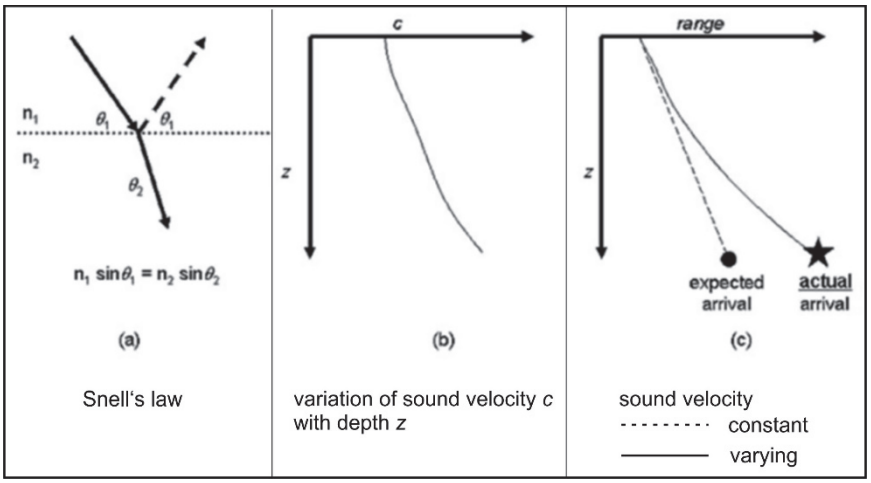

Figure 6: Variations in sound velocity influence the path of the acoustic wave (modified after Blondel, 2009). (a) Snell's law describes the refraction of an acoustic wave at an interface within a medium, e.g., a water body with different properties in each layer (n_1 and n_2). (b) A stratified water column results in variations in sound velocity with depth. (c) The different points of arrival of the acoustic wave relative to the source (range) when a constant velocity (dashed line) and a varying velocity (solid line) is assumed.

Following this, the acoustic wave is influenced by the properties of the seawater as well as by the geometry of its propagation. This applies to both ways: from the transmitter to the target and back from the target to the receiver, i.e., hydrophone or sonar system. The target is the seabed and can be considered as an interface between two media (i.e., sea water and sediment) with different properties such as density. The part of the acoustic wave that is reflected or scattered back from the target is recorded by the receiver. The oblique distance the acoustic wave has travelled from the transmitter to the target is called slant range, R (Blondel, 2009). The energy of the acoustic wave decreases the further it travels away from the source (geometrical spreading loss). The outer limit of the insonified area is called the far range and at this point the wave geometry can approximately be described as a plane wave, which leads to a decrease in energy that is scattered back to the transmitter (Blondel, 2009). The decrease is described as $\frac{1}{R^2}$ (Blondel, 2009). The decrease in energy of the acoustic wave is moreover related to the viscosity and chemical properties of the water column (attenuation loss) and therefore, the attenuation has to be considered when hydro-acoustic data are interpreted as it may lead to a decrease in resolution, especially in the far range as it adds to the geometrical spreading loss. In order to correct the signal for such losses in energy, the signal can be amplified by using Automatic Gain Control (AGC) and/or Time Variable Gain (TGV).

Besides the sound velocity within the medium, the frequency depends on the wavelength (Euqation 1) The wavelength is one factor, which controls the resolution of the acoustic image, because it determines to which dimension an object can be detected. In under water acoustics, operating frequencies for SSS and MBES can range between 1 kHz to 1 MHz (Blondel, 2009). Thus, the wavelengths of typical SSS frequencies are between 1.5 m and 1.5 mm. Other factors controlling the resolution are the characteristics of the pulse that is transmitted, i.e., length and type (Blondel, 2009). The most common types of pulses are burst (continuous sine wave) and chirp, which is a linear swept frequency formed by a cosines wave (Blondel, 2009). Both types are of a defined duration and are separated by a defined time. Thus, two consecutive pulses can only be recognized as individual pulses if the separating time is at least equal to the time of duration. A pulse of T = 1 ms scattered back from a target and travelling through a medium with the sound velocity c = 1500 m/s results in a spatial resolution of δ = 0.75 m:

$$\delta = \frac{cT}{2} \qquad \text{Equation 2}$$

2.1.2 Side-scan sonar (SSS)

The SSS provides acoustic images of the seabed based on the acoustic energy that is scattered back from the target to the instrument. A SSS is usually towed behind a vessel near the seabed (Figure 5) in order to achieve suitable conditions in terms of stability (e.g., low wave turbulences) and noise, e.g., from the vessels propeller. Unlike the MBES, a SSS usually does not provide information about the water depth. However, the height of the SSS above the seafloor can be determined. A SSS system typically has two transducers on each side, sending the acoustic signal, i.e., beam (Figure 7). The first incoming backscatter signals are from the water column, which is usually noise. The actual backscatter signal that comes from the seabed starts when the transmitted acoustic signal strikes the nadir (Figure 7) of the sonar. This first backscatter signal has a high strength because the attenuation due to geometrical spreading loss is minimal. It is useful to estimate the altitude of the sonar above the seabed and therefore to apply the slant range correction. As the signal propagates with time, it reaches oblique angles and produces the desired backscatter image.

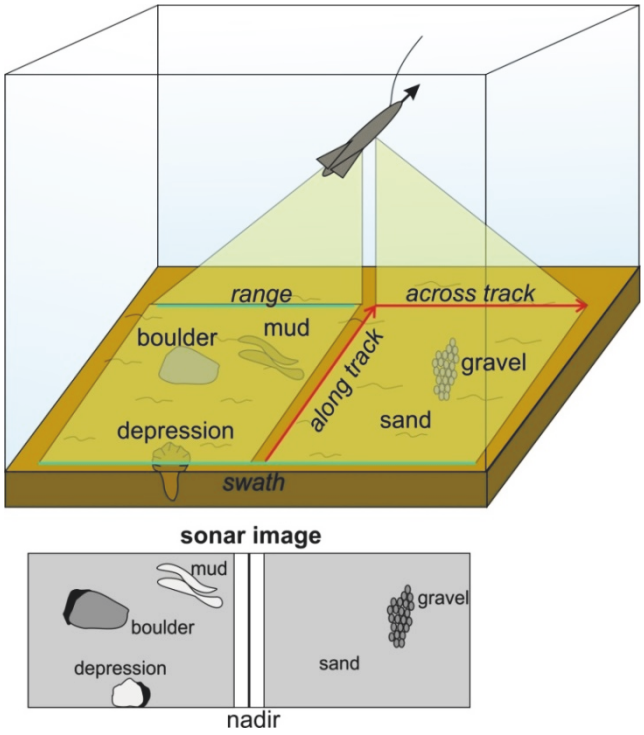

Figure 7: Schematic drawing of the side-scan sonar (SSS) configuration (modified after Boyd et al., 2005). The SSS is transmitting one beam to each side (range). It is towed in the direction of the vessels heading. The insonified area (light yellow shaded) on the seabed is called footprint and consists of the dimensions of the swath and the along track direction. According to their properties (e.g., roughness), the features on the seabed (mud patch, boulder, depression, sand and gravel patch) are represented in

the sonar image by different intensities of backscatter. The part directly below the SSS tow fish (nadir) is not insonified.

The insonified area is a narrow strip and when the vessel (and the SSS) is moving along track, it covers more and more of the seabed with time (Figure 7). The width in across track direction on each side of the towed SSS (range) can be between a few 10s of meters to several kilometers (GLORIA or TOBI system). The range in port and starboard direction add up to the so called swath. The beams are narrow along track (1° or less) and spreading wide in the across track direction, which leads to a higher resolution of the along track direction compared to across track (Blondel, 2009). The across-track resolution is given by:

$$\partial y = \frac{cT}{2sin\theta} \qquad \text{Equation 3}$$

Thus, it is determined by the pulse length of the signal (T), the sound velocity (c) and the incidence angle (θ). When θ approaches 90°, the resolution is described by Equation 2. The along-track resolution depends on the beam width (β) and the slant range (R):

$$\delta x = \beta R \qquad \text{Equation 4}$$

Thus, the resolution is not homogeneously distributed throughout the swath, which has to be considered during data interpretation. The resolution in the along-track direction (δx), moreover, depends on the range, the vessel speed over the ground (SOG) and the number of pulses travelling simultaneously through the water column. The maximum SOG can be calculated as follows (BSH, 2016):

$$max.SOG = \frac{c * \delta x * number\ of\ pulses}{2 * range} \qquad \text{Equation 5}$$

The distance from the transmitter to the target is the slant range and the distance from the SSS nadir to the target is called ground range (Figure 8a). When the acoustic wave reaches a target, i.e., the (rough) seabed or an object on it, the energy is reflected back to the SSS transducer as well as away from it along other angles (Figure 8b-d). This means, only a small proportion might be scattered back to SSS transducer, so that it can be recorded and produces an image of the seabed (Blondel, 2009). If the seabed shows strong variations in the morphology and the slope is facing away from the SSS, most of the energy will be reflected in specular direction away from the source (Figure 8b). This is why a sonar image of one part of the seabed can show less contrast than another, although it has similar properties except for the slope. In case of an approximate horizontal seabed, a greater proportion of the energy will be reflected back to the transducer (Figure 8c). However, depending on the seabed properties (e.g., density) less energy will be reflected back to the source in case of a very smooth (in the

scale of the respective wavelength) horizontal seabed surface, e.g., muddy sand, compared to a rough horizontal surface, e.g., gravel (Figure 8c). Due to the different shapes of the objects (e.g., individual pebbles), a number of small facets are available that can face in the direction of the sonar. Thus, a gravelly patch would appear with higher backscatter intensity compared to a muddy patch. However, there is no direct correlation between backscatter intensity and grain size (Goff et al., 2000): For example, if small bedforms, such as ripples, are present, two parts of a seabed with the same composition can appear different in the sonar image, just because on one part no bedforms are present ("smoother", low backscatter intensity) but on the other ("rougher", high backscatter intensity).

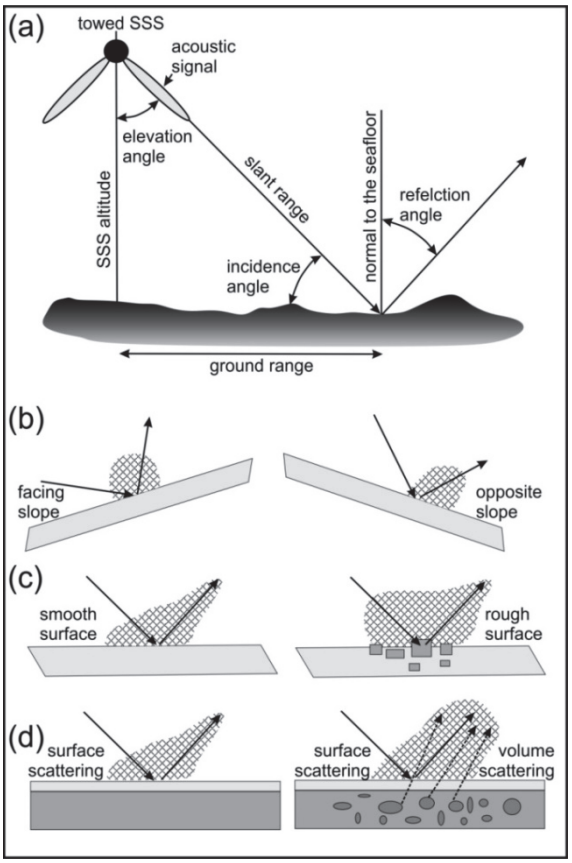

Figure 8: (a): Schematic representation of the acoustic signal path and (b-d): The dependency of the signals path on the seabed geometry and properties (modified after Blondel, 2009).

If an object on the seabed is large enough in terms of wave length, it will prevent parts of the signal from reaching the area behind it and thus also backscattering from these parts of the seabed. The received signal will be low (comparable to the signal received from the water column, i.e., noise) for a duration Δt depending on the height h of the object. The dimension of this "acoustic shadow" can be used to estimate the height of the object as follows:

$$h = \frac{H\Delta t}{t_F}$$ Equation 6

The height of the sonar above the seabed is H and t_F is the time where the "shadow" ends, measured from t = 0, i.e., the first signal received. This is useful for identifying objects on the seafloor such as mines and shipwrecks or to analyze the seafloor relief.

Depending on the seabed properties (e.g., density) and the frequency that is used, some of the energy will also penetrate the surface and be reflected from structures in the subsurface (volume scattering, Figure 8d) or will be attenuated to such an extent that it is lost (Blondel, 2009). In this case, the seabed will appear with low backscatter intensity ("smooth") at one wavelength but with higher backscatter intensity ("rough") at another wavelength, because buried objects or chaotic internal structures within the subsurface are scattering back the signal (Figure 8d).

The recorded backscatter signal is displayed as a function of time in the sonar image: For every ping, the backscattered intensity is plotted in across-track direction, resulting in a line of consecutive pixels in the sonar image. Time t and across-track distance y on the seafloor are not proportional and therefore a geometrical correction must be applied (slant range correction). In case of a plane seabed,

$$y = \sqrt{R^2 - H^2} \qquad \text{Equation 7}$$

can be used, where H is sonar altitude and R is the slant range. If the seabed is not plane, a geometrical correction has to be applied, which requires assumptions about the bathymetry (e.g., inclination of the slope) or additional bathymetry data recorded by a MBES. Moreover, the pixels have to be geographically corrected for the layback, i.e., the distance from the vessels GPS-antenna to the towed sonar. If the sonar is towed, it moves within the water column due to hydro-dynamic forces and turbulences created by currents, waves or the ship movements, which are transferred via the cable to the towed sonar. Various examples of disturbances in SSS backscatter images due to e.g., waves, propeller noise or a stratified water column are depicted in the "Guideline for seafloor mapping in German Marine Waters" (BSH, 2016).

2.1.3 Multibeam echo sounder (MBES)

The MBES is also based on hydro-acoustic theory, as described for the SSS the beam spreading, however, is different: Multiple individual beams create a swath (Figure 9a). The beam spread of each individual beam is usually around 1° to 3° and the total aperture is between 120° and 150° (Lurton, 2002). Typical frequencies a MBES is operated with are roughly between 200-

500 kHz in shallow water (e.g., on the continental shelf) and in deep water around 12-30 kHz (Lurton, 2002).

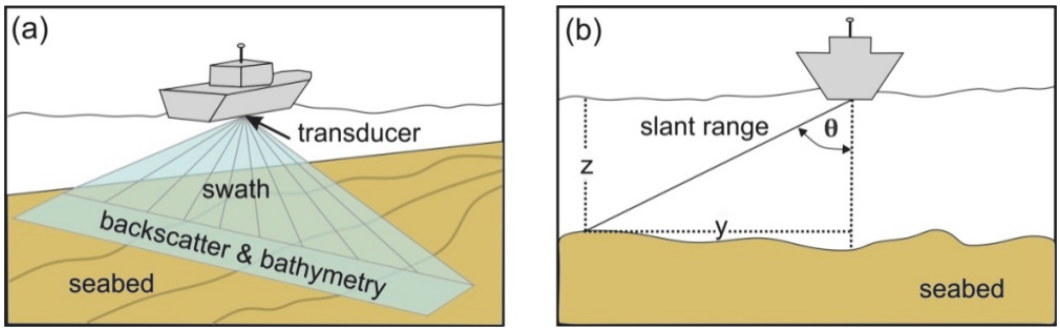

Figure 9: Schematic representation of the multibeam echo sounder (MBES) configuration (modified after Lurton, 2002). (a) The transducer emits multiple individual beams to the seabed, which form the swath. The returned signal contains the backscatter strength and water depth information (bathymetry). (b) The slant range is the oblique distance from the transducer to the seabed. The beam spread (θ) is the deviation of the beam from the vertical. The slant range and θ are needed to calculate the water depth (z) and the position (y) of the respective measurement on the seabed (Equation 8 and 9).

An advantage of the MBES is its ability to provide the backscatter intensity and bathymetric information as well. The array of individual beams allows measuring the backscatter or the water depth at numerous points simultaneously along the swath (across track) and thus, a long strip of consecutive data points is created when the vessel moves forward (along track). The resolution of MBES follows similar principles as SSS: The across track resolution can be described by equation 3 and the along track resolution by equation 4.

The MBES is hull-mounted and therefore the water depth can accurately be determined (Figure 9b), given that the sound velocity in the water column is known (Lurton, 2002): The water depth z is a function of the time (t) that the signal has travelled and can be calculated by Equation 8.

$$z = R\cos\theta = \frac{ct}{2}\cos\theta \qquad \text{Equation 8}$$

Where R is the slant range, θ is the spread of the individual beam and c is the speed of sound in the water column. The position of the depth measurement on the seabed y (Figure 9b) can be calculated as follows:

$$y = R\sin\theta = \frac{ct}{2}\sin\theta \qquad \text{Equation 9}$$

In order to determine the geographical position of an individual depth measurement a (differential) GPS is needed and the position of the antenna in relation to the MBES

transmitter. Equation 8 and equation 9 only apply to a constant speed of sound within the water column (Lurton, 2002). If this is not the case, a sound velocity profile is needed to calculate the acoustic path, using ray-tracing algorithms within the processing software. As described in chapter 2.1.1, the sound velocity and thus the transmission of the acoustic signal depends on the properties of the seawater, which makes it necessary to obtain continuous depth profiles of the sound velocity during the data acquisition with a MBES (Lurton, 2002).

Because the MBES is hull-mounted, it is influenced by the vessels motion (e.g., due to waves), which would lead to a displaced positioning of the beam (Figure 10). In order to correct the data for these kinds of motion, a sensor is needed to record the vessel motion.

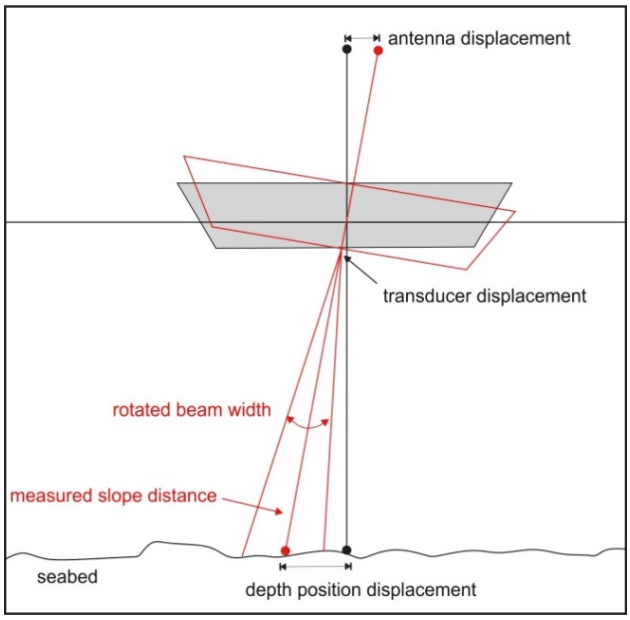

Figure 10: The MBES measurements are influenced by the vessels motion, e.g., due to waves. Thus, the antenna as well as the transducer is displaced from the vertical and the measured slope distance does not correspond to the real position on the seabed.

Another factor that influences MBES data is the tidal gauge. Bathymetric data from the same seabed area would deliver a shallower water depth when recorded during low tide compared to recordings at high tide (Lurton, 2002). Thus, it is necessary to include the gauge in the data correction process, especially in areas with a high tidal range. The area of the seabed that is insonified by the swath, i.e., the footprint, depends on the water depth as the beams spread according to the opening angle α and thus, in low water depths the footprint is smaller compared to high water depths. For example, a total aperture of 150° will result in a swath width that is 7.5 times the water depth (Lurton, 2002).

2.1.4 Artificial intelligence in sea bed mapping

The high resolution of SSS and MBES data (cm range) yields the potential to distinguish different sediment types and therefore habitat types as well as single seabed features, e.g., man-made object such as pipelines, on a fine scale. Since the importance of seabed mapping increased (see chapter 1.2), the amount of mapped seabed increased as well. The use of high resolution systems consequently also increases the amount of data or information on the seabed properties. In order to develop e.g., a habitat map based on these large amounts of data, an investigator has to interpret them. Usually, this very labor intensive and time consuming and the results are always biased by the investigators background. For example, a sedimentologist would have a different focus than an engineering geologist. Even within a discipline the interpretations of the same area of seabed would differ if it they are done by two different persons (Figure 11). They decide individually on e.g., where to place the boundary between fine grained sediment and a coarser grained patch. For one person the boundary is clearly identifiable and the other person is less sure and picks the boundary rather conservative.

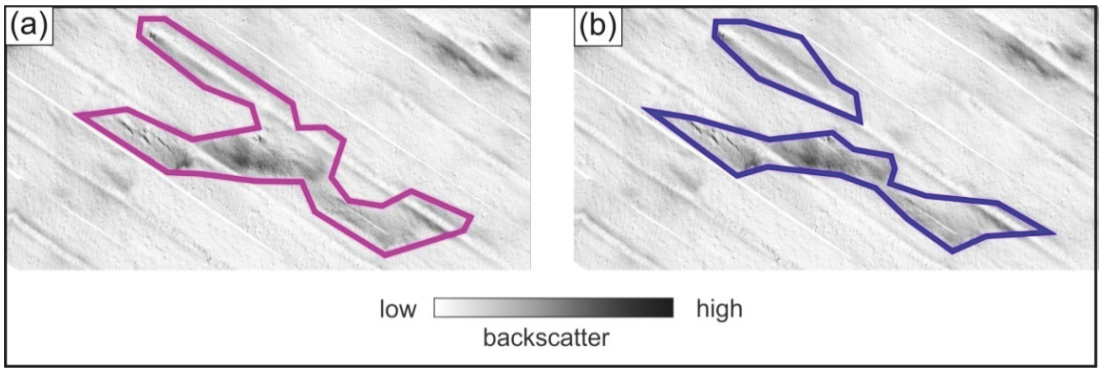

Figure 11: A coarse grained patch (high backscatter) in the same side-scan sonar (SSS) mosaic interpreted differently. Person A interpreted the boundary of the patch spaciously (a) and person B has decided to pick it rather conservative, which resulted in a slightly narrower shape and two patches (b). The SSS mosaic was obtained during survey AL520/2 (Holler et al., 2019b).

In order to minimize the workload and the human bias associated with interpreting large hydro-acoustic data sets, new approaches that involve artificial intelligence (AI) have been developed: Machine learning algorithms for image classification and image processing can be used to automatically classify certain seabed sediment types (e.g., Ierodiaconou et al., 2018) or to identify patchily distributed marine flora (e.g., Bartholomä et al., 2019) as well as single features such as boulders (e.g., Papenmeier, 2018) or trawl marks (Gournia et al., 2019). The application of machine learning algorithms to MBES data is particularly interesting as they

provide information on the bathymetry, which includes additional parameters such as slope, curvature or rugosity, which can be utilized in classification algorithms (Diesing et al., 2016, Schönke et al., 2022). SSS data usually deliver monochrome backscatter values on which statistical image classification algorithms can be applied that are e.g., based on detecting gradients in contrast, homogeneity or variance or a combination of those features, respectively, (Diesing et al., 2016). The automated recognition of elongated features in SSS data of the seabed, such as trawl marks, can for example be approached with edge detecting algorithms (Gonzales, 2004) or using Haar-like features (Gournia et al., 2019).

Within the realm of automated image classification there are two different main approaches: Supervised and un-supervised classification. A supervised classification such as Support Vector Machine (Hasan et al., 2012) is based on training data, which are created by the user and represent samples of all expected classes, e.g., sediment types (Calvert et al., 2014). This presupposes that the user has sufficient knowledge about the area to be classified. These parts of the image(s), which are not marked as training data, are then classified by the algorithm using the information given by the training data set. An un-supervised classification, however, does not involve training data, e.g., k-means clustering (Zhao et al., 2017). In this case, the algorithm identifies and creates the classes based on statistics applied to the spectral and spatial properties of the data.

In supervised and unsupervised image classification, two different classification options are possible: Pixel-based and object-based classification. When the pixel-based option is applied, the spectral properties of the individual pixel determine to which class it is assigned and neighboring pixels are not considered (Hussain et al., 2013). This method is less computationally intensive, but often leads to undesirable effects in the classified image, such as speckling noise (Phiri and Morgenroth, 2017). Object-based classification also considers neighboring pixels and groups them based on their spectral and spatial properties. This step in object-based classification is called image segmentation (Hussain et al., 2013). The segments or objects are then assigned to the corresponding class, which was either defined by the user via the training data-set (supervised) or was computed by the algorithm (un-supervised). The advantage of this method is that the resulting objects are a good approximation of the real-world features in the image and thus, may deliver more accurate results compared to pixel-based approaches (Weih and Riggan, 2010).

In recent years, image classification has gained importance, especially in terms of interpreting remote sensing data, such as satellite images or airborne LiDAR (Light imaging, detection and ranging) data sets (e.g., Yan et al., 2015, Michałowska and Rapiński, 2021) but also in the field

of seabed mapping and hydro-acoustic imaging (e.g., Brown et al., 2011, Burns et al., 2022). In general, each raster data set, which has one band (e.g., SSS backscatter data) or more (e.g., MBES bathymetry data) can be used in image classification. However, depending on the type of data, the method has to be chosen carefully: As SSS backscatter data are monochrome, a statistical method like a grey level co-occurrence matrix (GLCM), e.g., contrast, homogeneity, energy, entropy, correlation (Diesing et al., 2016) or using Haar-like features (Gournia et al., 2019) may be applicable, whereas for multi spectral data (e.g., MBES) a more complex classification method such as ISO clustering would deliver better results (Calvert et al., 2014).

2.2 Sediment sampling

In order to verify and substantiate the results from hydro-acoustics i.e., the sediment-types and their lateral distribution, it is crucial to obtain samples from the surface or sub-surface of the seabed. There are different approaches such as remote sampling with e.g., under-water video (UW-video) recordings and direct sampling in terms of sediment grab samples, box cores or measurements of the in-situ physical sediment properties (e.g., cone penetration testing). Due to the great variety of sediment sampling methods, only these that were used in the scope of this thesis are mentioned in this chapter.

The sediment samples can be analyzed for e.g., grain sizes and other physical properties such as water content, permeability and porosity. The sediment-type derived from SSS backscatter does not necessarily correlate with lateral grain-size distribution but can also be related to micro-topography (Goff et al., 2000, Collier and Brown, 2005). For instance, small ripples (< 10 cm) would increase the SSS backscatter strength but, depending on the used system and its resolution, they would not be resolved as individual features, which would lead to a backscatter signature indicating e.g., medium to coarse sand but in fact the seabed consists of fine sand with ripples. Addressing the problem of connecting hydro-acoustic data with the physical properties of the seabed is still ongoing and some studies presented approaches to correlate grain sizes/sediment-type with MBES data (Runya et al., 2021).

Figure 12: Two different devices to obtain surface sediment samples were used during the field work ofthis thesis. Left panel: The Shipek-grab onboard R/V Alkor. Right panel: The Van Veen grab onboard R/V Senckenberg.

For this thesis, surface sediment samples were obtained with a Shipek- and a Van-Veen-grab (Figure 12) in order to combine the results from the grain size analysis with SSS data and thus, determining the sediment type. Form the surface sediment samples the proportion of biogenic components (e.g., shell fragments) and the grain size distribution was derived. Two methods for grain size analysis were used: Most of the samples from the northern part of the German EEZ were analyzed with a laser particle sizer (LPS) and the rest of the samples were processed using wet sieving (gravel fraction), a settling tube (sand fraction) and a Sedigraph (mud fraction). Details on the methods and on how the samples were treated can be found in the corresponding publications (see chapters 3 and 4).

Moreover, UW-video surveys have become a widely used tool to further investigate the seabed remotely and connect the images with the findings from SSS and/or MBES data. For example, gravelly patches on a sandy seabed can be verified or the occurrence of boulders as well as investigating benthic species colonizing the boulders (e.g., *Alcyonium spec.*) or the seabed (e.g., *Lanice spec.*) is possible with UW-Video recordings (e.g., Buhl-Mortensen and Buhl-Mortensen, 2018, Bartholomä et al., 2019). The examination of man-made seabed features such as trawl marks with UW-Video is described by several authors and can help to determine their spatial distribution and/or their morphological features (e.g., Malik and Mayer, 2007, Mérillet et al., 2018, Buhl-Mortensen and Buhl-Mortensen, 2018).

2.2.1 Principles of dynamic free-fall penetrometers

In the field of marine research, determining the sediment strength by means of different parameters such as bearing capacity is often used in order to examine sediment mobilization, e.g., for the evaluation of slope stability or geotechnical investigations. Obtaining the sediment strength from sediment samples (e.g., grab samples) bear disadvantages as the samples may be disturbed and the in-situ properties are not preserved. Thus, penetrometers were developed in order to sample the sediment strength in-situ. In marine science, penetrometers are in use since the 1970s (Dayal et al., 1973).

Dynamic penetrometers, in contrast to quasi-static penetrometers, are not driven into the sediment by an engine with a constant velocity. Instead, the penetration velocity is dynamic, which means that the instrument impacts the seabed at a certain velocity that is reached through the free fall. During the penetration, it decelerates until the momentum is lost and the devices stops, which is related to tip resistance, side friction at the shaft and the mass of the displaced sediment (Dayal et al., 1973). The rate of change of momentum relies on the penetration depth (Dayal et al., 1973). From this deceleration the sediment strength can be calculated (see chapter 4 for details) using the tip resistance (Terzaghi, 1943, Stoll and Akal, 1999). The sediment strength refers to the maximum load capacity of soil before it experiences failure (Terzaghi, 1943). These principles were further modified and refined (e.g., Meyerhof, 1953, Dayal and Allen, 1975) by also considering penetration rate effects (e.g., Stoll and Akal, 1999, Aubeny and Shi, 2006) and subsequently a variety of instruments were developed covering a wide range of offshore applications such as slope stability assessment or for object burial experiments (Dayal, 1980, Richardson et al., 2001, Kopf et al., 2007). Usually, such instruments are constructed from a cylindrical main body onto which a tip is attached. The main body houses the sensors for measuring different parameters, such as deceleration, tip resistance and tilt. The geometry of the tip influences the measured sediment strength in that as the width of it will increase the sediment strength and the sensitivity of the device (Terzaghi, 1943, Stark, 2010)

The great advantage of a probe-shaped dynamic free-fall penetrometer is that it is cost and time effective as its dimensions are usually rather small compared to conventional CPT-lances (Stoll and Akal, 1999). Thus, it can be handled from a various kinds of vessels and also in rough weather conditions. Dynamic free-fall penetrometers can be used to investigate the in-situ sediment properties of a marine habitat; for example, sub-aquatic dues or tidal channels (Stark, 2010).

From other studies it was known that a dynamic free-fall penetrometer is suitable to detect sediment mobilization (Stark, 2010) and that bottom trawling can mobilize great amounts of sediment (Palanques et al., 2014, Paradis et al., 2021). Thus, the dynamic free-fall penetrometer *Nimrod* (Stark, 2010) was used in the scope of this thesis in order to investigate the in-situ sediment properties of a trawled and un-trawled seabed and its sub-surface (see chapter 4). The instrument (Figure 13) was developed at MARUM – Center for Marine Environmental Sciences, University of Bremen. It bears the advantages that it has small dimensions (mass ca. 16 kg) and is independent from the speed of the winch and motions of the vessel as it would be the case with a conventional CPT-lance (Stark, 2010).

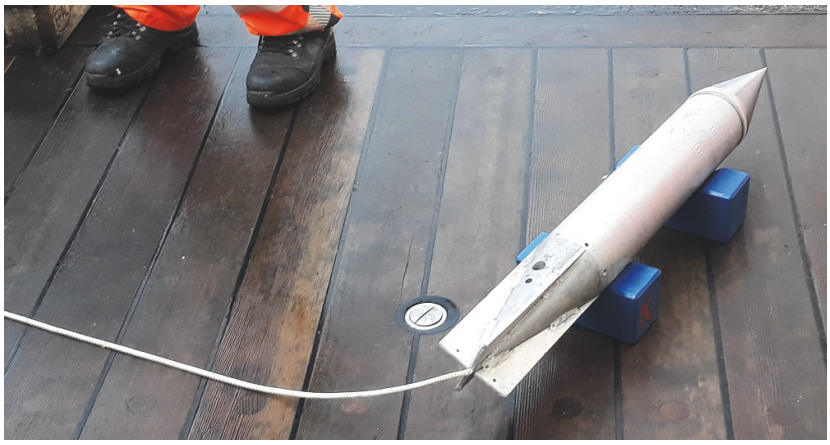

Figure 13: Thy dynamic free-fall penetrometer *Nimrod* (Stark, 2010) onboard R/V Heincke during expedition HE544 (Holler and Bruns, 2020).

3 Identifying trawl marks in North Sea sediments

Ines Bruns[1,2], Peter Holler [1], Ruggero M. Capperucci [1], Svenja Papenmeier [3] and Alexander Bartholomä [1]

[1] Senckenberg am Meer, Department for Marine Research, Südstrand 40, 26382 Wilhelmshaven, Germany

[2] Department of Geosciences, University of Bremen, Klagenfurter Straße 4, 28359 Bremen, Germany

[3] Leibniz Institute for Baltic Sea Research Warnemünde, Seestraße 15, 18119 Rostock, Germany

Published on 25 October 2020, © Geosciences

Please cite this as a journal article and not as a thesis chapter: Bruns, I.; Holler, P.; Capperucci, R.M.; Papenmeier, S.; Bartholomä, A. Identifying Trawl Marks in North Sea Sediments. *Geosciences* 2020, *10*, 422. https://doi.org/10.3390/geosciences10110422

The article was reformatted in order to match the thesis and the references can be found in the overall reference list (chapter 8). The contributor roles are listed as stated in the original article (see 2.7) as well as in greater detail in the section "Thesis outline and author contributions".

3.1 Abstract

The anthropogenic impact in the German Exclusive Economic Zone (EEZ) is high due to the presence of manifold industries (e.g., wind farms, shipping, and fishery). Therefore, it is of great importance to evaluate the different impacts of such industries, in order to enable reasonable and sustainable decisions on environmental issues (e.g., nature conservation). Bottom trawling has a significant impact on benthic habitats worldwide. Fishing gear penetrates the seabed and the resulting furrows temporarily remain in the sediment known as trawl marks (TM), which can be recognized in the acoustic signal of side-scan sonars (SSS) and multibeam echo sounders (MBES). However, extensive mapping and precise descriptions of TM from commercial fisheries at far offshore fishing grounds in the German EEZ are not available. To get an insight into the spatial patterns and characteristics of TM, approximately 4800 km2 of high-resolution (1 m) SSS data from three different study sites in the German EEZ were analyzed for changes in TM density as well as for the geometry of individual TM. TM were manually digitalized and their density per square kilometer was calculated. In general, TM density was highest in August and October. Moreover, different gear types could be identified from investigating individual TM in SSS data. Beam trawl marks were observed to have widths of up to 22 m whereas otter board marks showed widths up to 6 m. The

persistence of TM was estimated to 2–7 days minimum for all three sites based on the SSS data from 2015–2019. A maximum persistence could be defined at one site (Dogger Bank) and it was five months for the investigation period 2016–2017. Besides the main factors driving TM degradation (wave-base impact, sediment-type), different methods for TM detection (SSS, MBES, under-water video) are discussed. The study provides valuable information on the physical impact of bottom trawling on the seabed and can support existing monitoring strategies.

Keywords

seabed sediments; seabed mapping; marine habitat mapping; anthropogenic impact; side-scan sonar; German Bight

3.2 Introduction

The German Exclusive Economic Zone (EEZ) in the North Sea, is extensively used for infrastructure and resource extraction, such as wind farms, offshore cables, pipelines, shipping routes as well as fishery (Stelzenmüller et al., 2015, BSH, 2019). The impact on the seabed due to different kinds of bottom contacting trawling gears has been globally documented by several authors, e.g., Oberle et al. (2016a), Amoroso et al. (2018), and it has multiple effects on the benthic habitats. For instance, the mortality rates of non-target species can increase due to the damage caused by the bypassing trawl gear (Lindeboom and de Groot, 1998, Kaiser and Spencer, 1996) and the flattening of small bedforms can influence juvenile fish as they use them as a shelter (Depestele et al., 2016). The abundance of target species may significantly decrease, which makes the implementation of protected areas necessary, such as the Plaice Box in the southern North Sea (Figure 3.1). Since 1995, large trawlers (>221 kW engine power, >24 m length over all, LOA), which use larger trawl gears and therefore have higher catch rates compared to small trawlers (<221 kW engine power, <24 m LOA), have been banned in order to allow the recovery of the plaice (Pleuronectes platessa) population in that area (Commission of the European Communities, 2005). In addition, sediment re-suspension and removal result in changes in the geochemical properties of the sediment because nutrients or pollutants such as heavy metals are reworked as well (van der Molen et al., 2013, Coughlan et al., 2015) and the vertical sediment distribution is altered due to the (partial) removal of the fine-fraction (Palanques et al., 2014), which may affect benthic species. The impact of bottom trawling on such species also depends on how well they are adapted to regular natural disturbances: The fauna of habitats where sediments are mobile

are less affected than species that inhabit rather stable environments (Kaiser and Spencer, 1996). However, long-living species may be more sensitive to trawling than species with high reproduction rates (Hiddink et al., 2017).

The physical impact of bottom trawling on the seabed can be recognized by furrows (trawl marks, TM), which were created by the trawl gear and temporarily remain in the sediments. They can be observed in hydro-acoustic backscatter data, in some cases over large areas and in high densities, e.g., Depestele et al. (2016), Werner et al. (1990), Friedlander et al. (1999), Smith et al. (2007). Such TM were manually mapped from side-scan sonar (SSS) data by following and counting them in order to determine their density and direction (Friedlander et al., 1999, Smith et al., 2007) or from under-water (UW) videos also to provide an estimation of their abundance (Mérillet et al., 2018). Recently, an approach to automatically detect and quantify TM in SSS data was presented (Gournia et al., 2019). These studies stress that the methods of habitat mapping are applicable to map TM as well as the interest in estimating fishing effort based on TM abundance.

The persistence of TM is of interest when estimating the physical impact of bottom trawling on the seabed and it ranges between a few days in coastal areas (Depestele et al., 2016) and a few years in rather offshore waters (Gilkinson et al., 2015): Gilkinson et al. (2015) examined the effects of experimental clam dredging on the seabed (65–75 m water depth) of the Scotian shelf, Canada. The authors found TM to be still visible in SSS data after three years and up to one year in UW-videos. Furthermore, they could show the degradation of TM and that storm events are the main factor in reworking the sediments and, therefore, in flattening the TM.

Experimental studies conducted in coastal areas of the North Sea revealed that TM were visible in SSS data for up to 52 h (ca. 15 m water depth) (Lindeboom and de Groot, 1998) and observations in bathymetry and backscatter data from a multibeam echo sounder (MBES) could show that the TM were still detectable after four days (15–22 m water depth) and also degraded with time (Depestele et al., 2016). The penetration of the trawling gear into the seabed and the persistence of the TM was shown to be higher in muddy sediments compared to sandy sediments in studies in the Baltic Sea (Krost et al., 1990), Narragansett Bay (New England, USA) (DeAlteris et al., 1999), and in the Mediterranean Sea (Smith et al., 2007) using SSS and UW-video. Different factors like carbonate content and bioturbation play a role in TM persistence, as shown by Mérillet et al. (2018) in the Bay of Biscay. Thus, it can be assumed that a complex relationship between the environmental parameters such as natural disturbances (sediment reworking due to wave impact and tidal currents) and the sediment type is controlling the persistence of TM. Moreover, the used trawling gear is of importance

as the penetration depth depends on the weight of the gear (Eigaard et al., 2016), which also influences the persistence of TM, making the relationship even more complex.

In the German EEZ (North Sea), beam trawls (TBB) and bottom otter trawls (OTB) are common trawling gears for catching demersal fish (Schulze, 2018, Pedersen et al., 2009). The weights of such gears are variable (up to several tons) and usually, the size of the gear is related to the size of the vessel (i.e., engine power) (Eigaard et al., 2016). The penetration depth of the otter doors can be up to 35 cm in muddy sediments (≤ 10 cm in sandy sediments) and beam trawls have a penetration depth of ≤10 cm on both, muddy and sandy sediments (Eigaard et al., 2016). The TM of OTB, observed in SSS data, are described as narrow furrows creating irregular patterns across the seabed (Krost et al., 1990, Sala et al., 2019, Malik and Mayer, 2007). The width of TM induced by TBB is equal to the beam width of the trawl gear and TBB are often towed in pairs, resulting in parallel running TM (Kaiser and Spencer, 1996, Depestele et al., 2016, Sala et al., 2019).

Currently, an extensive mapping and description (geometry, spatial density, persistence) of commercial TM based on SSS data are not available in the German EEZ. The TM stemming from commercial fisheries differ from those examined in the experimental studies, as commercial TM include several trawl gears (differing in type and size) and can reflect fishing behavior (e.g., high density during fishing season).

SSS has been used for seafloor mapping since decades and serves as a tool for investigating the seafloor, as it allows large areas to be mapped with metric to centimetric resolutions, e.g., Lucieer (2008), Blondel (2009), BSH (2016), Holler et al. (2017). In the scope of the German national seabed mapping program "*SedAWZ*" ("Full coverage sediment mapping in the German Exclusive Economic Zone"), commercial TM induced by otter and beam trawls were observed in SSS data and examples were included in the "Guideline for Seafloor Mapping in German Marine Waters" (BSH, 2016). However, detailed descriptions of TM in terms of trawling gears and related TM geometry, density, and spatial pattern were not carried out, as this was not among the aims of the project. An extensive and comprehensive mapping of TM will allow it to document the spatial impact of bottom trawling in the German North Sea. In addition, the collection of time series data can offer new insights into the short- and long-term impact related to fisheries. As information on the persistence of TM strongly differ between a few days and several years, depending on the trawling gear and the specific characteristics of the site (e.g., hydro-dynamics, sediment) (Lindeboom and de Groot, 1998, Depestele et al., 2016, Gilkinson et al., 2015), obtaining more data from further sites would lead to a better understanding of the persistence of TM and therefore trawling impact. This information is

crucial to evaluate to which extend the seabed is influenced by bottom trawling in order to make decisions in marine spatial planning (MSP), e.g., restrictions of fishery in certain areas.

In order to address the impact of bottom trawling on the seabed, three study sites within the North Sea-part of the German EEZ were selected (Figure 3.1) and TM from roughly 4800 km^2 of SSS data were mapped. MBES data were collected along the same lines and used for a morphological description of the TM and for comparing the different acoustic signatures on SSS and MBES data. Time series data were obtained on specific sub-areas (Figure 3.1) in order to examine potential indicators for the degrading of TM and their persistence.

The main objective of the study is to provide a comprehensive mapping of commercial TM in the North Sea-part of the German EEZ in order to:

1. Point out spatial patterns of TM specifically for each study site.
2. Connect those patterns with the fishing behavior (trawling gears, fishing season).
3. Estimate the impact (intensity and persistence) of fishing activities on the sea floor.
4. Investigate the role of specific factors (sediment type, water depth related wave impact) in the generation and degradation of TM.

3.3 Materials and Methods

3.3.1 Study Sites and Physical Settings

The development and the actual sedimentary and morphological characteristics of the German North Sea have been mostly influenced by the late Pleistocene sequence of glacial and interglacial cycles.

During the last glaciation (Weichselian), the glaciers did not reach the area of the modern German Bight but during the Saalian and earlier glacials, moraines and meltwater deposits were formed (Zeiler et al., 2008). After the Last Glacial Maximum (ca. 10,000 y BP), the sea level began to rise and glacial/periglacial deposits were reshaped by waves and currents, which is still ongoing (Schwarzer et al., 2008). In the German Bight, Holocene sediments consist of the reworked glacial/periglacial materials, forming mobile sand layers and lag deposits (Schwarzer and Diesing, 2006). The North Sea is a shelf sea and water depths in the German EEZ are increasing slightly from <10 m near the coast to >50 m in the north-westernmost part. In coastal sectors the hydrodynamics are mainly tide driven, whereas waves play a bigger role in the central part of the North Sea (Aldridge et al., 2015). The distribution of sediments reflects such a hydrodynamic regime (Stanev et al., 2009, Sündermann and Pohlmann, 2011).

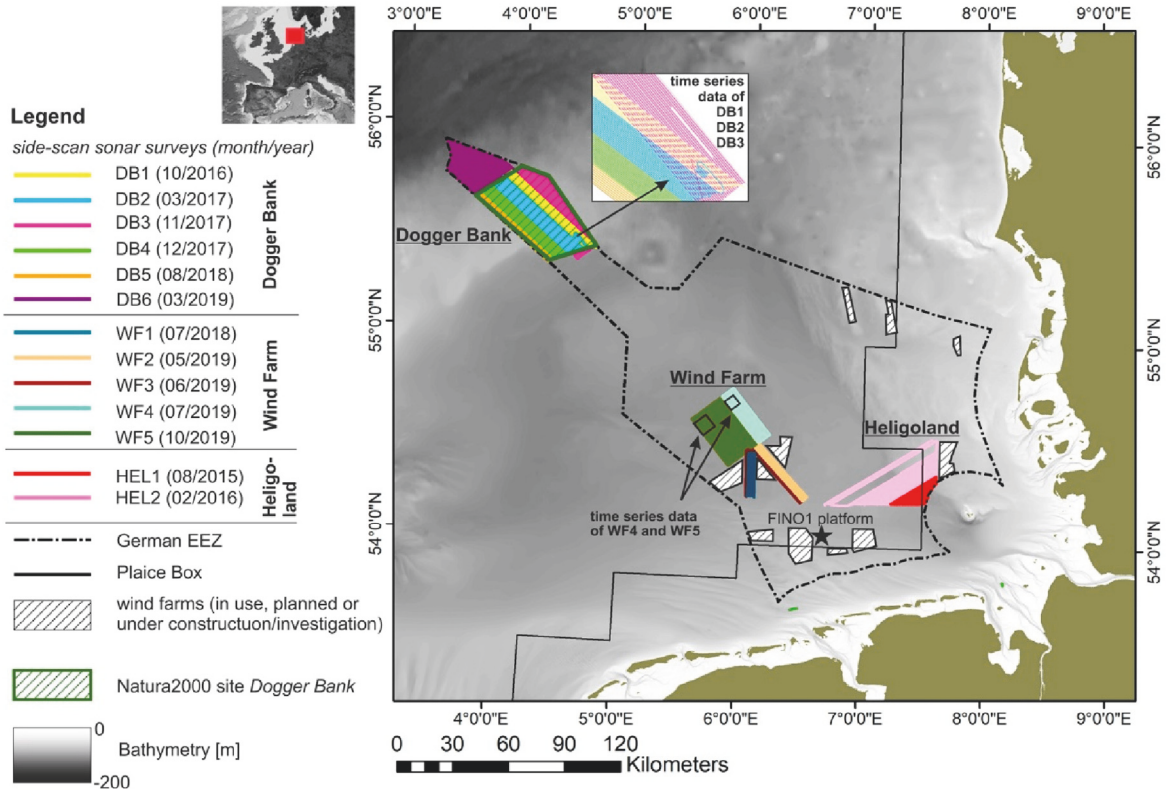

Figure 3.1: Map of the German EEZ (North Sea) with the areas of the different side-scan sonar surveys (Table 3.1) grouped by study sites (Dogger Bank, Wind Farm and Heligoland). Bathymetry is provided by EMODnet-Bathymetry-Consortium (2018), overview of Europe: Imagery reproduced from the GEBCO Grid (GEBCO-Compilation-Group, 2020).

3.3.1.1 Study Site "Dogger Bank" (DB)

The Dogger Bank is a topographic height in the central North Sea where water depths are ranging between 20–40 m. Holocene sediments have thicknesses of 1–5 m, in some parts up to 30–40 m (Fitch et al., 2005). In this study the part of Dogger Bank, which is located in the German EEZ (known as "Tail End", approx. 130 nautical miles north of the mainland) was examined. Here, water depths are between 35–40 m (Figure 3.1). Seabed sediments are mainly fine to medium sand with low mud content (Laurer et al., 2014, Papenmeier et al., 2019, Holler et al., 2019a). In 2004, the German part of the Dogger Bank was integrated into the international Natura2000 network for nature conservation (Figure 3.1). Due to its specific biodiversity, which is related to the high primary production rates, it is particularly worth protecting (Neumann et al., 2017, Bildstein et al., 2017). Hence, multi-lateral discussions on e.g., restricting bottom trawls and implementing enhanced enforcement regulations are ongoing and fishing may be restricted in the future in order to allow benthic species to gain biomass (STECF, 2019). Currently, trawling is allowed within the DB study site and beam trawls (TBB) and otter trawls (OTB) are common (Pedersen et al., 2009). Based on data from the vessel monitoring system (VMS), the fishing effort of was calculated for the German EEZ using the swept area ratio (SAR), which is the area that was touched by the trawl gear during one year normalized over the respective grid cell (0.05°*0.05° in this case) (ICES, 2018c). This means, an area equivalent to the grid cell was trawled during that particular year. For the years 2016 and 2017, the SAR for TBB was between 0.1 and 1.4 and for OTB it was between 0.1 and 0.9 in the area of the DB study site (ICES, 2018c). The fishing effort relies mostly on large trawlers (>221 kW and >24 m LOA) (Schulze, 2018), which are towing gears with varying size. In general, common TBB widths are 5–20 m and OTB can have door spreads of up to >100 m (Eigaard et al., 2016).

3.3.1.2 Study Site "Wind Farm" (WF)

The area is located north of the offshore wind farms ("BARD offshore 1" and "EnWB Hohe See"; approx. 50 nautical miles north of the mainland) in the south-western part of the German EEZ (Figure 3.1). Water depths are 39–42 m and seabed sediments consist of sand to muddy sand (Laurer et al., 2014).

The site directly borders several wind farms (planned and already completed, Figure 3.1). It is assumed that wind farms lead to increased fish abundance as fishing is prohibited and the fish migrate also to adjacent areas, which can increase the fishing effort near such vicinities (Methratta and Dardick, 2019).

At the WF site, the SAR ranged between 0.6–2.5 (TBB) and 0.2–1.8 (OTB) for the years 2016 and 2017 (ICES, 2018c). Here, also mainly large trawlers (>221 kW and >24 m LOA) are operating (Schulze, 2018) with the related gear sizes (TBB: 5–20 m width; OTB door spread: up to >100 m) (Eigaard et al., 2016).

3.3.1.3 Study Site "Heligoland" (HEL)

The third study site is located approx. 13 nautical miles northwest of the island Heligoland (Figure 3.1). The water depth increases from northeast (25 m) to southwest (40 m) of the site. Coarser sediments (sands) are present in the northeastern part, whereas the mud content increases up to >10% in the southwestern part (Laurer et al., 2014, Holler et al., 2019a).

The HEL site includes a small area of the Plaice Box (Figure 3.1), which is closed for large trawlers (>221 kW and >24 m LOA). An increased fishing activity of large trawlers was observed at the borders of the Plaice Box and therefore also within the HEL site (Pedersen et al., 2009). The SAR was up to 2.9 in 2015 (TBB). In 2016 and 2017 it was 0.1–1.3 (TBB) and 0.1–0.4 (OTB) (ICES, 2018c). The small trawlers (<221 kW, <24m LOA), which are allowed to operate within the Plaice Box, are equipped with smaller gears (TBB: 4–8 m width, OTB door spread: several tens of meters) compared to the large trawlers (Eigaard et al., 2016).

3.3.2 Bottom Contacting Trawling in the German EEZ, North Sea

In order to identify the TM, the different construction of the related trawl gears, which are common at the study sites (TBB and OTB), have to be considered.

TBB have a rigid beam to open the net and the mouth width of TBB is therefore constant (Figure 3.2). In order to move over the seafloor, runners (called "shoes") are attached to each side. Ground ropes with additional tickler chains are fixed to the bottom side of the net in order to penetrate the first few centimeters of the substratum and startle demersal fish. In sandy and muddy sediments the penetration depth is <10 cm and TBB are often towed in pairs (Eigaard et al., 2016, Schulze, 2018). Most of the impact of TBB is induced by the ground gear as it affects the seabed surface and the subsurface (Eigaard et al., 2016). In German waters, target fish for TBB are mainly demersal flatfish, like plaice and sole (Pedersen et al., 2009).

In contrast to TBB, the mouth width of OTB is variable. They have “doors” or “otter boards” attached to each side (Figure 3.2), which open the net and, according to the towing speed, control the mouth size (door spread). The doors of OTB are rather narrow compared to TBB and therefore have a greater penetration depth: <10 cm in sandy sediments and up to 35 cm in muddy sediments (Eigaard et al., 2016). The impact of OTB is mainly produced on the surface of the seabed by the otter doors (Eigaard et al., 2016) and the width of an individual OTB mark is related to the door length and the angle of attack (Figure 3.2) (Krost et al., 1990). OTB can be also towed in pairs, being called otter twin trawls (OTT), but this is rather uncommon in the study sites (Schulze, 2018). OTB target also demersal flatfish species as well as gurnard or sand eel (Pedersen et al., 2009).

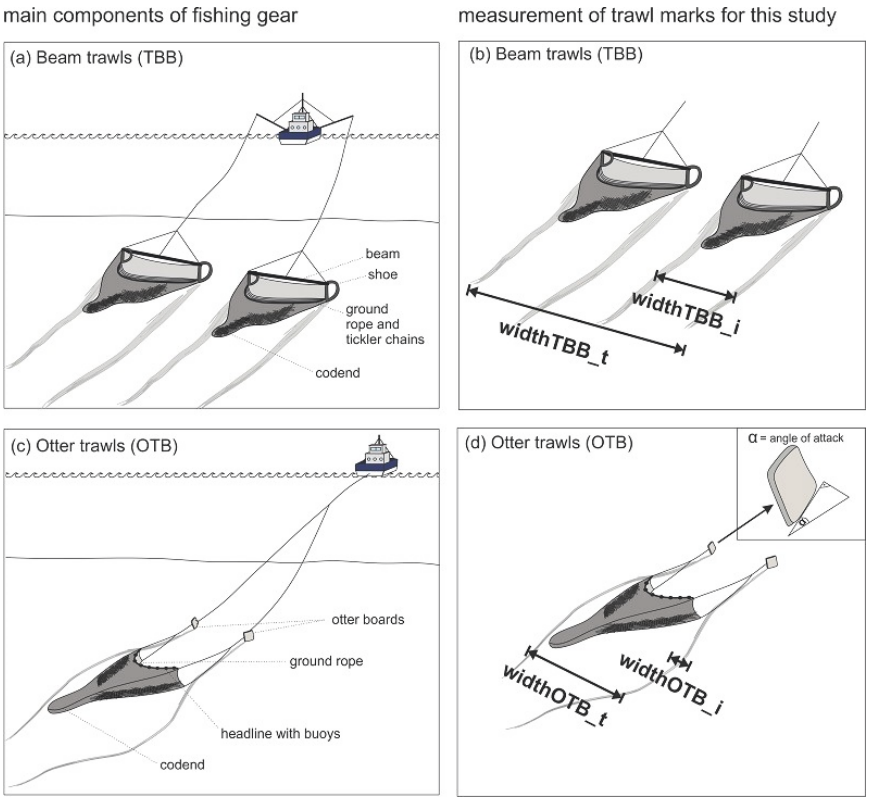

Figure 3.2: Schematic drawings of common bottom contacting trawl gear in the German EEZ (North Sea) and corresponding width measurements. (a) Main components of pair-towed beam trawls (TBB). (b) Measurement of the trawl gear (TBB) width presented in this study: total width = $width_{TBB\_t}$, individual width = $width_{TBB\_i}$. (c) Main components of a bottom otter trawl (OTB). (d) Measurement of the trawl gear (OTB) width presented in this study: total width = $width_{OTB\_t}$, individual width = $width_{OTB\_i}$.

3.3.3 Data Acquisition and Processing

3.3.3.1 General Survey Information

Within the framework of the "*SedAWZ*" project, SSS and ground-truthing data (grab samples and under-water videos) were used to create a sediment distribution map for the German EEZ (BSH, 2016). Multiple surveys were carried out in recent years, which served as a base for the TM mapping and their description in this study. In order to provide a comprehensive mapping of TM, three study sites and a high number of surveys were selected (Figure 3.1), which allows it to point out spatial patterns of TM specific to the respective site. Two sites include time series data to investigate the degrading and the persistence of TM (sites DB and WF, Figure 3.1). Environmental factors (sediment type, water depth and related wave impact, fishing effort) slightly differ between the sites. Therefore, it was possible to examine the role of these factors in TM characteristics (spatial patterns, degrading/persistence) in each site. Further details of the individual surveys per study site are listed in Table 3.1.

Table 3.1: Details of the surveys carried out with RV Heincke (HE), RV Alkor (AL) and RV Senckenberg during 2015–2019. In favor of readability official survey names are abbreviated with a pseudonym. The pseudonyms are used in the text and figures. SSS = side-scan sonar (further specifications can be found in Table 3.2), MBES =multibeam echo sounder, UW= under-water, LPS = Laser Particle Sizer (volume based particle size estimation), SVA = hydraulic grain sizes on the base of settling velocity analysis.

Study Site	Survey Pseudo-nym	Official Survey Name	Date of Survey	Survey Area [km^2]	Water Depth [m]	Device (SSS)/Coverage of Survey Area	Device (MBES)/Coverage of Survey Area	UW-Video Camera	Grain Sizes
Dogger Bank (DB)	DB1	HE474	15–18 October 2016	340	30–40	Edgetech 4200MP/100%	Kongs-berg EM710/40%	Kongsberg Colour Zoom, GoPro Hero4+ black	LPS
	DB2	HE478	09–13 March 2017	425	30–40	Edgetech 4200MP/100%	-	Kongsberg Colour Zoom, GoPro Hero4+ black	LPS
	DB3	HE500	02–09 November 2017	700	30–40	KLEIN4000, Benthos SIS-1624/50%	-	-	-
	DB4	HE502	10–14 December 2017	350	30–40	Edgetech 4200MP/100%	-	-	-
	DB5	Senckenberg 32_2018	22–24 August 2018	230	30–40	KLEIN4000/100%	-	-	SVA
	DB6	AL520_02	20–31 March 2019	640	40–55	KLEIN4000/100%	-	Kongsberg Colour Zoom, GoPro Hero4+ black	SVA
Wind Farm (WF)	WF1	Senckenberg 25_2018	17 July 2018	90	39–41	KLEIN4000/50%	-	-	-
	WF2	Senckenberg 14_2019	20–23 May 2019	133	39–41	KLEIN4000/100%	-	-	-
	WF3	Senckenberg 18_2019	24–26 June 2019	100	39–41	KLEIN4000/100%	-	-	-
	WF4	Senckenberg 21_2019	23–25 July 2019	260	41–42	KLEIN4000/100%	-	-	-
	WF5	HE544	15–29 October 2019	655	41–42	KLEIN4000/100%	-	-	SVA
Heligoland (HEL)	HEL1	Senckenberg 30_2015	03–06 August 2015	144	27–41	Benthos SIS-1624/100%	-	-	SVA
	HEL2	HE456	09–20 February 2016	672	27–41	Edgetech 4200MP/100%	-	-	SVA

3.3.3.2 Grain Size Analysis and Under-Water (UW) Video Recordings

In order to ground-truth the results from SSS data concerning the sediment type, surface sediment samples were obtained by means of Shipek and Van-Veen grabs (Figure 3.3) in the course of the "*SedAWZ*" project. The itemization of the sediment fractions (gravel, sand, mud), which was done for the present study, provides extra information to the prior known sediment distribution. In total, 158 samples (DB1 10 samples, DB2 9 samples, DB5 18 samples, DB6 26 samples, WF5 15 samples, HEL1 36 samples, HEL2 44 samples) were collected based on the real-time SSS data. The sediments were decalcified with acetic acid and organic matter was removed with hydrogen peroxide. For surveys DB1 and DB2, grain sizes were measured with a laser particle sizer (Table 3.1, LPS). The measurements for the rest of the surveys were done as follows: gravel, sand and mud fraction were separated via wet sieving. The grain sizes of the dried sand fraction were calculated from settling velocities by means of a settling tube (Brezina, 1979). For the mud fraction, X-ray transmission time series were measured by using a Micromeritics Sedigraph particle analyzer (Brezina, 1979, Stein, 1985, Cramp et al., 1997). The mode (most abundant grain size in a sample) was averaged over the samples within each sampling site.

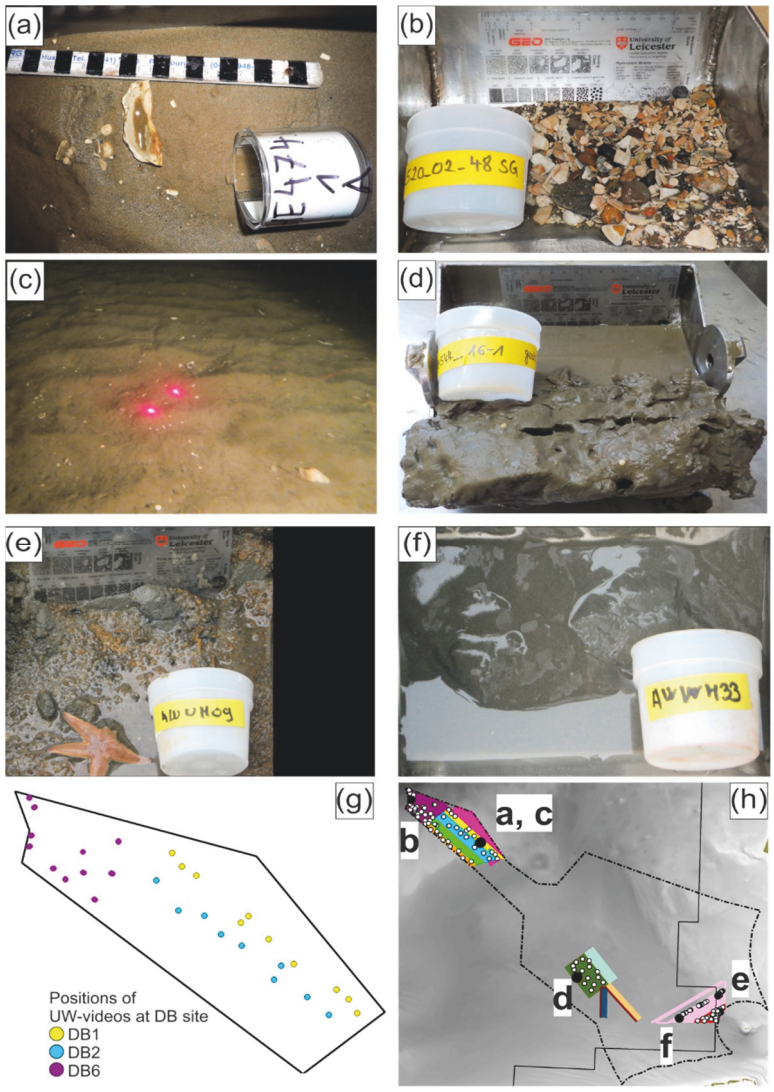

Figure 3.3: Exemplary pictures of grab samples and UW-video. (a) Fine sand with occasional shell debris at the Dogger Bank site. (b) In the northernmost part of the Dogger Bank site patches occur, where the gravel content increases up to 75%. (c) Still image of a UW-video transect showing ripples with wave lengths of 10–20 cm, which are indicating active sediment transport (likely wave driven) at the Dogger Bank site. Distance of the laser points is 10 cm. (d) Muddy sand to fine sand is the main sediment-type at the Wind Farm site. (e) Gravelly sand with occasional benthos at the northern part of the Heligoland site. (f) In the southern part of the Heligoland site, the seabed sediments consist of muddy sand. (g) Positions of the UW-video stations at DB site. (h) Positions of the sediment samples (white circles); the locations of the examples that are shown in (a–f) are highlighted (black circles).

The UW-cameras (Table 3.1) were attached to a sledge operated in drift mode, without an active steering. The individual hauls (30 stations, Figure 3.3) were conducted for 5–10 min with a speed of ≤1 knot (ca. 0.5 m/s). Videos provide 48 frames per second (FPS) with 1920 × 1440 pixels (GoPro) and 30 FPS with 640 × 480 pixels (Kongsberg). The UW-videos were obtained in order to ground-truth the sediment type within the "*SedAWZ*" project and for the present

study, they were examined regarding the detection of TM. The videos were not manipulated (e.g., with a video editing program) in order to enhance the image quality.

3.3.3.3 Side-Scan Sonar (SSS) Data Acquisition and Processing

The hydro-acoustic surveys were originally designed for seabed sediment mapping within the *SedAWZ* project, following the recommendations for an optimal combination among resolution, spatial coverage and time (BSH, 2016). Hence, they were not specifically designed for investigating TM. The SSS was towed with approx. 5 knots (ca. 2.5 m/s) and the swath (300–400 m) and line spacing (300–400 m) were planned in order to cover at least 100% of the seafloor. Only for surveys DB3 and WF1 the coverage was of ca. 50%, due to limitations in survey time. Three SSS systems were used during the surveys (Benthos, Edgetech, and KLEIN, Tables 3.1 and 3.2). Despite the slightly different technical characteristics, the systems are able to deliver comparable datasets. A minimum resolution (across and along track) of 1 m was achieved for all the surveys and datasets.

The quality of SSS data varies across the different surveys due to a combination of several factors. Environmental variables such as weather and sea condition, turbidity of the water, etc., change during the same survey and among the surveys, which influence the quality of the data (signal/noise ratio, backscatter absorption, presence of artifacts). The TM signature and its detection on SSS data are therefore affected by those factors. This is especially important for assessing the persistence and degradation of the TM. However, rough sea conditions were avoided during the surveys and SSS records were corrected in order to obtain reliable and comparable datasets. The software SonarWiz6.05/SonarWiz7 (Benthos and Edgetech SSS systems) and SonarPro14 (KLEIN system) were used for acquisition. Automatic gain control (AGC) was turned off and time varying gain (TVG) was active. Post-processing was performed with SonarWiz7.01 applying the following steps:

1. slant-range correction
2. empirical gain normalization (in order to correct over- and under-amplified areas)
3. de-stripe filter (in order to remove artifacts due to tow-fish movements)
4. layback correction (in order to ensure precise positioning within the mosaic)

The resulting mosaics were exported at 1 m (=1 pixel) resolution. Changes of TM with time in terms of changing backscatter values were examined by calculating histograms (grey-level distribution of the pixels across the area) and corresponding statistics of six mosaics. The histograms were computed from the whole mosaics (see Section 3.4.5). For each pixel of the

respective mosaic (raster data), a point feature was rendered with ArcGIS, containing geographic information and the backscatter value (0–255) of each pixel (=point). In this way, it was possible to use the histogram function of the Geostatistical Analyst provided by ArcGIS, which allows to display the graph as well as to derive lower- (mode, standard deviation) and higher-order statistics (skewness and kurtosis).

Table 3.2: Further specifications of the SSS systems, which were deployed during the surveys (Table 3.1). The frequencies were operated parallel.

SSS system	Frequency	Horizontal Beam Width	Across-Track Resolution
KLEIN4000	100 kHz/400 kHz	1 ° /0.3 °	9.6 cm/2.4 cm
Benthos SIS 1624	100 kHz/400 kHz	0.5 ° /0.5 °	5 cm/5 cm
Edgetech 4200 MP [1]	300 kHz/600 kHz	0.5 ° /0.26 °	3 cm/1.5 cm

[1] Recording only with 300 kHz (surveys DB1, DB2, HEL2).

3.3.3.4 Multibeam Echo Sounder (MBES) Data Acquisition and Processing

In order to describe the morphology of the TM, high resolution bathymetric data were collected simultaneously with the SSS records by means of a Kongsberg EM710 MBES. The system is permanently mounted aboard the RV Heincke and coupled with a PHINS (Photonic Inertial Navigation System) motion sensor for pitch, roll, heave, and yaw real-time compensation. SVPs were used for sound velocity calibration, and positioning was achieved by means of a DGPS system. The MBES operates at frequencies of 70 to 100 kHz and with an opening angle of 65°. A swath width of approx. 120 m (ca. 4× water depth) was achieved. For the present study, a subset of the data was further processed using the Multibeam Imagery tool from SonarWiz7.01. The resulting grid has a lateral resolution of 0.75 m. A non-optimal correction of the vessel motion is likely responsible for the artifacts in the external parts of the swath and for the general bathymetric “noise”, which affected the final outcomes. However, the general aspect and the morphometry of the TM could be detected.

3.3.3.5 Trawl Mark Mapping

For each study site the TM were manually mapped (i.e., digitized) from the 1 m resolution SSS mosaics and stored as ESRI-shapefile (polyline). TM were classified according to the trawling gear type, based on their different patterns in the SSS mosaics: TBB marks show a constant width all along the course of the track, due to the fixed mouth size; in addition, they are towed in pairs (Figure 3.2a). On the contrary OTB marks are rather narrow and present irregular patterns as the door spread differs in width (Figure 3.2c). For each gear type a shapefile was

created for the respective survey. The number of mapped trawl marks is influenced by the SSS data quality. As stated earlier, the SSS data quality changes across the surveys and TM might be not detected due to artifacts caused by e.g., turbulences in the water column. Therefore, the mapped TM represent a minimum number (and density).

Files were merged for each study site and the azimuth (trawling direction) of the TM was calculated, in order to point out potential preferred trawl routes. Hereafter, the direction is given in a bidirectional manner (e.g., NW-SE, implying both directions are possible) because the heading of the vessel cannot be derived from TM. The azimuth calculation was done by means of the ArcGIS field calculator and the results are displayed as rose diagrams (Figure 3.4).

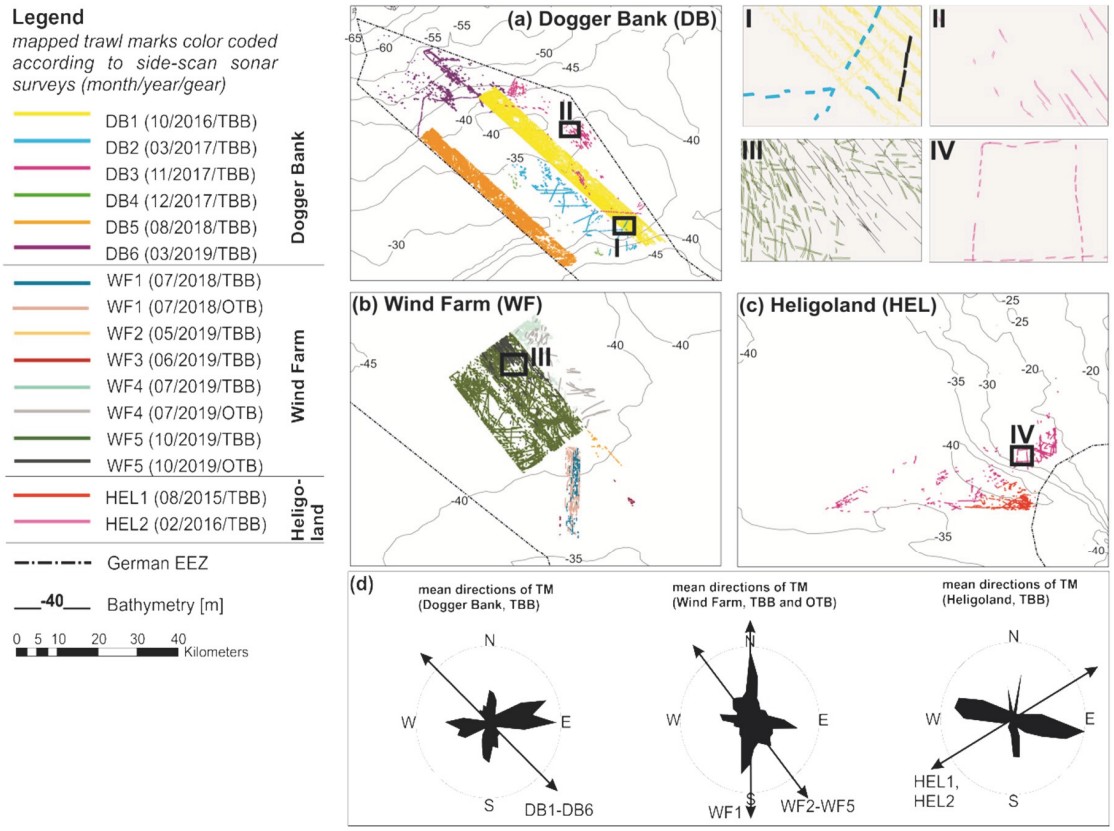

Figure 3.4: Overview of manually mapped TM in the three research areas (a) Dogger Bank, (b) Wind Farm (c) Heligoland. Zoom-ins (I–IV) show different kinds of spatial pattern of TM. I: High spatial density of clustered TBB marks in October 2016 (DB1, yellow) and consecutive TBB marks from March 2017 (DB2, blue). Black lines indicating TBB marks from the fishing vessel, which was observed during survey DB1. Five months later, this TBB marks could not be identified anymore in the SSS data of survey DB2. II: Low spatial density of clustered TBB marks in November 2017 (DB3). III: High spatial density of clustered and consecutive TBB marks (WF5, dark green) as well as low spatial density OTB marks (WF5, dark grey). IV: consecutive TBB marks (HEL2). (d) Rose diagrams display the mean direction of TM for each

survey area (gears combined) as well as the direction of the SSS-survey (arrows). Bathymetry contours are provided by EMODnet-Bathymetry-Consortium (2018).

In addition, TM files were merged according to gear type (=neglecting the survey information and study site) showing the overall density for both TBB and OTB. With the help of the "line density" ArcGIS function a TM density distribution was rendered, with a grid resolution of 1 × 1 km. Such function counts the occurrence of lines within a given radius (1 km in this study), regardless to the length of the individual TM. This means that a grid cell can show low TM density although the area touched by the trawl gear is high due to few but long-distance TM. By comparing the line density values of the surveys, the relative changes in the fishing intensity can be resolved.

In order to further determine the geometry (i.e., metrics) of TM from the corresponding gear type, 100 TM were randomly picked from the SSS data of each study site and specific metrics were determined (Figure 3.2):

- width of individual TBB mark was measured ($width_{TBB\_i}$)
- total distance from starboard to portside TBB ($width_{TBB\_t}$)
- distance between the otter boards (door spread, $width_{OTB\_t}$)
- width of the marks created by the otter doors ($width_{OTB\_i}$)

3.3.3.6 Observation of Fishing Vessels

In the course of surveys DB1, WF4, and WF5 operating fishing vessels were observed, which allowed to immediately record new TM and thus determine their date of origin. An estimation of the persistence and an investigation of potential signs of degradation of TM at the study sites DB and WF was possible by performing re-surveys:

- DB1: observation of a single vessel, re-survey after five months (DB2)
- WF4: observation of a single vessel starting a new haul, re-survey after 36 hWF5: observation of multiple vessels, re-survey after six days including three days of rough sea conditions (significant wave height approx. 4 m)

3.4 Results

3.4.1 Sediment Types—Grain size and UW-Video Analysis

The DB site is dominated by sandy sediments (mode = 177 µm) with a mud content of ≤5% and ≤1% of gravel (Figure 3.3a,c and Figure 3.5a). Only in the northernmost part, gravelly patches are occurring and the gravel content increases up to 75% (Figures 3.3b and 3.5a).

Similarly, the WF site is dominated by sandy sediments (mode = 149 µm) and the proportion of mud is slightly lower in the northwestern part (5–10%) than in the rest of the area (mud content up to 23%, Figures 3.3d and 3.5b). Gravel is absent in all samples.

The HEL study site shows slightly coarser sand than at the other sites: mode = 210 µm with <5% mud and without gravel in the northeastern part (Figure 3.5c). In the central part, there are patches with high gravel content (20–40%, Figures 3.3e and 3.5c), and the southwest is characterized by an increase in mud content (10–20%, Figures 3.3f and 3.5c).

UW- video analysis from DB site confirmed the findings from the backscatter data (in terms of sediment-type) and grain size data. The picture shows sand with occasional shell deposits and ripples with approx. 10 cm wavelength (Figure 3.3c). For the other sites, no UW-video is available (Table 3.1).

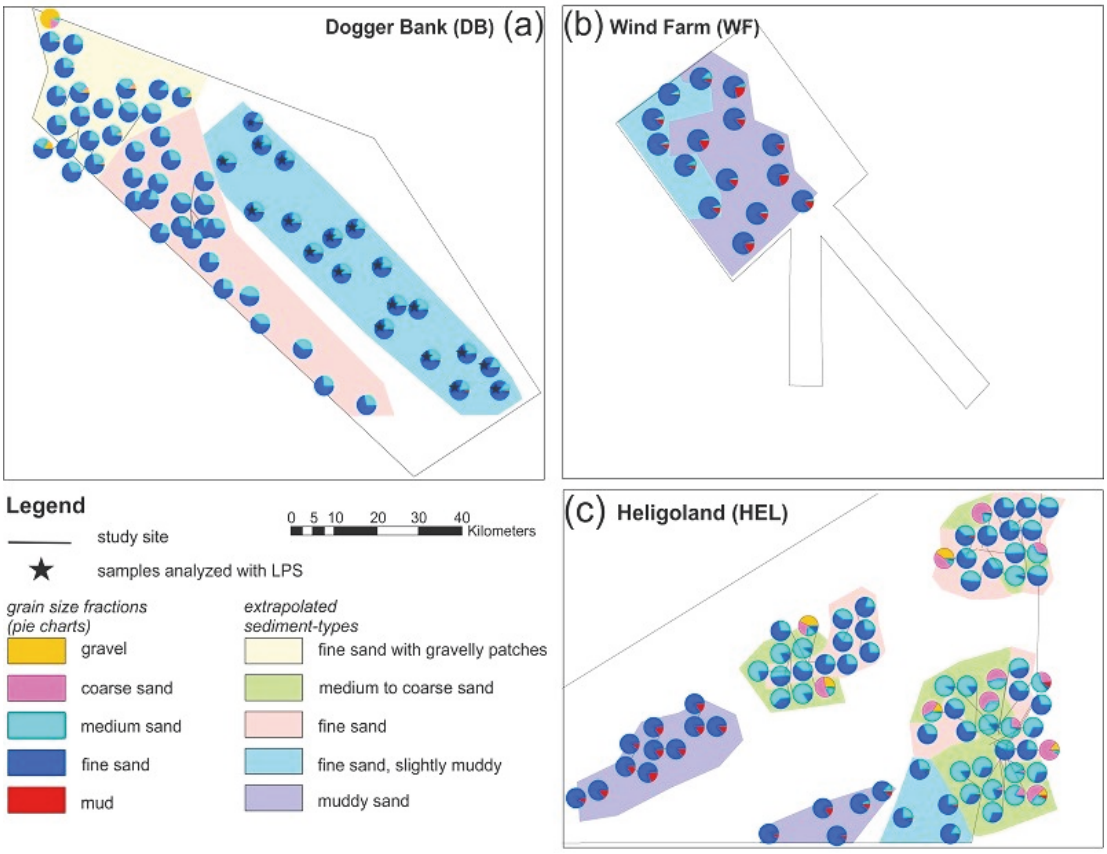

Figure 3.5**:** Sediment composition in the three study sites: (a) Dogger Bank: Mainly fine sand with mud (mode = 177 µm) and gravel content <10%, except for occasional patches where gravel content is >60% (northernmost part). (b) Wind Farm: Fine sand to muddy sand (mode = 149 µm) with an average mud content of 12% and without any gravel. (c) Heligoland: Fine sand to muddy sand (mode = 210 µm, 10–20% mud) with occasional gravelly sand (20–40% gravel) in the central and northernmost part. Samples marked with a star: Grain sizes measured with laser particle sizer (LPS, see Table 3.1).

3.4.2 Acoustic Signature of Trawl Marks

The mapping revealed that TM have different levels of visibility in backscatter data. In some cases, they are not clearly distinguishable from the background (Figure 3.6a), and in some cases they appear rather distinct (Figure 3.6b, TBB mark of the observed vessel, DB1). Moreover, TM appear with different backscatter values depending on the study site: At the DB site, TBB marks, compared to the surrounding sediments, show higher backscatter values in their center, which is bordered by slightly lower backscatter (Figures 3.6b and 3.7b). This detailed backscatter signature is not always present. TM can appear with higher backscatter (compared to the surrounding) over their whole width (Figure 3.6b) as well, which is most commonly observed in clustered TM.

TBB marks within the WF site mostly show the detailed backscatter signature but the lower backscatter parts are more pronounced compared to TM at the DB site (Figure 3.8).

OTB marks could be identified in SSS data only at the WF study site. They show lower backscatter in the center and higher backscatter at the outer, signal facing edge (Figure 3.9).

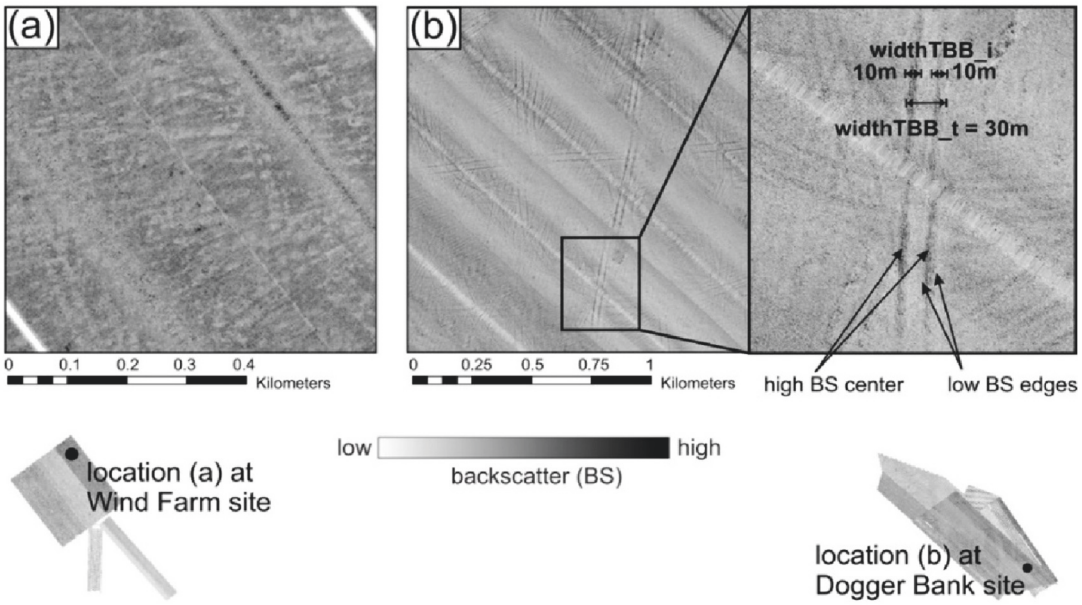

Figure 3.6: (a) SSS-mosaics showing examples of high spatial density clustered TBB marks without details and a rather blurry appearance, which are therefore difficult to be distinguished from the background and hardly traceable (Wind Farm site, July 2019). (b) TBB mark (roughly N-S oriented) from the observed fishing vessel during survey DB1 (October 2016). The newly made TM is better visible also in the far range of the SSS swath than its neighbors, which appear rather faint and mainly in the central two thirds of the SSS-swath.

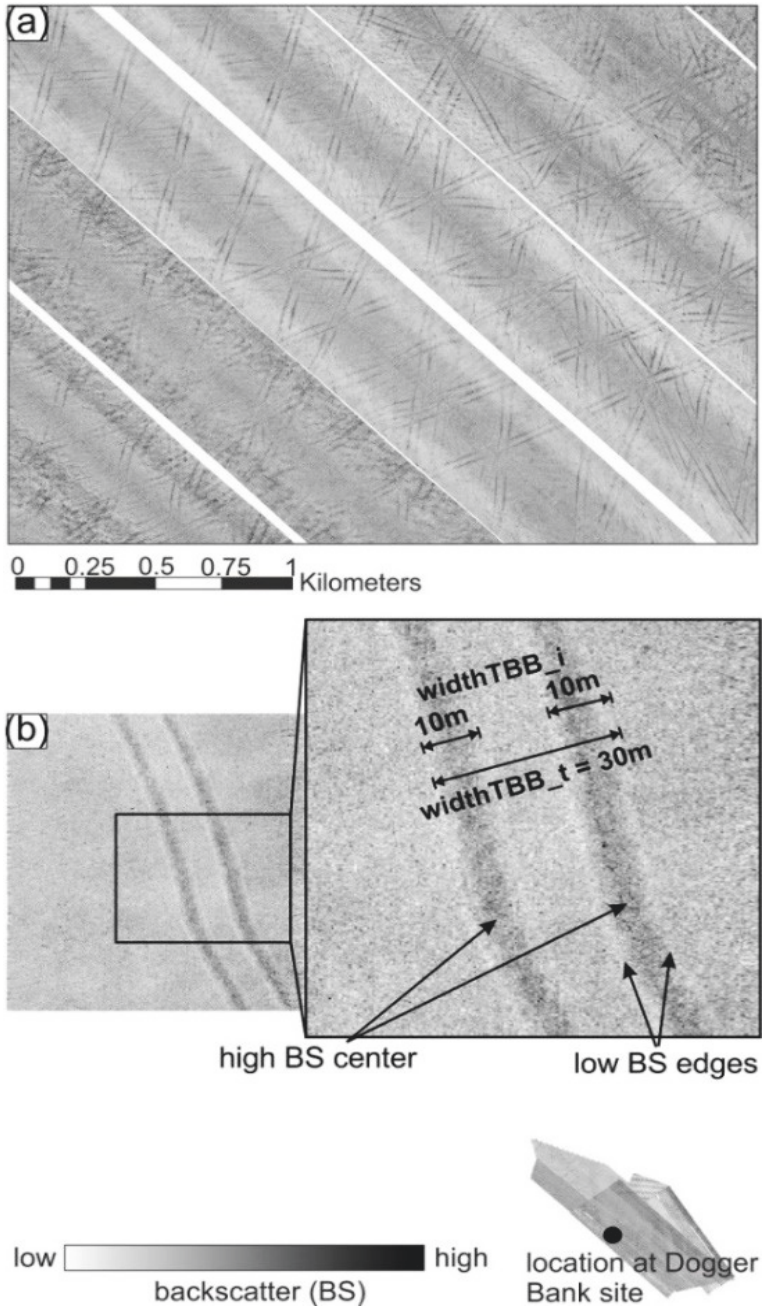

Figure 3.7: (a) Example of high spatial density consecutive TBB marks in the SSS-mosaic of Dogger Bank site (DB5, August 2018). (b) Detailed picture of such TBB marks. They show higher backscatter compared to the surrounding sediment, boarders by slightly lower backscatter. The whole width ($width_{TBB\_t}$) is roughly 30 m whereas individual beam trawls have widths of ca. 10 m ($width_{TBB\_i}$).

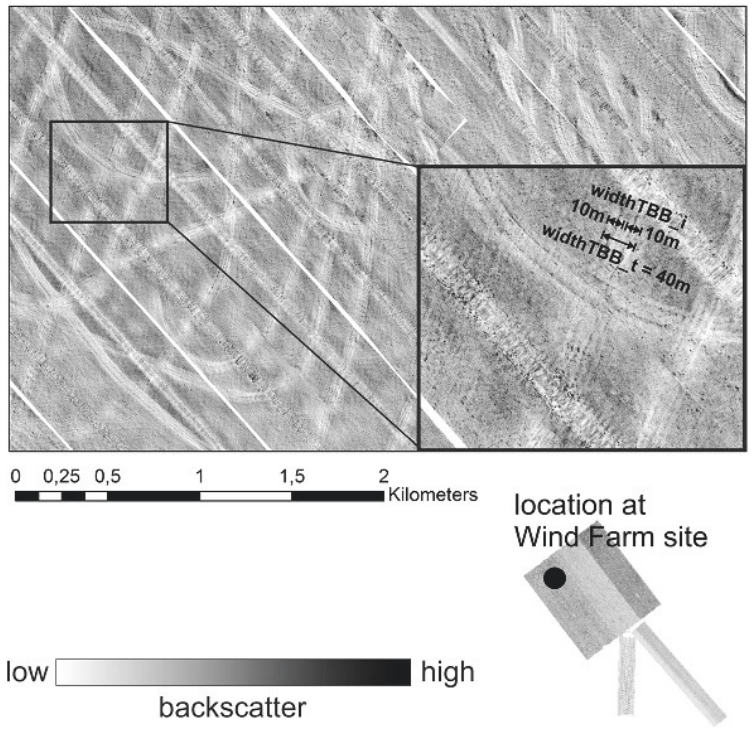

Figure 3.8: SSS-mosaic depicting examples of high spatial density consecutive TBB marks at Wind Farm site (October 2019). Compared to the Dogger Bank site, new TBB marks at the Wind Farm area appear with larger areas of low backscatter around the high backscatter center. Total width ($width_{TBB\_t}$) of TBB marks is roughly 40 m and the individual width ($width_{TBB\_i}$) is 10 m.

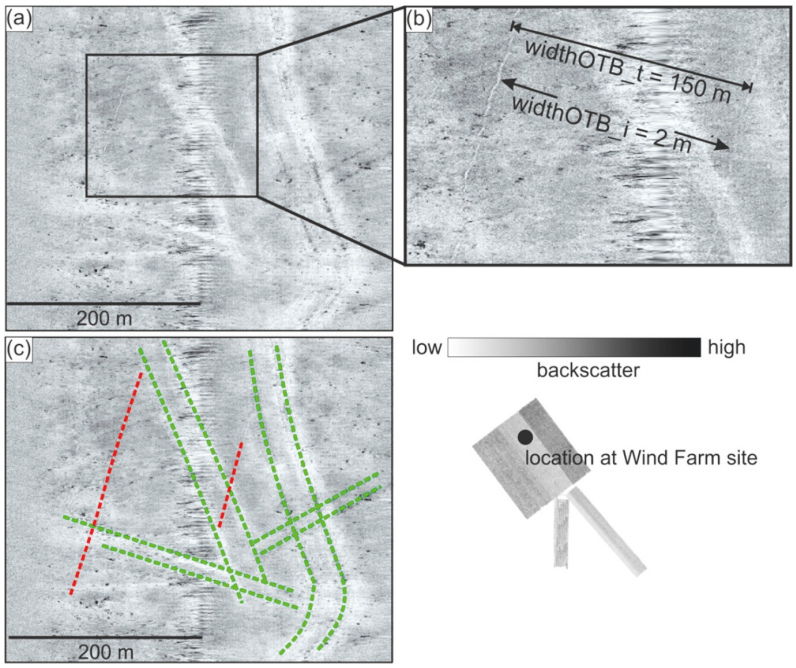

Figure 3.9: (a) Examples of TBB marks and OTB marks in the SSS data in waterfall mode at the Wind Farm site (swath = 400 m). TBB marks and OTB marks are intersecting each other and OTB marks are less striking than TBB marks. (b): Zoom-in and width measurements of the OTB mark. Total width of

the OTB mark ($width_{OTB\_t}$) is 150 m and the width of the individual marks caused by the otter boards ($width_{OTB\_i}$) is 2 m. (c): Enhanced TM from panel (a); TBB (green) and OTB (red).

Regarding the backscatter signatures of TBB marks at the HEL site, they are characterized by higher backscatter in the northeastern part of the site and with lower backscatter compared to the surrounding in the southwest (Figure 3.10). The former also show a detailed signature, similar to TBB marks at DB site.

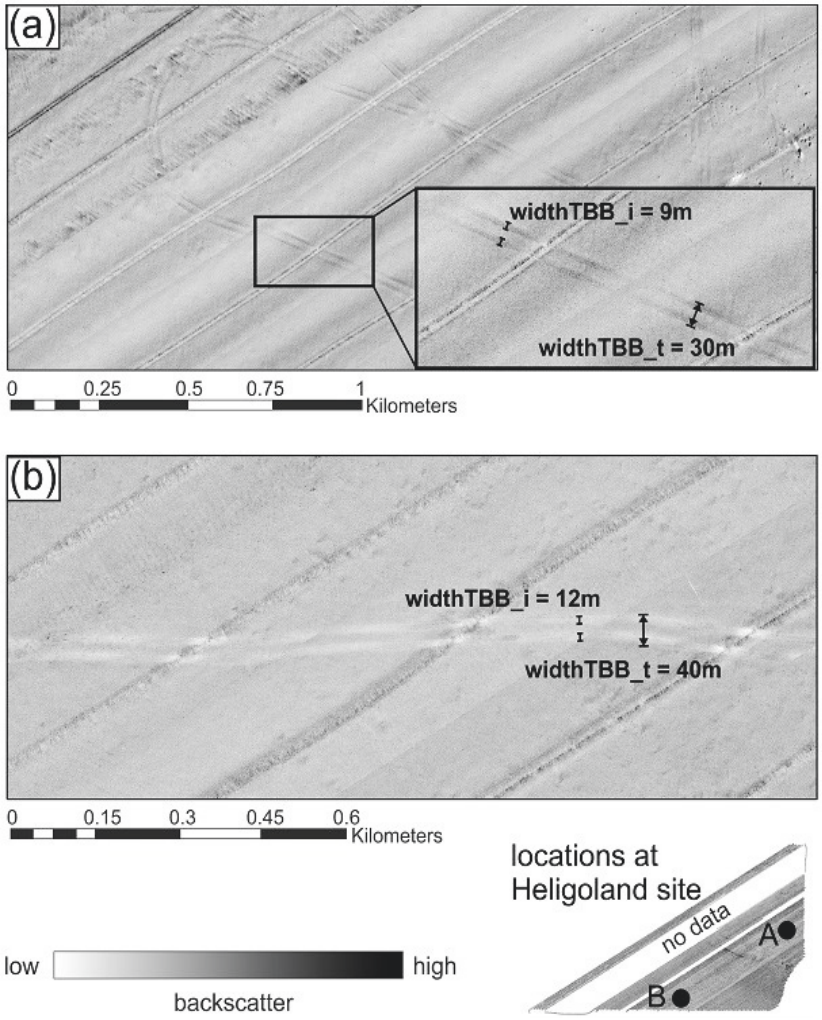

Figure 3.10: Examples of TBB marks from the Heligoland site. (a) In the Northeastern part they appear with higher backscatter values compared to the surrounding and (b) with lower backscatter values compared to the background in the southwestern part of the site.

3.4.3 Trawl Mark Geometry and Morphology

Based on the specific pattern shown in the backscatter data, it was possible to differentiate between TBB and OTB marks: two parallel marks with 10–12 m width ($width_{TBB\_i}$) and an average distance of ca. 40 m ($width_{TBB\_t}$, Table 3.3, Figure 3.7) were classified as pair-towed TBB

marks. Slightly smaller TBB marks (9.5 m on average) were found at the HEL site (Table 2.3). At the WF study site, highest widths of TBB marks could be measured (mean ca. 11 m, Table 3.3).

Table 3.3: Trawl mark geometry (=widths [m]) and corresponding statistics of TM according to Figure 3.2 measured in the three research sites. Otter trawl (OTB) marks could only be identified in SSS-data of the WF study site. Mean = arithmetic mean, SD = standard deviation.

	Dogger Bank (DB)		**Wind Farm (WF)**				**Heligoland (HEL)**	
	width TBB_t	width TBB_i	width TBB_t	width TBB_i	width OTB_t	width OTB_i	width TBB_t	width TBB_i
Min	34.20	5.20	19.20	5.60	30.20	1.60	24.60	4.00
Max	52.40	14.80	51.60	22.00	281.60	5.90	54.40	13.80
Mean	40.20	10.17	40.80	11.39	126.22	3.06	33.03	9.50
Median	39.95	10.00	42.00	11.40	127.80	3.05	31.10	9.45
SD	3.39	1.71	6.79	2.52	53.60	0.88	6.55	1.90

Similar could be observed on the bathymetric data: TBB marks appear as parallel tracks and show a distance of 30–40 m and an individual width of 8–12 m. Figure 3.11 shows an example of such marks with both straight and curved forms. The TBB marks are slightly depressed (5–10 cm) with respect to the surrounding areas.

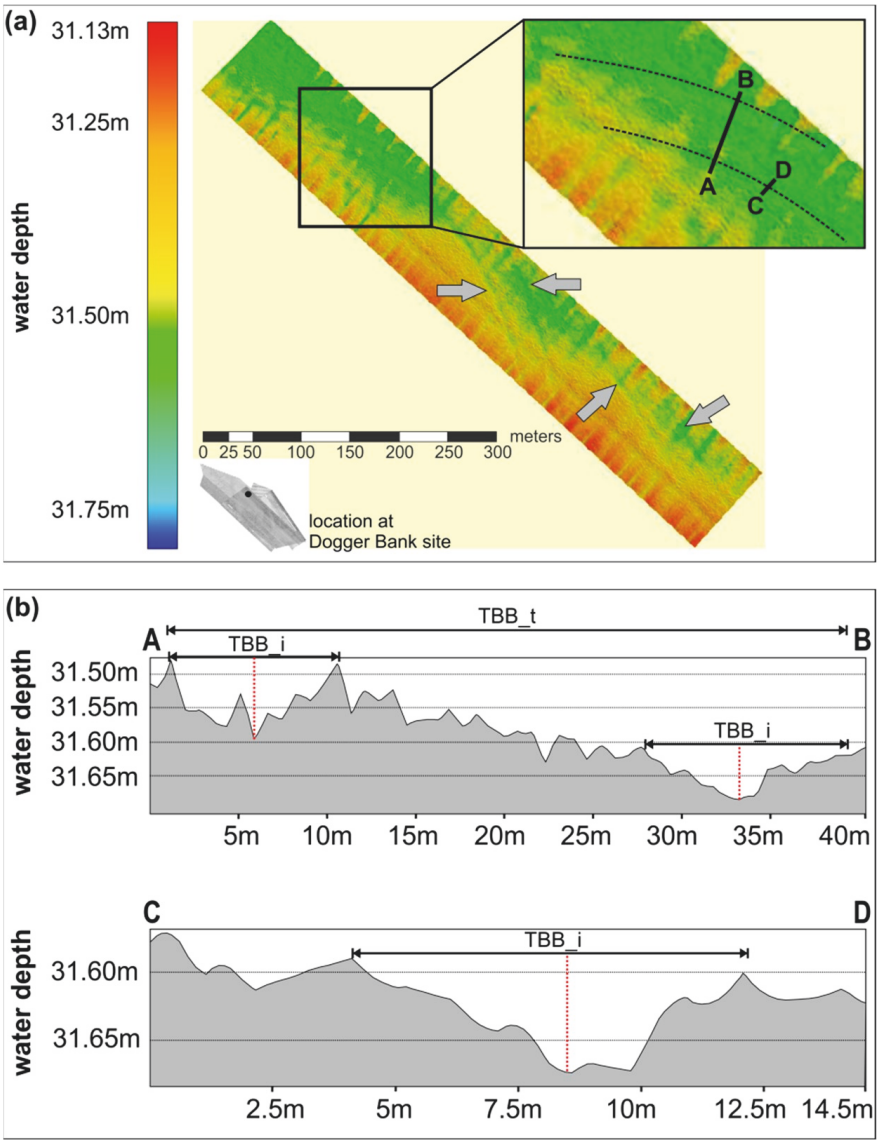

Figure 3.11: (a) Exemplary multibeam echo sounder (MBES) data showing TBB marks (grey arrows, black dashed line) at DB site. (b) Cross-section A-B depicts the morphology of TM from a pair towed TBB with an individual gear widths ($width_{TBB\_i}$) of approx. 10 m each and a total width ($width_{TBB\_t}$) of ca. 33 m. The same mark appears slightly narrower in cross-section C-D ($width_{TBB\_i}$ approx. 8 m). The change of morphology (red dashed line) due to the impact of the TBB is <10 cm in both cases. However, the metrics are difficult to determine due to the insufficient quality of the MBES-data (see discussion). Please note the different scales in A–B and C–D.

OTB have a variable door spread and therefore produce rather irregular patterns compared to TBB tracks: In this study, OTB marks could only be recognized at the WF study site and semi-parallel marks have distances (i.e., door spreads, $width_{OTB\_t}$) up to 281 m (126 m on average) and the individual marks created by the otter boards are ca. 3 m wide ($width_{OTB\_i}$, Table 3.3, Figure 3.9).

3.4.4 General Trawl Mark Mapping

As the bathymetry is quite gentle in all three study sites (Figure 3.4), a significant relation between water depth and TM density could not be found. The main orientation of the TM is NW-SE and N-S (Figure 3.4). TM could not be observed in UW-video recordings, although TM density was very high, e.g., during survey DB1 (October 2016, Figure 3.4, Figure 3.12).

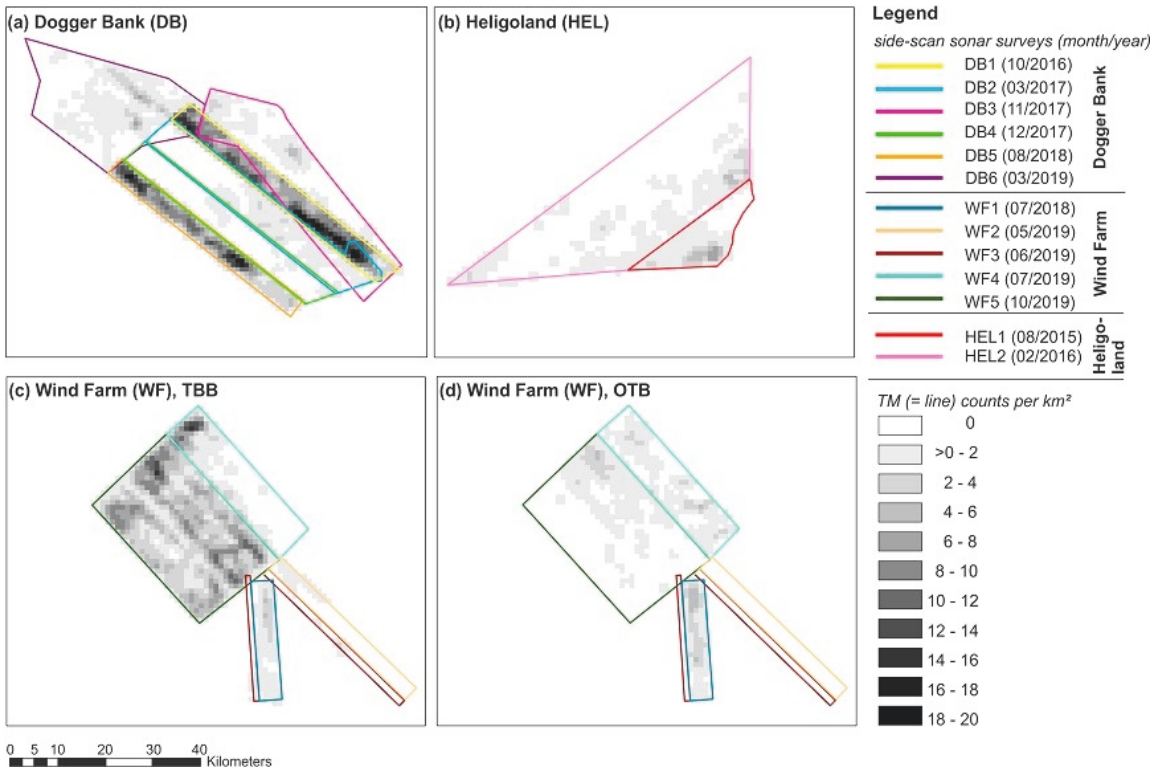

Figure 3.12: The maps show TM (= line) counts per km² for each study site. (a) At the DB site, TM density is up to 20 counts per km². (b) The HEL site shows a TM density of ≤ 6 counts per km². (c) TBB mark density at the WF site is higher (up to 20 counts per km²) than (d) OTB mark density (<5 counts per km²). OTB marks could be identified only in the WF site.

In the DB2 dataset a TBB track was mapped in the E-W direction for roughly 10 km, crossing the entire SSS mosaic (Figure 3.4, DB1). Similar to the DB2 survey, several consecutive TBB tracks of approx. 12 km length were observed across the whole SSS mosaic collected during the DB3 survey.

Mapping also revealed that TM can occur as consecutive tracks or clustered (Figure 3.4), which is however difficult to differentiate at locations were TM density is high and individual TM are strongly overlapping, or when TM are poorly preserved.

The spatial density ("line density") of TM changes between the different surveys (i.e., months) as it can be seen at DB site: the highest density of TM could be observed in surveys DB1 and

DB5 (October 2016 and August 2018, up to 20 counts per km², Figure 3.12), the least in DB3 (December 2017, 2–4 counts per km², Figure 3.12). Within the WF study site, TM density is highest in July 2019 (WF4) and survey WF5 from October 2019 (up to 20 counts per km², Figure 3.12). In contrast to the other study sites, OTB marks were recognized at the WF site, but with lower density (max. 5 counts per km², Figure 3.12) compared to TBB marks. The HEL study site shows highest densities in August 2015 (HEL1, up to six counts per km²), whereas counts were ≤4 per km² in February 2016 (HEL2, Figure 3.12). OTB marks are absent here as well.

3.4.5 Trawl Mark Preservation and Potential Signs of Degradation

SurveysDB1, DB2 and DB3 overlap in the southern part of the DB study site (Figure 3.1). The resulting time-series data collection took place after five (DB2) and 13 (DB3) months (Table 3.1) from the first dataset. None of the previously mapped TM was still visible in the later SSS datasets.

The TBB marks in Figure 3.13a could be dated to the period of the 22–24 October 2019; fishery was active at the same time as the SSS survey. SSS data of the re-survey show a decreased visibility of the TM: the “new” marks were clearly to follow and showed details, whereas “old” TM can be identified but appear rather pale and blurry (Figure 3.13b). The histogram of the mosaic with the “old” TM (Figure 3.13b) shows a higher standard deviation (σ = 19.27) than the mosaic with “new” TM (σ = 14.06, Figure 3.13a). The skewness was calculated to be −0.91 for the initial mosaic and −1.23 for the second. The mode of the grey values of the “new” state mosaic is 172 and the mode of the “old” state mosaic it is 177. The kurtosis did not change between the two mosaics (leptokurtic distribution, 7.13).

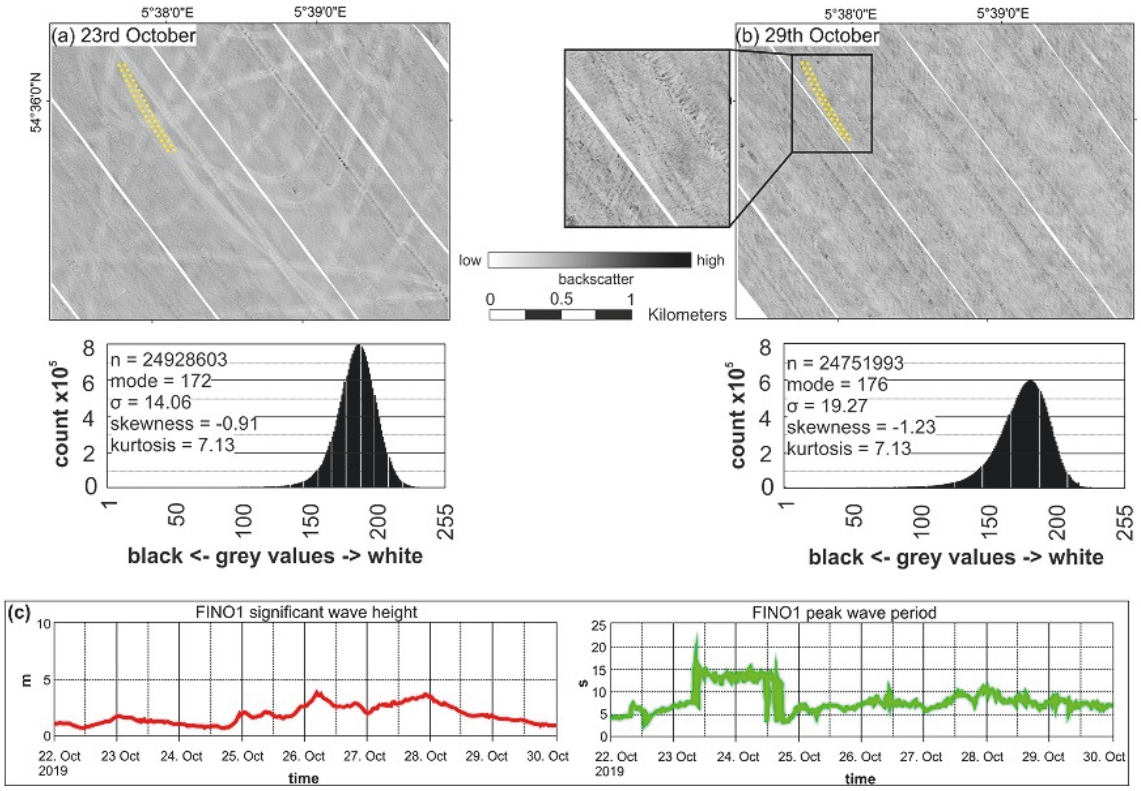

Figure 3.13: (a) TBB marks at the Wind Farm site (WF5) created on 22nd and 23rd October, which were recorded on 23rd October (WF5). (b) The re-surveyed area from 29th October after six days in total including three days of rougher sea conditions. TBB marks were rather difficult to identify. (c) During the storm, significant weave heights were approx. 4 m (FINO1 data, BSH (2020), red graph) and peak wave period was around 5–10 s (FINO1 data, BSH (2020), green graph). Position of FINO1 platform can be found in Figure 3.1.

On the SSS-record in Figure 3.14, a V-shaped pattern of TM is visible, which was classified as OTB mark. High backscatter values and corresponding acoustic shadow clearly define these TM regarding the background. When the TM were surveyed again, the transition to the surrounding sediments was rather gradual: The TM showed lower backscatter compared to the surrounding and the high backscatter parts were absent. The corresponding backscatter histograms reveal a shift of the standard deviation (σ) from higher to lower values for both SSS frequencies (Figure 3.14). The skewness is clearly negative (−1.39 and −1.06) in the mosaics of the first survey and changes to values near zero for the mosaics from the second survey (−0.31 and −0.15). The distribution is leptokurtic and shows higher values (7.5 and 9.04) for the initial mosaic and decreases to 4.02 and 4.23 in the second. The noise caused by the propeller and wake of the fishing vessel (Figure 3.14a,c) is also absent in the second survey (Figure 3.14b,d).

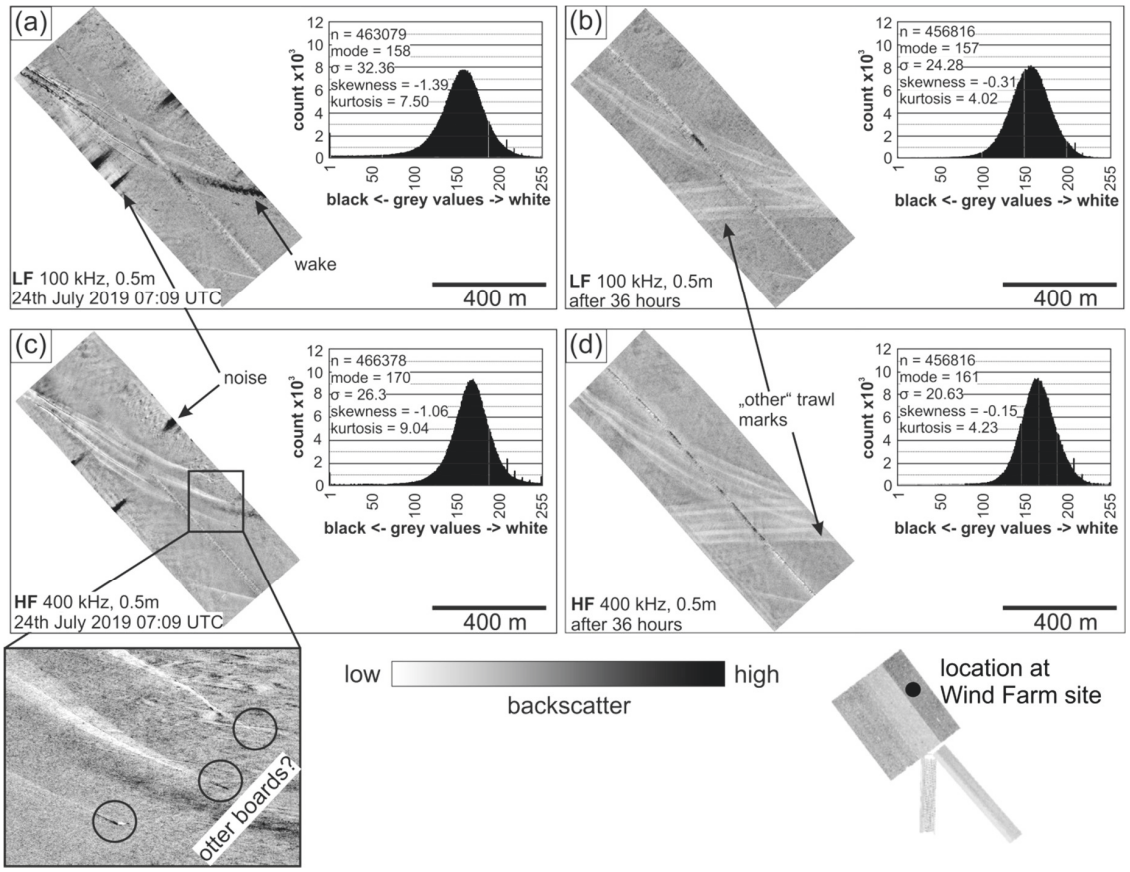

Figure 3.14: TM from an observed vessel that started trawling while crossing the profile track of RV Senckenberg at the Wind Farm site (WF4). Panel (a) displays the 100 kHz record and (b) the 400 kHz record. The wake and noise were less pronounced in the high frequency. It can be seen that the mark widens from NW to SE according to the trawlers travel direction, which indicates the proceeding divergence of the gear due to increasing towing speed. The three objects (circles, zoom-in of panel (c) are probably otter boards, why the fishing gear is assumed to be an OTT). Panel (b,d) show the same mark 36 h after the first recording. The transition to the surrounding sediments is now rather gradual. Moreover, "other" TM were created in the meantime.

3.5 Discussion

This study revealed differences in TM density among the individual surveys. The highest spatial density of TM was found in the surveys of the summer months (August and October). Fishing activity depends on the abundance of target fish as well as weather conditions. Kaiser et al. (1996) also found the highest density of trawling activity in early summer to summer due to the opening fishing season in the Irish Sea. In the German EEZ, the largest catches of plaice and sole (targeted by TBB and OTB) are mostly observed within the 3rd and 4th quarter of the year (Schulze, 2018). Storms are most common in the winter and therefore these months are expected to show the least amount of TM. For instance, storm "Herwart" (Haesler and Lefebvre,

2017) affected German waters with significant wave heights (Hs) up to 8 m and wave periods (T) between 10 s and 15 s at the end of October 2017 (BSH, 2020). It is suggested that the wave-base reworks the seabed during winter storms and the TM are flattened faster compared to summer, which could explain the relatively low density of TM detected in November and December at the DB site. The effective wave-base reaches about twice as deep during stormy weather than under normal weather conditions, even during a mild storm (Hs = 2.4 m, T = 6 s) (Son et al., 2012, Flemming, 2005). Gilkinson et al. (2015) found that winter storms (for Hs > 6 m at 67 m water depth on the Scotian Shelf) are the main reason for sediment reworking, causing degradation of TM.

In this study, TM were hardly to distinguish from the background in some cases (Figure 3.6a). The limited traceability produces an error in overall TM density, which is hardly to quantify as trawling is not equally distributed but can overlap (Rijnsdorp et al., 1998, Gerritsen et al., 2013). Hence, the density measure (line density), which is presented in this study cannot be understood as an absolute measure of trawling intensity and, moreover, it reflects a minimum density as stated earlier (see Section 3.3.3). TM are often not visible in the far range of the SSS swath, which is most prominent at DB site (Figure 3.6b). It is estimated that, on average, one third of a TM is not visible due to this problem. This, however, does not contribute to an error in TM spatial density, because the length of TM is neglected in the calculation.

The main orientation of the TM in the study sites is WSW-ENE (DB site), N-S (WF site), and WNW-ESE (HEL site, Figure 3.4). Malik and Mayer (2007) as well as Smith et al. (2007) describe that trawling is often conducted parallel to isobaths, which generates a bathymetry-related orientation of the TM. In our study, the bathymetry is rather gentle (Figure 3.4) and the orientation of the TM is therefore independent from the water depth. In the study sites, wind and waves are mainly westerly oriented (NW, SW, Sündermann and Pohlmann, 2011) and tides northerly (Sündermann and Pohlmann, 2011), which could explain the preferred bearings of the fishing vessels.

At sites DB and HEL, TM are oriented approx. W-E and are rather perpendicular to the acoustic data collection grid (Figure 3.4). In SSS data, elongated features such as cables and pipelines are more likely to be detected if orientated along tracks (Klaucke, 2018). The survey direction plays therefore no significant role in the detection of TM in these areas. However, at WF site TM have mainly N-S orientation, which is parallel or sub-parallel to the survey direction (Figure 3.4). OTB marks that are only found at the WF site could be more sensitive to directionality of the SSS-signal because they are rather narrow. This would result in missed OTB marks perpendicular to the survey direction, affecting the measure of density in Figure 3.12 and

making the comparability of TM spatial density between the sites difficult. Enhancing acoustic shadows and increasing across-track resolution by towing the SSS nearer to the seafloor and/or narrowing the swath could, moreover, have improved data quality and therefore TM detection.

TM could not be detected in UW videos, despite the high spatial density of TM in some of the surveys (e.g., DB1, Figure 3.4, Figure 3.12). Malik and Mayer (2007) reported similar results for the Gulf of Maine (<100 m water depth), due to the limitations in the camera steering options and in the positioning (mismatch between the TM detected in the acoustic data and the camera positioning). The camera system used in this study captures only a section of the seafloor (ca. 1 m^2), likely too small in comparison with the TBB mark widths (>5 m). Moreover, a steering option would probably increase the chance to catch TBB on UW footage. In addition, the ripples in the DB study site indicate sediment movement due to currents and waves and their size is similar to the penetration depth for TBB in sandy sediment (≤10 cm, Eigaard et al. (2016) and Figure 3.11), which further complicates TBB mark identification.

In contrast, Mérillet et al. (2018) observed TM on UW-videos (sledge-mounted camera, no active steering). However, they examined OTB marks in rather muddy sediments (sand, muddy sand, and mud), which were <0.5 m wide (furrows created by otter boards). This could have influenced the visibility of TM in UW-video footage as narrower OTB marks could be resolved more easily by a camera section of 1 m^2. Smith et al. (2007) detected TM in UW-video footage on muddy but not on sandy seabed (visible in SSS-data in both sediment-types). Gilkinson et al. (2015) described that TM created by a hydraulic dredge (uses cutting blades and water injections instead of tickler chains) are detectable in UW-videos of sands (primarily medium grained) in 65–75 m water depth but after one year they were not detectible in UW-video material anymore while they were still visible in SSS data up to three years. This supports the assumption that the gear penetration at the DB site is too low or the TM are too old (i.e., flattened) to have the furrows detected with UW-video.

3.5.1 Acoustic Signature of Trawl Marks

TBB marks show higher backscatter values in their center and lower backscatter values at their edges, compared to the surrounding sediments (Figure 3.15). In the WF site, the low backscatter area is more pronounced (Figure 3.15) and in some parts of the HEL site, high backscatter in the center of TM is completely missing (Figure 3.15). That can be explained with the reworking of the sediments due to the trawling gear: fine grained, silty material gets re-suspended during trawling and settles in the furrow and the adjacent areas, which was also described by Gilkinson et al. (2015). This would result in lower backscatter (smoother surface)

compared to the surrounding sediment. Depending on the local hydrodynamics, bottom currents can instead transport the material away and settle it down elsewhere, which was described by Palanques et al. (2001) and Mengual et al. (2016). As a result, they observed a coarsening of the sediments along the trawled tracks, due to the removal of the fine-grained fraction (silt to clay). Where the seabed consists of coarser sediments, like at the DB site and in the NE part of the HEL site, (with >90% of sand, Figure 3.5) such a fine sediment removal is less pronounced, as the mud fraction is nearly missing. In these areas, the increase of the backscatter values in the center of the TM is therefore due to the mechanical interaction of the trawling gears with the seafloor. Feldens et al. (2018) could show that lower frequencies (200 kHz in this case) are able to increase the detection of specific seafloor features (e.g., when they appear rather subtle), which can be assigned to different contributions of volume and surface scatter, and texture to the backscatter signal. Similarly, it was observed that TBB marks in survey DB5 were more evident in the 100 kHz than in the 400 kHz SSS frequency records. This should be examined further.

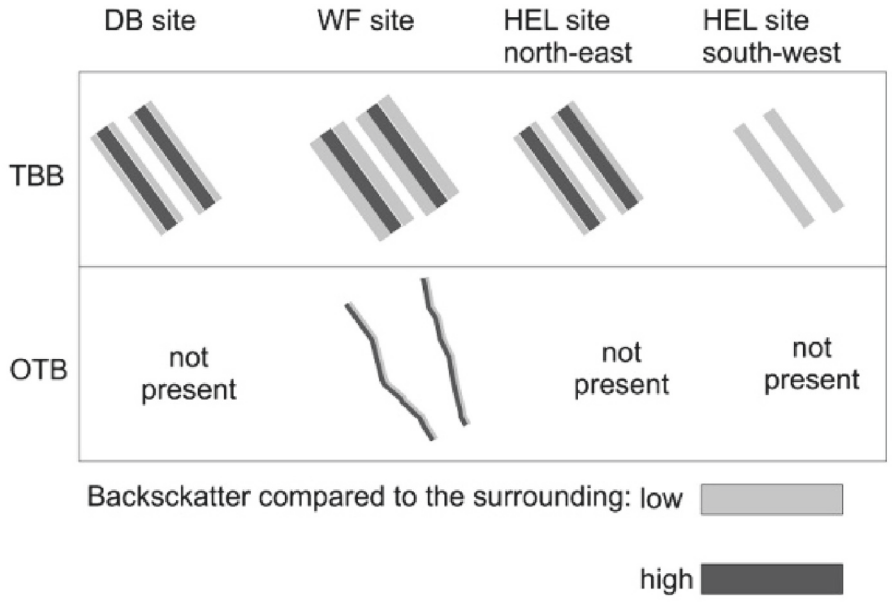

Figure 3.15: Schematic sketch of the backscatter signatures of TM (TBB and OTB) in the different sites. The corresponding SSS mosaics can be found in Figures 3.6-3.10 and 3.14.

3.5.2 Trawl Mark Geometry and Morphology

Different trawl gears could be assigned to the TM in the SSS backscatter showing significantly different patterns and metrics. TBB marks appear in rather regular and parallel-like patterns compared to OTB marks, as already described by Eigaard et al. (2016). The beam widths ($width_{TBB\_i}$) range between 4 m and 22 m in our study sites (Table 3.3), which corresponds to

fishing vessel engine power of 200–900 kW for TBB trawler targeting demersal fish (Eigaard et al., 2016). Large beam trawlers (>221 kW) are active in all three study sites, whereas small beam trawlers (<221 kW) are operating mainly within the 12-nautical-mile-zone and, less frequently, also NW off Heligoland within the EEZ (Schulze, 2018). Therefore, TBB marks at sites DB and WF were likely made by large beam trawlers catching demersal fish. According to their size, TBB marks at the HEL site were probably created by a mix of large and small beam trawlers.

In regard to the otter trawlers fishing in the North Sea area, a door spread of approx. 50–300 m occur corresponding to vessels of 10–40 m LOA (Eigaard et al., 2016). A maximum door spread ($width_{OTB\_t}$) of 281 m and a mean door spread of 126 m (Table 3.3) were measured at the WF site. Such wide door spreads occur in fleets targeting demersal fish and mixed bentho-pelagic species, while smaller door spreads are usually used for catching crustaceans, sprat or sand eel (Eigaard et al., 2016). Individual OTB marks in this study present widths ($width_{OTB\_i}$) ranging from >1 m to 6 m with an average of approx. 3 m (Table 3.3). Lucchetti and Sala (2012) noticed widths of 30–40 cm in the Mediterranean Sea. Krost et al. (1990) described OTB marks with widths of <1–2 m in the Baltic Sea and related them otter door lengths of approx. 2 m, considering the angle of attack (ca. 30°). Lucchetti and Sala (2012) mentioned a door spread of <50 m and Krost et al. (1990) related the observed OTB marks to small fishing vessels, which probably use smaller gears. It is likely that higher door spreads in the present study are caused by larger nets and otter doors than in the other studies, which could explain the discrepancy in widths of the door marks. Sala et al. (2019) found maximum door spreads of 292 m (mean 90 m) in a vessel and gear metrics database of the Mediterranean Sea. Otter board lengths were approx. 3 m (mean 1.9 m), which would result in a furrow of 3.5–4 m width, assuming an angle of attack (Figure 3.2) of 30–40°. This is in accordance with the findings of this study; OTB marks have mean widths of 3 m (Table 3.3).

As expected, OTT marks could not often be identified in backscatter data as OTT fishing is quite rare compared to the other métiers (Schulze, 2018). One example which is probably an OTT mark could be found (Figure 3.14). Due to the fact that the corresponding vessel was observed, the TM could be assigned to a single haul but if the TM would have been observed without context it also could be interpreted as two single OTB marks with more or less the same bearing. Overlaps of fishing routes of individual vessels or within fleets is not uncommon (Rijnsdorp et al., 1998) and therefore OTT/OTB might be overseen.

Malik and Mayer (2007) found trawl tracks of >12 km length corresponding to a 6–8 h haul at 2–3 knots trawling speed. The trawling speed is approx. 5 knots for TBB catching demersal fish

(ICES, 2018b), which can produce a consecutive trawl track of >50 km length for a 6 h haul. In this study consecutive tracks of approx. 10 km length were found in all three research sites but their length is limited by the SSS covered area and by the orientation of the TM respect to the collected dataset. Some TM could only be followed over distances of <1 km, which is also reported by Malik and Mayer (2007) as connected to scallop dredging. However, VMS data show that dredges for scallops are only used in coastal waters in the German North Sea (Schulze, 2018). As a consequence, the shorter tracks can rather be related to limited traceability due to difficulties in distinguishing TM from the background, SSS survey size and the occurrence of low spatial density clustered TM in consequence of degradation.

Exemplary MBES data from survey DB1 show a morphological change of <10 cm in a TBB mark (Figure 3.11). Bathymetry data show TBB morphologies of a similar size and aspect to the SSS records. The shoes of the TBB should produce depressions in the seafloor, bordered by centimeter scaled ridges due to the sediments pushed away by the shoes. On the bathymetric data such a sequence (ridge-depression-ridge) could be observed, although the miscompensation of the motion sensor and the resulting morphological artifacts do not allow a clear distinction of those geometries respect to the "bathymetric noise". The TM are clearly more evident in the SSS than in the MBES records. The morphological change of the TBB marks (Figure 3.11) is in accordance with Eigaard et al. (2016), where a penetration depth of <10 cm was stated for TBB on sandy sediments. Depestele et al. (2016) described changes in seabed bathymetry of 2–6 cm caused by a 4.4 m wide TBB on a sandy sediment (median grain size 144 µm). This change is slightly less than observed in the data of the present study, which can be explained by the size of the gear; the TBB mark (Figure 3.11) has a width of approx. 10 m and therefore the related gear is assumed to be larger and heavier. However, multiple passages of the trawl gear can also increase the morphological change (Depestele et al., 2016). If the TBB in Figure 3.11 was created by multiple gear passages is unknown but the ridge-depression-ridge sequence would probably have another form (e.g., more than two ridges) because it is considered unlikely that the gear passed the exact same track multiple times.

3.5.3 Persistence of Trawl Marks and Signs of Degradation

TM preservation varies based on multiple factors like sediment type, hydrodynamics (e.g., tidal currents, waves, storm events) and trawling patterns. In this study, a minimum preservation time of 5–7 days and a maximum preservation time of <5 months could be defined in the DB site: Several TBB marks were observed across the whole SSS mosaic of DB2 and as the data collection spanned between 9th and 13th March 2017 (DB2), it is reasonable to assume a minimum preservation time of roughly 5 days at this location. In DB 3, similar to

DB2, several TBB tracks of approx. 12 km length were identified, which corresponds to seven days survey time (Table 3.1). The same order of magnitude for minimum preservation time of TBB marks could be observed at study sites WF (TM of ca. 10 km =^ five survey days) and HEL (TM of ca. 7 km =^ four survey days). During the DB1 survey, a trawling vessel was real-time observed during fishing operations. The TM was recorded (Figures 3.4 and 3.6b) and re-surveyed during DB2 (March 2017). It could not be identified again, which means the maximum preservation time is <5 months at this site within the investigation period. Lindeboom and de Groot (1998) described a preservation time of 52 h in coarse sand in the southern North Sea, using a smaller beam trawl (4 m beam width) deployed in shallower water (approx. 15 m water depth), which could explain the shorter persistence compared to results of this study.

Mérillet et al. (2018) observed that bioturbation could lead to a lower persistence of TM. In general, bioturbation is higher in muddy than in sandy sediments (Zhang et al., 2019), therefore, bioturbation is likely not a significant controlling factor for the preservation of TM in the three study sites, where sediments are mainly made by sand with a very low mud content. However, in their model, Zhang et al. (2019) described a pattern of increased bioturbation activity at Dogger Bank during summer. As a consequence, the TM at the DB site should be less stable during summer months, which is in contrast with the highest TBB mark densities recorded in that period in our datasets.

In the present study, it could be observed in SSS data that TBB marks can show a detailed backscatter signature (higher backscatter values in the center and lower backscatter values at the edges, Figure 3.15), whereas other TBB marks do not (clustered and blurry TBB marks, Figure 3.6a). The absence of these detailed patterns seems to be related to the progressing degradation of TBB marks and therefore, consecutive TM with a detailed backscatter signature are suggested to be rather “new” than clustered TM without these details. However, it has to be noted that differentiating between a “new” mark with low penetration and an “old” mark with high penetration is not possible (Smith et al., 2007). For instance, electric pulse trawls have gained importance, e.g., within the Dutch fleet, which use electric pulses instead of the heavy tickler chains (Turenhout et al., 2016). Thus, the gears have lower weights compared to conventional TBB, resulting in a lower penetration depth (Depestele et al., 2019).

The evaluation of degradation and persistence of TM has to consider the limitations of the SSS system: The “new” TBB mark in Figure 3.6b can be traced across the whole SSS swath but neighboring TM are not visible in the far range of the SSS swath as most of the energy of the SSS signal is returned from areas closest to the source and the resolution decreases in the far range

due to the angle of incidence and the signal travel time (Lurton, 2002). The size of the TM in respect to the SSS mosaic resolution plays also an important role. As the TM vanishes, their size is expected to reduce and therefore to be less detectable at the given SSS resolution of 1 m.

As expected, post-storm TBB marks from survey WF5 were less prominent (i.e., they were characterized by a lower backscatter intensity) and therefore more difficult to be distinguished from the surrounding sediments (Figure 3.13a,b). By considering the corresponding histograms, it could be found that the mosaic, which is displaying "new" TM has a lower standard deviation regarding the grey values (σ = 14.06, Figure 3.13a), than the mosaic with "old" TM (σ = 19.27, Figure 3.13b), indicating a lower contrast in the mosaic of the initial survey. This is unexpected because the contrast should decrease when TM are less pronounced. The skewness is showing a more negative value in the re-survey mosaic (−1.23; initial mosaic −0.91) and therefore the majority of the values within the distribution shifts in the direction of lower backscatter values (="whiter" grey values) of the mode (176), although the low backscatter values of the TM are missing. This counter-intuitive change of the grey value distribution can be explained by lower data quality of the re-survey due to slightly rougher sea conditions compared to the initial survey (Figure 3.13c), resulting in an increased number of artifacts. It is hardly to quantify on which extend the data quality influences the change among the histograms. However, the subjective comparison (examination with the naked eye) of the two mosaics suggests that the TM are significantly less evident in Figure 3.13b.

Gilkinson et al. (2015) described an "initial decrease in sharpness" of TM (4 m wide dredge) after the first year of observation followed by a "more gradual degradation of the tracks and their edges" in the next years until they were undetectable after three years in the SSS data (0.25 m resolution) of the mobile sand sheet on the Scotian Shelf in 65–75 m water depth. The authors concluded that storms are of major importance regarding sediment reworking. TBB marks at our WF site were hardly visible in SSS data after six days including three days of rough sea conditions (Figure 3.13). Gilkinson et al. (2015), moreover, noticed a reversal in backscatter (from lower to higher compared to the surrounding) during the degrading process. In the present study, all TBB marks at the DB site show similar backscatter values (i.e., higher) compared to the surrounding. This means they either all have to be of the same age at the time of the survey or the effect of backscatter-reversal does to apply to our study site. At site HEL, both cases are present (high and low backscatter compared to the surrounding) but the high backscatter TM occur in coarser sediments than low backscatter TM, which likely depends on sediment-type rather than on the degrading processes.

The TM in Figure 3.14 shows a V-shaped pattern, indicating the proceeding divergence of the gear due to increasing vessel speed. High backscatter values with a corresponding acoustic shadow are clearly visible in the course of individual TM (Figure 3.14a,c), indicating pushed up sediments followed by morphological depressions. The high backscatter features at the ends of the individual furrows (i.e., TM) are interpreted as otter boards. It is assumed that this signature is related to an OTT, as the two nets share one otter board in their middle (=3 otter boards in total, (Eigaard et al., 2016). Within 36 h, the morphological change vanished to the state, which is shown in Figure 3.14b,d. The standard deviation (σ) calculated from the histograms shifts from higher (Figure 3.14a,c) to lower values (Figure 3.14b,d). This indicates a decrease of contrast, which is likely due to the flattened TM with less pronounced acoustic shadows and the absence of the artifacts caused by propeller noise of the fishing vessel. In the mosaics of the initial survey, the grey value distribution is clearly negative skewed (−1.39 and −1.06), indicating that the majority of the grey values are concentrated right of the mode (158 and 170), i.e., around lower backscatter values (="whiter" grey values). In the re-survey mosaic, the skewness is closer to zero (−0.31 and −0.15) and the distribution, therefore, is now concentrated nearer around to the mode (157 and 161). This seems reasonable, as the artifacts are missing and the TM has decreased in contrast. The kurtosis in the re-survey mosaics (4.02 and 4.23) is rather comparable to the normal distribution (kurtosis = 3) than in the initial mosaics (7.5 and 9.04), which is, as well, likely due the absence of artifacts and contrasts in the TM. Due to the striking artifacts (propeller noise) in the initial mosaics, it can be assumed that this contributes considerably to the change among the histograms. The subjective comparison (with the naked eye) of the mosaics, however, reveals rather gradual edges of the TM after 36 h, indicating a degraded TM. Depestele et al. (2016) reported that the TM of a 4.4 m wide TBB hardly changed their aspect after 12–44 h and a 4.4 m pulse trawl (similar to TBB but uses electric pulses instead of tickler chains) faded after 55–107 h. They conducted their studies in coastal areas (15–22 m water depth, median grain size 144µm) where tidal and wave related currents are more pronounced than in the three study sites. Nevertheless, the preservation time of the OTT marks observed in this study is even shorter.

The degradation rate seems to be more dependent on the gear type and on the size (i.e., weight). Palanques et al. (2001) observed OTB marks in muddy sediments on the Ebro Shelf (20–70 m water depth): these TM did not show any changes after a few days but after a year they appeared with lower backscatter values. They related the relative longevity to the cohesive properties of the muddy sediment (mud content >60%). In the WF study site, the mud content is relatively low, while it is likely that the altering of the OTT mark is faster.

At sites DB and HEL, any OTB mark was detected, whereas at the WF site OTB marks were present. The fishing activity related to OTB trawls is reported to be similar at all the three study in the years 2016 and 2017 (ICES, 2018c). Therefore, either OTB marks are not detectible in the DB and HEL sites or fishing did not take place during and/or before our survey. Similar to TBB in offshore waters, OTB fishing is targeting demersal flat fish. In this study, high relative TBB densities in the months of general high fishing activity (i.e., summer, Figure 3.12) were recorded and it is expected that OTB fishing is conducted at the same times because the gears are targeting similar fish populations. Consequently, it is likely that OTB marks were not recorded because the relative narrow furrows were masked by TBB marks and/or OTB have, compared to TBB, lower penetration depths in sands (Eigaard et al., 2016) and therefore the preservation potential of the marks is lower. In addition, the otter boards can float within the water column or touch the seabed at irregular intervals (BSH, 2016). This leads to characteristic "dashed line-patterns" (Figure 3.9a), which makes the tracking of OTB marks over longer distances more difficult.

3.6 Conclusions and Outlook

Together with the detailed description of TM patterns specifically related to different trawl gears, the mapping presented in this study provides an insight into the physical disturbance on the seabed caused by bottom contacting trawling, which can help to evaluate the impact of fishing activities on sediments, seafloor morphology, and macrobenthos (flora and fauna).

In general, fishing activity maps are derived from positioning and logbook data of fishing vessels (VMS data; ICES, 2018d). These data are usually aggregated over one year, if using SAR (ICES, 2018c, ICES, 2018d) and no further distinction about specific time windows is possible (e.g., seasons). SSS data can therefore provide additional and valuable information on a higher timely resolution concerning the fishing effort and its potential seabed disturbance. However, collecting recurrent (yearly or monthly) SSS datasets over large areas is very cost intensive and time consuming. Thus, it would be beneficial to examine potential advantages of the direct connection of SSS and VMS data in order to improve monitoring programs.

The present study reveals seasonal changes in the spatial density of TM: It was highest in August and October and lowest during the winter months (November to March, Figure 3.12) and TBB marks could be identified in all sites. Although the fishing effort for both gears is similar, OTB marks, surprisingly, only appear at WF site. This is probably related to a reduced persistence of OTB marks in sands as well as limited detectability in SSS-data due to their metrics, which is especially important if the quality of the backscatter data is not constant; the

detection of narrow TM is rather difficult in rather "noisy" data. Moreover, the visual examination of backscatter data for TM mapping and descriptions strongly depends on the editor. Therefore, methods to reduce the "noise" in SSS data should be applied as well as standard guidelines and/or automated feature detection approaches are needed in order to improve the robustness of TM detection.

The extensive mapping of TM was based on approx. 4800 km^2 of SSS data. SSS has the advantage of a wider swath (e.g., 400 m in this study) compared to MBES (e.g., 120 m in this study), which allows to survey an area with 100% coverage in a shorter time using SSS. In this study, TM were more evident in SSS than in MBES data, which is, however, likely due to the quality of MBES data. The carefully application of MBES data corrections by means of vessel motion and SVPs is therefore important in order to get more reliable morphometric measures, because the depth information is a great benefit of MBES. This could also help to identify the mechanical impact of the different gear parts (tickler chains and shoes). Moreover, a comparison of the backscatter data from both systems (SSS and MBES) would allow it to investigate how the detection of TM on acoustic records may be influenced by the geometric array of the acoustic device. However, the SSS shows an unparalleled ability to map large areas with reasonable time and cost efforts.

In contrast to the hydro-acoustic data, TM could not be resolved in UW-videos in this study, although the possibility of observing TM in UW footage was already described in literature. That likely depends on the area investigated by a single video frame (video square footage = 1 m^2 in this study) in relation to the size (both vertical and horizontal) of the TM. Steering options of the camera and a wider image section may help to detect TM. However, for a comprehensive mapping over larger areas, the UW video system does not represent a suitable tool, whereas it can significantly contribute to the investigation of specific aspects related to the impact of trawl gears such as changes in sediment composition and in seabed roughness, and modifications in the macrobenthos communities.

TM characteristics and preservation potential strongly depend on the individual sites as both are influenced by multiple factors, which are not constant over time and space, like bed shear stress due to currents and waves as well as general fishing activity. Statements in the literature on the persistence of TM strongly differ (from a few hours to several years) and therefore one of the main goals of this study was to evaluate TM persistence in the German North Sea. A Minimum TM persistence was estimated to be 2–7 days and the maximum persistence at Dogger Bank <5 months. As the lowest TM density was found during the winter months, general rougher sea conditions and an increased probability of storm events

compared to the summer months are likely to control the preservation of TM during that time: The TM are more likely to be flattened and/or less fishing activity is present, which could be further investigated by a combined analysis of mapped TM and VMS- data.

At the WF site, time series data of TM were compared in order to investigate degrading of TM by calculating histograms of grey values of the respective mosaics. In the manner how histograms were treated in this study, they have proven to be impractical to reliably quantify the changes in backscatter intensity, since differences in data quality (artifacts due to, e.g., weather conditions or propeller noise) have considerable impact on the grey scale distribution. The application of additional filtering methods is highly recommended when quantifying the backscatter changes of a degrading TM based on histogram statistics. However, the subjective examination (with the naked eye) could reveal that TBB marks showed a decrease in backscatter intensity after four days including two days of rough sea conditions (Hs = 4.5 m, T = 5–10 s) in October (Figure 3.13). This example shows that TM are less evident after a storm event in the SSS data, and the question arises how much impact on the habitat (i.e., sediment re-working) is generated by such storm events in relation to the impact caused by bottom trawling in that area. In July (survey WF4), an OTT mark was re-surveyed after 36 h and showed signs of degradation as presented in Figure 3.14. If and how the alteration of such marks proceeds until they are completely removed should be examined by observing a full sequence of decay, maybe also with regard to storm events, using SSS and MBES.

3.7 Author Contributions

Conceptualization, I.B., P.H., and A.B.; methodology, I.B.; validation, I.B., P.H., R.M.C., S.P., and A.B.; formal analysis, I.B., R.M.C., and S.P.; investigation, I.B., P.H., and S.P.; resources, A.B.; data curation, P.H., S.P., and I.B.; writing—original draft preparation, I.B.; writing—review and editing, R.C.M., A.B., S.P., and P.H.; visualization, I.B.; supervision, A.B.; project administration, A.B.; funding acquisition, A.B. All authors have read and agreed to the published version of the manuscript.

3.8 Funding

This research was conducted in the framework of the ASKAWZ project, which is a research and development cooperation between Senckenberg am Meer and the German Federal Maritime and Hydrographic Agency (BSH, Bundesamt für Seeschifffahrt und Hydrographie, ASKAWZ III Contract-No. 10038520). ASKAWZ is part of the *SedAWZ* project, which is coordinated by BSH

and funded by German Federal Agency for Nature Conservation (BfN, Bundesamt für Naturschutz).

3.9 Acknowledgments

The authors are grateful to the Captains and Crews of RV Alkor, RV Heincke and RV Senckenberg for the professional support on the vessel. The authors would like to thank the late H. Christian Hass (Helmholtz Centre for Polar and Marine Research, Alfred Wegener Institute, List, Germany) for contributing to the acquisition of multiple datasets from the "*SedAWZ*"-project at Dogger Bank site (hydro-acoustic raw data, photo and video material and grain sizes). We would also like to thank Maik Wilsenack for technical support, our lab staff Astrid Raschke for the grain-size analysis as well as all our student assistants contributing to the surveys and the lab work.

3.10 Conflicts of Interest

The authors declare no conflict of interest. The funders had no role in the design of the study; in the collection, analyses, or interpretation of data; in the writing of the manuscript, or in the decision to publish the results.

3.11 References

Please find the references within the overall reference list of this thesis (chapter 8).

4 Physical impact of bottom trawling on seafloor sediments in the German North Sea

Ines Bruns[1], Alexander Bartholomä[2], Francine Menjua[1], Achim Kopf[3]

[1]Department of Geosciences, University of Bremen, Klagenfurter Straße 4, 28359 Bremen, Germany

[2]Senckenberg am Meer, Department for Marine Research, Südstrand 40, 26382 Wilhelmshaven, Germany

[3]MARUM Center for Marine Environmental Sciences, University of Bremen, Loebener Straße 8, 28359 Bremen, Germany

Submitted to Frontiers in Earth Science (section Marine Geoscience) on 01.06.2023.
The article was published in revised form on 09.11.2023: Bruns I, Bartholomä A, Menjua F and Kopf A (2023), Physical impact of bottom trawling on seafloor sediments in theGerman North Sea. Front. Earth Sci. 11:123316. doi: 10.3389/feart.2023.1233163

4.1 Abstract

Bottom trawling is a well-known global phenomenon and has significant physical impact on the seabed habitat, such as compression, displacement and mobilization of the sediment. Thus, it is necessary to examine how it alters the seabed e.g., in order to support strategies in marine spatial planning and nature conservation. Numerous studies aim at quantifying the physical impact of bottom trawling on the seabed based on laboratory experiments and/or modeling approaches but, to our knowledge, none of them include in-situ techniques. The North Sea is heavily influenced by bottom trawling and thus, we selected an area in the southern North Sea where side scan sonar data identified areas showing the physical impact of bottom trawling by means of trawl marks. Here, we deployed the dynamic penetrometer Nimrod to determine the changes in sediment strength (quasi-static bearing capacity) compared to the reference sites (absent trawl marks). Our results attest a higher penetration depth of Nimrod and a lower sediment strength in the trawled area compared to the un-trawled reference sites. This is likely related to an increase in water content and a decrease in bulk density of the sediment that was re-worked by bottom trawling. A spatial analysis of the quasi-static bearing capacities in the trawled area and the backscatter characteristics of the trawl marks suggest that the lowest sediment strength is rather obtained where a single bottom trawling took place recently. In contrast, regions with repeated trawling events in the past show elevated sediment strength.

4.2 Introduction

Bottom trawling is one of the most widespread human impacts on the seabed and relevant on a global scale (Oberle et al., 2016a, Amoroso et al., 2018). Besides reduced populations of target species due to overexploitation, intensive bottom trawling can increase the damage and mortality of non-target benthic fauna caused by the bypassing trawling gear (e.g., Lindeboom and de Groot, 1998, Buhl-Mortensen et al., 2016, Mérillet et al., 2017). The gear itself may weigh up to several tons (Eigaard et al., 2016). The impact on the soft, porous seabed surface and subsurface induced by the trawling gear represents an additional, severe disturbance to the natural forcing by waves and currents on benthic species, in particular species with a long-life span that require longer recovery times (Sciberras et al., 2018). For species in the southern North Sea (Frisian Front), it was found that fragile, small-bodied infauna like the white furrow shell (*Abra alba*) and epifauna are more vulnerable to the impact of bottom trawling than large-bodied infauna, e.g., the burrowing mud shrimp *Upogebia deltaura* (Tiano et al., 2020). Moreover, bottom trawling can alter the seabed in terms of removal of bedforms such as ripples as well as displacement, compression and re-suspension of the sediment (e.g., Ivanović and O'Neill, 2015, Depestele et al., 2016, Lindholm et al., 2015, Arjona-Camas et al., 2019). Sediment with reduced stability, e.g., due to bioturbation, is more likely to get re-suspended by bottom trawling (O'Neill and Ivanović, 2015), and hence may hamper benthic habitability for several populations (Lindeboom and de Groot, 1998, Depestele et al., 2016).

The alteration of the seabed is visible as linear morphological depressions (trawl marks) in side scan sonar (SSS) and multibeam echo sounder (MBES) data as well as in under-water video footage (e.g., Friedlander et al., 1999, Smith et al., 2007, Mérillet et al., 2018, Bruns et al., 2020, Schönke et al., 2022). Trawl marks have widths of a few decimeters up to several meters and the gear can penetrate <10 cm up to 35 cm into the seabed (e.g., Krost et al., 1990, Friedlander et al., 1999, Eigaard et al., 2016, Bruns et al., 2020). The dimensions of trawl marks depend on the gear type (e.g., beam trawl, otter trawl) and the sediment type. Larger gears produce wider marks, for instance, the width of beam trawls usually is between 4 m and 12 m, which is reflected by trawl marks of the same width (e.g., Eigaard et al., 2016, Bruns et al., 2020). In contrast, the two otter boards of otter trawls create narrow furrows (approx. 30 cm to 3 m) separated according to the distance between the otter boards, which can be up to 250 m (e.g., Eigaard et al., 2016, Bruns et al., 2020). Due to a higher weight also the penetration depth increases (Eigaard et al., 2016) and, for example, a 4 m wide beam trawl would penetrate less deep compared to a 12 m wide gear. In muddy sediments the penetration depth is usually higher than in coarser sediments such as fine sand (Ivanović et al., 2011, Eigaard et al., 2016).

The backscatter signature of trawl marks shows that reworking of the sediment (displacement, compression, re-suspension) can lead to an increased roughness of the seabed compared to the surrounding, depending on the sediment type and the state of degradation of the trawl marks (Bruns et al., 2020).

For other areas, it has been shown that intensive bottom trawling can influence erosion and sedimentation rates. For the Western Irish Sea Mud Belt, Coughlan et al. (2015) could show that the upper 20 - 50 cm of the sedimentary record (approx. the last 20 years) were eroded due to high bottom trawling activity. In two submarine canyons off the Italian south coast where the material that was re-suspended by bottom trawling is deposited, an increased sedimentation up to one order of magnitude was observed (Paradis et al., 2021).

Moreover, bottom trawling may alter the integrity of the near surface sediment layers (O'Neill and Ivanović, 2015), for example by destroying biogenic structures such as tubes or mounds (Schwinghammer et al., 1998). The upper layers are more likely to be mobilized or eroded, respectively, which in turn could lead to the mobilization of deeper layers (O'Neill and Ivanović, 2015). Long term bottom trawling and the related re-suspension of the seabed sediment can cause significant changes in the grain size distribution: The re-suspended fine grained material settles directly within the trawled area if a significant sediment transport is absent and thus the fine fraction is increased on the seabed surface (Trimmer et al., 2005). If tides and currents are strong the fine grained re-suspended material is transported into adjacent areas, which leads to a decrease of the fine-grained fraction in the trawled area (Palanques et al., 2014, Mengual et al., 2016).

If bottom trawling was relevant for sediment re-mobilization and changes in the physical properties of the sediment (e.g., grain size) this would also be reflected by geotechnical properties such as sediment strength and its resistance to mobilization. Studies that investigated the influence of bottom trawling on geotechnical properties, and therefore the physical impact with the help of experimental and modeled data, are available (e.g., Paschen et al., 2000, Ivanović et al., 2011, Ivanović and O'Neill, 2015), but there is a lack of in-situ data for the support of those findings. Stark et al. (2011b) detected sediment mobilization by using the dynamic penetrometer *Nimrod*, where mobilization is manifested by a layer with lower sediment strength above a stronger layer in the penetrometer data. Following this, the question arises if the physical impact of bottom trawling can be described, and even quantified, by means of vertical and lateral variations in the sediment strength using in-situ techniques such as *Nimrod* deployments.

Along this line of reasoning, we performed geotechnical in-situ measurements of the sediment strength in the southwestern German North Sea using the dynamic free-fall penetrometer *Nimrod,* which was developed at MARUM, University of Bremen (Stark et al., 2011a, Stark et al., 2011b, Stark et al., 2012). At the time of the survey, the trawl mark density in the north western part of the survey area was relatively high, i.e., up to 20 marks per km^2 and very recent trawling activity could be detected (Bruns et al., 2020). With the experiences of the former studies we assumed that sediment mobilization triggered by the high trawl mark activity can be demonstrated by means of the dynamic free-fall penetrometer *Nimrod*. For comparison, we also sampled an area without trawl marks. In the past, Stark et al. (2011b) used the dynamic penetrometer *Nimrod* to show sediment mobilization due to tides and currents in the German Bight. However, it is a completely new approach to connect in-situ sediment strength data to bottom trawling impact, as will be demonstrated in this manuscript.

4.3 Material and Methods

4.3.1 Study site

The study site (hereafter referred to as *HE544* site, named after the expedition number of R/V Heincke, a 55 m-long research vessel operated by AWI Bremerhaven; https://www.portal-forschungsschiffe.de/en/vessels-heincke.html) is located in the southern North Sea and the western German Exclusive Economic Zone (EEZ, Figure 4.1). Surface sediments in the German EEZ predominantly consist of Pleistocene glacial and periglacial deposits, which were reworked during the Holocene after the area was flooded around 9000 - 8000 BP (Eisma et al., 1981, Zeiler et al., 2008). Sediment types are mainly sand to fine sand and some parts can be classified as muddy sand to sandy mud e.g., south of the island Heligoland or in the western German Bight (Laurer et al., 2014). The survey *HE544* was conducted in 2019 approx. 50 nautical miles north of the German coast where the water depth ranged around 39 - 42 m (Figure 4.1). Hydrodynamics are mainly tide driven in the coastal areas, but rather wave driven in offshore areas (Aldridge et al., 2015). *HE544* site is located in the wave driven area and the kinetic energy at the seabed is approx. 40 - 60 Nm^2/s (EMODnet, 2019). The sediment type at *HE544* was classified as “fine sediment to sand” by Holler et al. (2020). It is homogeneously distributed across the *HE544* site (Holler et al., 2020). Corresponding surface sediment samples attested the absence of gravel, a small proportion of shell fragments (<2 %) and a mud content ranging from 3-10 % in the northern and western part of the site and up to 20 % in the remaining area (Bruns et al., 2020, Holler and Bruns, 2020).

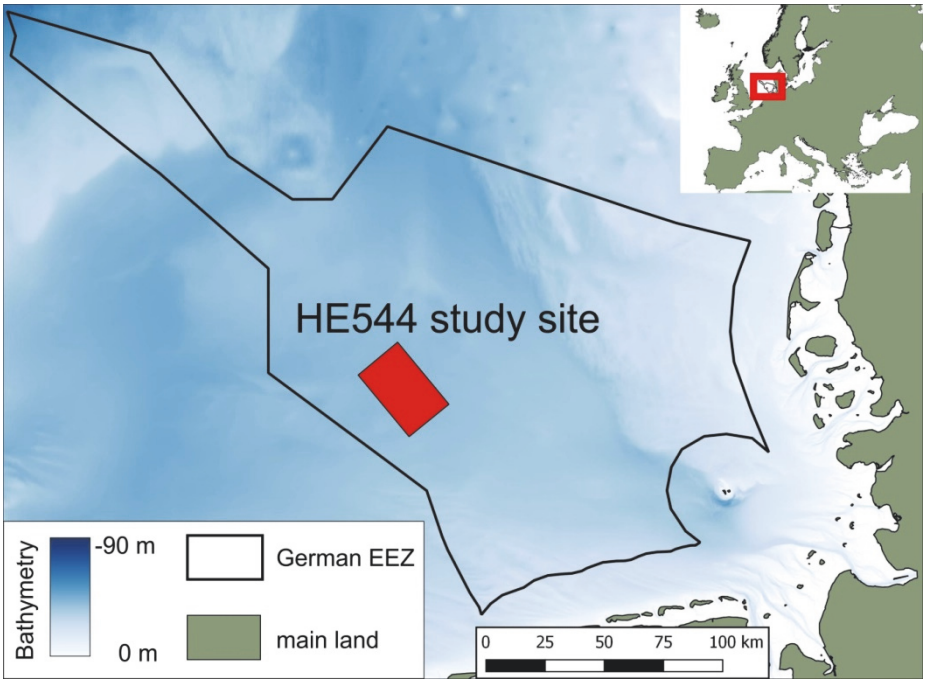

Figure 4.1: The *HE544* study site in the German Exclusive Economic Zone (EEZ), North Sea. The site is approx. 60 nautical miles off the coast of Lower Saxony, Germany. Bathymetry is provided by EMODnet-Bathymetry-Consortium (2018).

The fine sediments are colonized by large populations of benthic organisms such as the brown shrimp (*Crangon crangon*) or flatfish, such as sole (*Solea solea*). Bottom trawling in the German EEZ (North Sea) is mostly related to smaller vessels operating in coastal areas to catch e.g., the brown shrimp (Schulze, 2018). The fishing effort made by larger trawlers, targeting flat-fish such as sole (*Solea solea*) or plaice (*Pleuronectes platessa*) is less in comparison and takes place farer offshore, i.e., outside the 12-nautial-mile-zone (Schulze, 2018). These trawlers commonly use beam trawls and otter trawls (Schulze, 2018). The corresponding trawl marks could be observed in SSS and MBES data on the seabed of *HE544* site (Bruns et al., 2020). Marks created by the individual beam trawls had mean widths of approx. 11 m, and because they are towed in pairs the total width was approx. 40 m (Figure 4.2a) and see also Bruns et al. (2020). In contrast, otter trawls have no fixed width over the course of one haul as they have no rigid beam to open the net. Instead, they have otter doors attached to the trawl rig, which are diverging according to towing speed (Figure 4.2b). As seen, mouth sizes of otter trawls ranged between 30 and 280 m and the marks created by the otter boards were ca. 3 meters wide (Bruns et al., 2020).

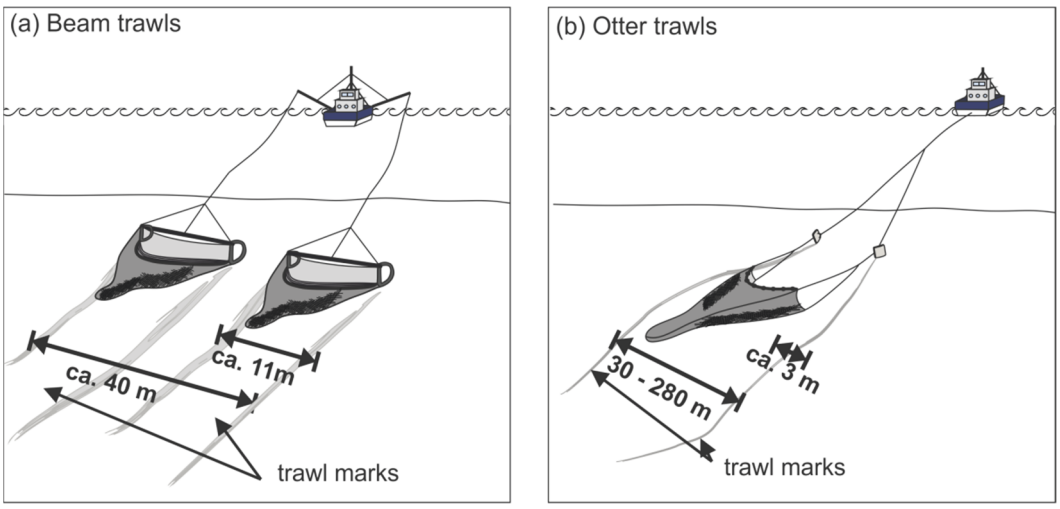

Figure 4.2: Schematic sketch of the trawl gear and the corresponding trawl marks, which were observed in the side scan sonar data of the study site (modified after Bruns et al., 2020). (a) Beam trawls are towed in pairs and the trawl marks have an individual width of 11 m and a total width of 40 m on average (Bruns et al., 2020). (b) Otter trawls produce individual trawl marks of approx. 3 m width and the total width ranges from 30 m to 280 m because the distance between the two otter boards is variable (Bruns et al., 2020).

4.3.2 Data acquisition

The survey for this study was conducted with R/V Heincke from 14th to 30th October 2019 (survey number HE544) in the southern North Sea (Figure 4.1). The overall aim of the cruise was to extend the mapping in the course of the German national mapping program "*SedAWZ*" and to examine anthropogenic seabed features by means of trawl marks (Holler and Bruns, 2020).

4.3.2.1 Sediment samples

During expedition *HE544*, 15 surface sediment samples were obtained (Figure 4.3a). A Shipek grab was used and the samples were analyzed for grain size distribution. It was already described by Bruns et al. (2020) that the proportion of the mud fraction ranges between 3 % and 20 % (gravel is absent) and that the sediment type is homogeneously distributed across the study site with a slight decrease of the mud fraction towards the northwestern part of the site. For this study, the same samples were considered but further statistics in terms of sorting, skewness and kurtosis were calculated in order to characterize the sediment type in detail. For the calculation GRADISTAT (Blott and Pye, 2001) was used. The following procedure was applied to the samples (see also Bruns et al., 2020): (i) decalcification with hydrochloric acid, (ii) removal of organic carbon with hydrogen peroxide, (iii) separation of the mud and sand fraction via wet sieving, (iv) the grain sizes of the dried sand fraction were determined from settling velocities by means of a

settling tube, (v) for the mud fraction X-ray transmission time series were measured using a Micrometrics Sedigraph particle analyzer.

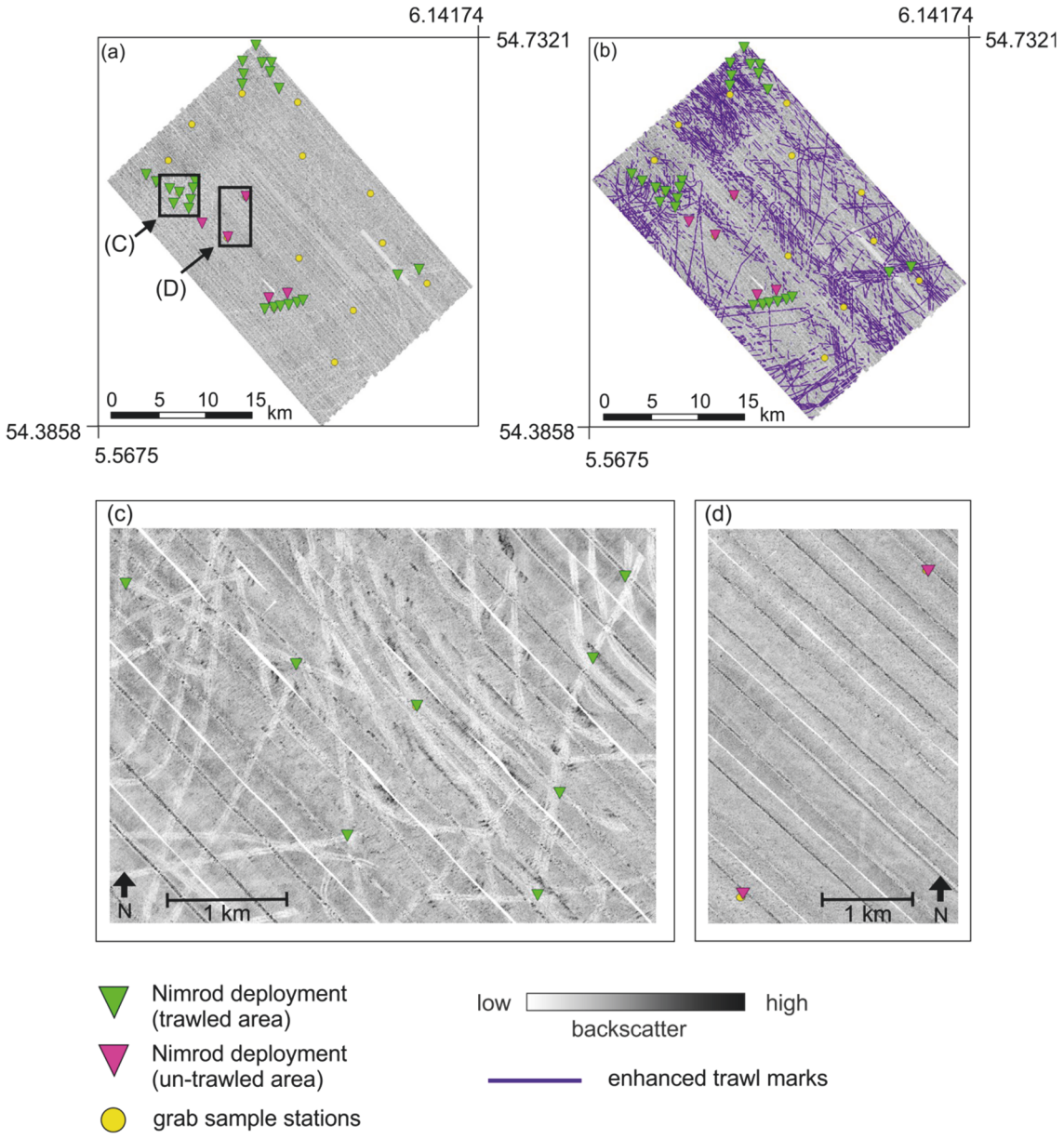

Figure 4.3: (a) SSS mosaic of the *HE544* study site with the grab sample stations (yellow circles) and the *Nimrod* deployment stations on trawled (green triangles) and un-trawled (pink triangles) areas. The trawled areas are characterized by multiple linear features, i.e., trawl marks, which appear with a lower backscatter intensity compared to the background. (b) The same SSS mosaic with enhanced (manually mapped) trawl marks (beam trawls and otter trawls). For details concerning the mapping of trawl marks see Bruns et al. (2020). (c) Zoom-in of a trawled area as an example. *Nimrod* penetrated the seabed directly within trawl marks. (d) Zoom into an un-trawled area as an example. Trawl marks are mostly absent; however, some trawl marks are still indistinctly visible in between the deployment stations.

4.3.2.2 Hydro-acoustic survey

The SSS mosaics that were acquired during the survey *HE544* were used to map the sediment type as well as the trawl marks (Bruns et al., 2020). On the basis of these existing mosaics, the sample locations for the in-situ measurements with the dynamic free-fall penetrometer *Nimrod* were identified. The towed SSS dual frequency system KLEIN4000 (100 kHz and 400 kHz) was operated with 400 m swath (100% coverage of the area without overlap) and approx. 5 knots towing speed (ca. 2.5 m/s), resulting in an across-track resolution of 9.6 cm and 2.4 cm, respectively. Data acquisition was performed with SonarPro14 and data processing with SonarWiz7.01. The post-processing included the following steps: (i) slant range correction, (ii) empirical gain normalization, (iii) de-stripe filtering, (iv) layback-correction and the resulting mosaic has a resolution of 1 m as described by Bruns et al. (2020).

At the *HE544* site, trawl marks were abundant: Bruns et al. (2020) calculated them to be up to 20 marks per km^2 and described the trawl marks as distinctly visible in the SSS mosaic, indicating recent bottom trawling activity. Beam trawl marks were distributed across the whole study site, while otter trawl marks were present only in the northeastern part of the site (Bruns et al., 2020). Moreover, Bruns et al. (2020) observed fishing vessels operating simultaneously to the SSS survey operations. Thus, it is very likely that sediment mobilization took place recently and/or at the time of the *HE544* data acquisition. The trawl marks form a mesh-like pattern (Figure 4.3a,b) and due to their clarity in the georeferenced SSS-mosaic, our data were suitable to serve as a base to select stations for *Nimrod* deployments in the trawled areas (Figure 4.3c) and the un-trawled areas (Figure 4.3d).

4.3.2.3 *Nimrod* dynamic free-fall penetrometer

General description and sampling set up

With the dynamic free-fall penetrometer *Nimrod*, the deceleration of the device during the shallow sub-seabed is measured together with pore pressure and tilt variations during profiling. From these parameters the quasi-static bearing capacity can be derived, which is a measure for sediment strength (e.g., Stark et al., 2011b). We combined SSS backscatter data with the penetrometer data to examine if trawling causes alteration of the seabed in terms of differences in sediment strength. The dynamic free-fall penetrometer *Nimrod* was developed at the research center “MARUM – Center for Marine Environmental Sciences” (University of Bremen). It is operated under free-fall conditions as its speed is not limited to the speed of the winch and the weight of the cable as with conventional penetrometers (e.g., cone penetration testing, CPT). *Nimrod* is attached to a tether and can be deployed manually in shallow water environments of

up to 200 m water depth (Stark et al., 2011a, Stark et al., 2011b, Stark et al., 2012). The main body consists of a cylindrical aluminum case housing the sensors and memory card. Fins are attached to the tail (Figure 4.4a) and the relation of the center of mass to the center of volume allows a stabilized deployment of the device even if waves and currents are present. The diameter of the device is 0.11 m and the sampling rate is 1 kHz (Stark et al., 2011a, Stark et al., 2011b, Stark et al., 2012). The weight of *Nimrod* is 13 - 16.6 kg and depends on which frontal end is used; hemispheric or conical tips with different opening angles are available (Stark et al., 2011a, Stark et al., 2011b, Stark et al., 2012). Stark et al. (2011b) could achieve penetration depths of ca. 10 cm and below in sandy North Sea sediments using the conical tip with 60° opening angle. The estimated penetration depth of the trawl gear is ≥ 10 cm (Bruns et al., 2020, Eigaard et al., 2016) and therefore, a conical tip with a narrower opening angle of 25° (0.2 m length and 16.6 kg total weight of *Nimrod*) was manufactured for this study in order to achieve higher penetration.

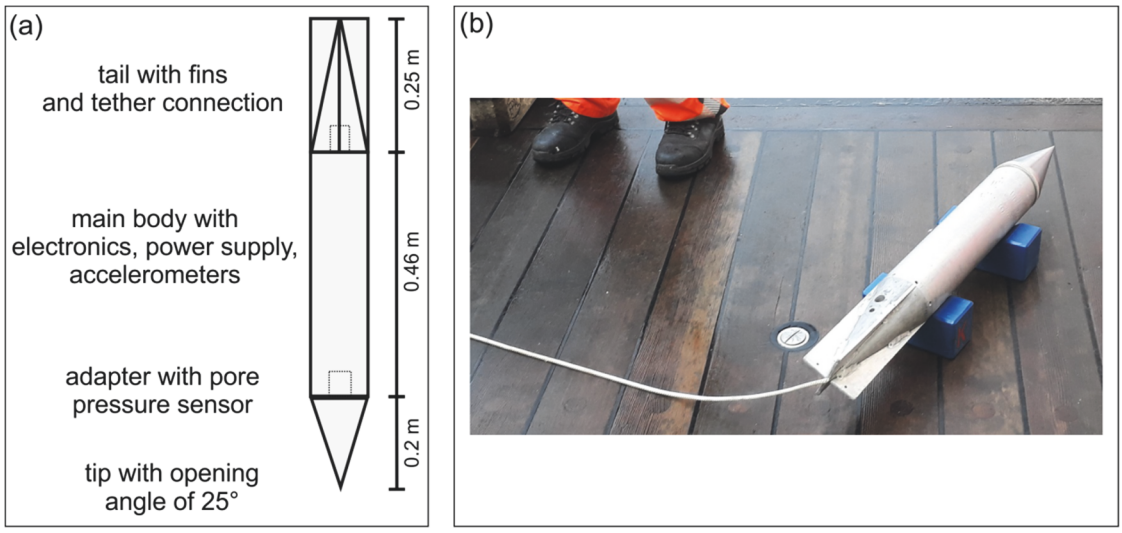

Figure 4.4: (a) Schematic drawing of Nimrods design (modified after Stark et al. 2009). Four tip geometries are available and for this study, a conical tip with 25° opening angle was used. (b) Nimrod onboard R/V Heincke. A tether with small buoyancy was attached to Nimrod in order to prevent disturbances during the free fall.

In this study, 24 *Nimrod* deployments were successfully performed on beam trawl marks that were identified from SSS data (Figure 4.3a,c). For comparison, 5 deployments were conducted in an area that showed no trawl marks in the SSS data (Figure 4.3b,d) and therefore was classified as un-trawled. Because of the small dimensions (approx. 3 m) of the otter board marks (Bruns et al., 2020), it was decided not to directly target them with *Nimrod*. In contrast, beam trawl marks have a mean width of 11 m (Bruns et al., 2020) and are therefore less difficult to target. However, the impact of otter trawls might contribute to signals the *Nimrod* data in areas where both kinds

of trawl marks were present. In order to ensure that *Nimrod* penetrates the beam trawl marks, deployments were profiled across parts of *HE544* site where they appeared in dense mesh-like patterns (Figure 4.3b). The sample locations were determined by means of a high accuracy DGPS.

Data processing

In contrast to conventional CPT probes, which have strain gauges to measure sleeve friction and cone resistance, *Nimrod* measures deceleration, tilt and pore pressure from which the sediment strength expressed as quasi-static bearing capacity is derived. The quasi-static bearing capacity varies over the penetration depth of each individual deployment. It increases with depth until the maximum is reached and *Nimrod* is not able to penetrate further into the sediment. The data processing was performed following the procedure presented by Stark et al. (2011a), Stark et al. (2011b) and Stark et al. (2012).

The bearing capacity q_u is derived from the deceleration of the probe with depth:

$$q_u = q_c + q_q + q_\Upsilon = cN_c + qN_q + \frac{1}{2}\Upsilon B N_\Upsilon \qquad \text{Equation 4.1}$$

This includes cohesion q_c, surcharge q_q and unit weight of the soil q_Υ (Terzaghi, 1943, Das, 1990). In this case, the factor q_c can be neglected, because non-cohesive fine sand was examined. The surcharge q_q describes the load of the surrounding sediment; it is zero. At the seabed surface and increases with depth. B is the width of the penetrating probe (11 cm in this case) and N is the bearing capacity factor, which mainly depends on the soil friction angle (Das, 1990). Moreover, the opening angle of the conical tip (25°), the surface roughness of the cone, the inclination of the probe (inclination of the seabed can be neglected in this case), the excess pore pressure and the relation between the width of the probe (conical tip with cylindrical body, Figure 4.4a) and the penetration depth have to be considered (Stark et al. (2011b) and references therein).

The bearing capacity is expressed by the sediment resisting force, because it describes the maximum resistance force of the sediment (or a sediment layer), which it can bear until it fails and the probe continues penetrating (Terzaghi, 1943, Das, 1990, Aubeny and Shi, 2006).

$$q_u = \frac{F_{sr}}{A} \qquad \text{Equation 4.2}$$

A is the horizontal area on which the load is applied and F_{sr} is the sediment resistance force. When the probe decelerates (*dec*), F_{sr} acts against it, which includes the sediment shearing resistance force F_s and the buoyancy of the probe in the soil F_b (Aubeny and Shi, 2006).

$$m_{Nim} dec = F_b + F_s = F_{sr} \qquad \text{Equation 4.3}$$

In this case, the mass of *Nimrod* m_{Nim} in water is 16.6 kg.

The dynamic penetrometer *Nimrod* decelerates during penetration, which leads to a strain dependency and therefore the strain-rate factor f_{ac} is introduced in order to allow the comparison of different dynamic penetrometers and standardized methods (Stark et al. (2011b) and references therein):

$$f_{ac} = 1 + K \log(\frac{v}{v_0}) \quad \text{Equation 4.4}$$

It includes the actual velocity of penetration *v* and the reference velocity v_0, which is 0.02 m/s and the standard for quasi-static penetration tests, after Cai et al. (2009). The empirical factor *K* is dimensionless and can range between 1 and 1.5 (Stoll et al., 2007). This leads to an uncertainty of 15 % (Stark et al., 2011b). In the present study, *K* was set to 1.25 and the range of uncertainty was considered in the results, following the approach of Stark et al. (2011b).

The dynamic sediment resistance force F_{sr} and the dynamic bearing capacity $q_{u_{dyn}}$ are now divided by strain-rate factor f_{ac} in order to convert them to quasi-static values (Stark et al., 2011b):

$$q_{u_{qs}} = \frac{q_{u_{dyn}}}{f_{ac}} \quad \text{Equation 4.5}$$

The optimization of the strain rate correction for high velocity impact penetrometers is still a subject of research (Lucking et al., 2017, Roskoden, 2020). For further details on the dynamic penetrometer *Nimrod* and the respective data processing and calculations, see Stark et al. (2011a), Stark et al. (2011b) and Stark et al. (2012).

4.4 Results

4.4.1 Grain size analysis

For this study, the grain size distribution of the samples obtained by Bruns et al. (2020) was examined further by means of statistics. All samples show an unimodal distribution with modes between 2.5 ϕ and 3 ϕ (Figure 4.5a). The mud content (> 4 ϕ) ranges between 3 % and 20 %. The statistical analysis shows that the samples are well to very poorly sorted (σ_1 between 0.4 and 2.4 ϕ), very fine skewed (Sk_1 between 0.2 and 0.8) and extremely leptokurtic (K_G > 3). The classifications are based on Folk and Ward (1957). The *Nimrod* deployments were carried out in areas where the mud content was below 15 % (Figure 4.5b) and thus, the sediment there is well to moderately sorted.

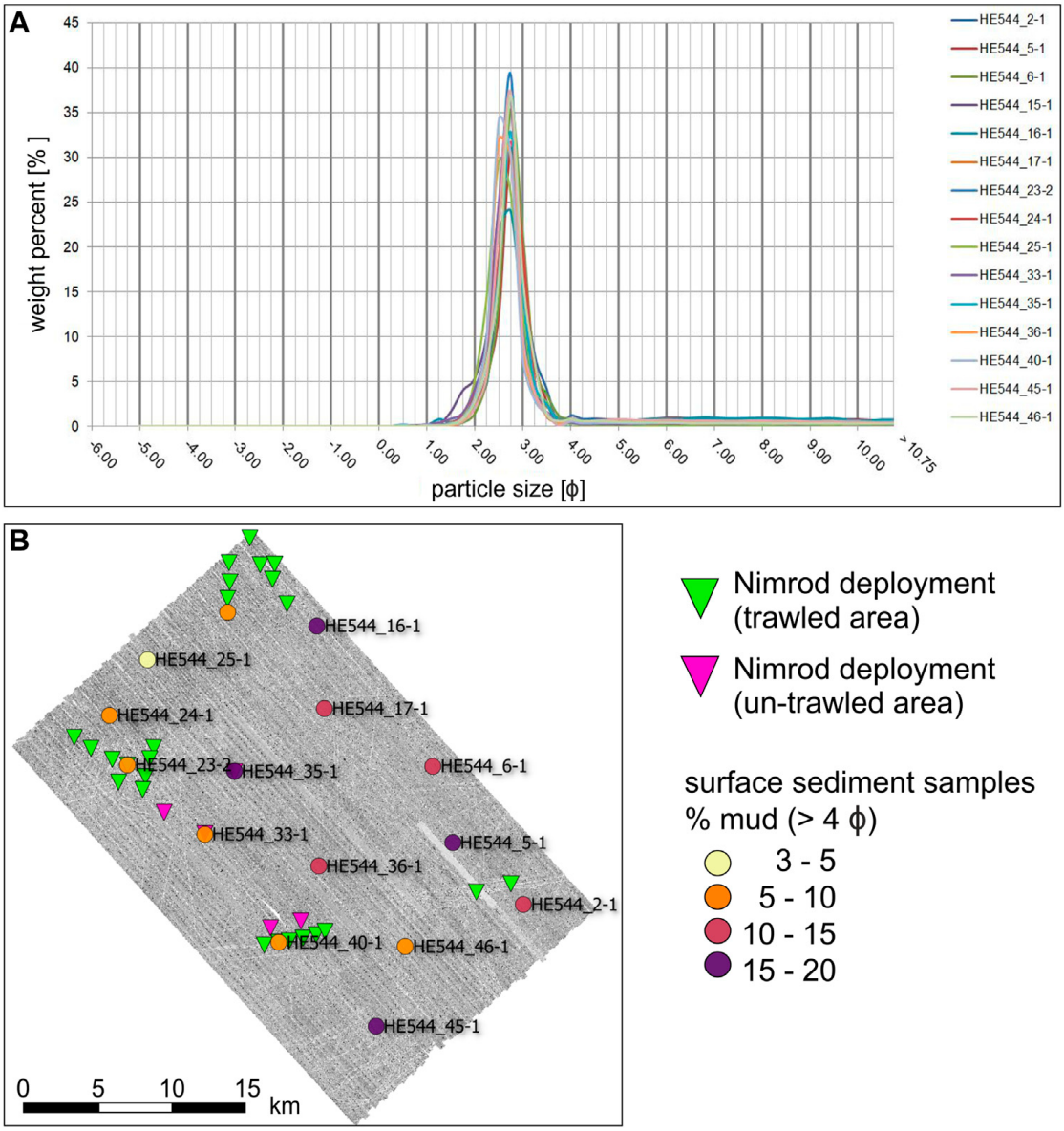

Figure 4.5: The grain size distribution at *HE544* site. (a) The samples show an unimodal distribution with modes between 2.5 ϕ and 3 ϕ. The mud content (> 4 ϕ) ranges between 3 % and 20 %. The statistical analysis shows that the samples are well to very poorly sorted (σ_1 between 0.4 ϕ and 2.4 ϕ), very fine skewed (Sk_1 between 0.2 and 0.8) and extremely leptokurtic (K_G > 3) (b) The *Nimrod* deployments were carried out in areas where the mud content was below 15 %.

4.4.2 Penetrometer data

The maximum penetration depth (pen_{max}) and the maximum quasi-static bearing capacity ($qsbc_{max}$) were determined for each *Nimrod* deployment. From pen_{max} and $qsbc_{max}$, the mean values (pen_{maxM} and $qsbc_{maxM}$) were calculated for each area (trawled and un-trawled) at *HE544* site: for the un-trawled area (Figure 4.6) $qsbc_{max}$ ranges between 58.92 ± 8.84 kPa and 127.3 ± 19.1 kPa ($qsbc_{maxM}$ = 77.7 ± 11.67 kPa). For the trawled area (Figure 4.6b, Table 4.1) $qsbc_{max}$ is

between 7.89 ± 1.18 kPa and 109.1 ± 16.4 kPa ($qsbc_{maxM}$ = 58.6 ± 8.8 kPa). The value pen_{max} varies between 0.04 mbsf (meters below seafloor) and 0.39 mbsf (mean 0.18 mbsf) regarding the un-trawled area (Figure 4.6a, Table 4.1). The trawled area (Figure 4.6b, Table 4.1) shows a range in pen_{max} of 0.02 mbsf up to 0.72 mbsf (pen_{maxM} 0.31 mbsf). At un-trawled stations, $qsbc_{maxM}$ is higher compared to trawled stations, which corresponds to the lower pen_{maxM}. The very high values of $qsbc_{max}$ >100 kPa observed at three deployment stations at *HE544* site may reflect shelly layers or other obstacles with high sediment strength which are possibly located a few centimeters to a decimeter below the seabed surface and hindered the probe to penetrate deeper. This would also explain the rather low penetration depths (pen_{max}) of 0.1 to 0.2 mbsf at the three stations.

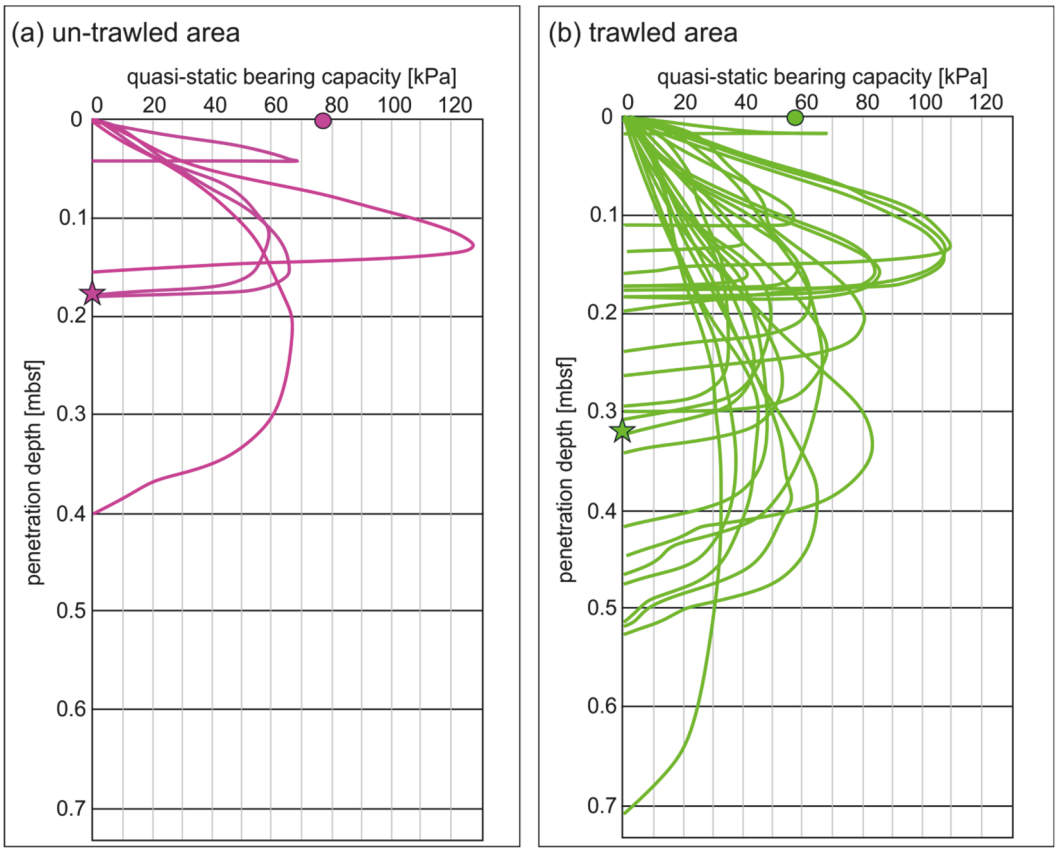

Figure 4.6: Penetration depth (mbsf = meters below seafloor) plotted against the quasi-static bearing capacity (kPa) derived from *Nimrod* measurements. In general, the quasi-static bearing capacity increases with depth until the maximum is reached and the penetrometer is not able to penetrate further into the seabed. (a) In the un-trawled area, lower penetration depths and higher quasi-static bearing capacities were obtained compared to the trawled area (b). The mean maximum penetration depth of un-trawled stations (a, pink star, 0.18 mbsf) is roughly half as low as the mean maximum penetration depth observed at trawled stations (b, green star, 0.31 mbsf). The mean maximum quasi-static bearing capacities are 77.7 ± 5.8 kPa (a, pink circle) and 58.6 ± 4.4 kPa (b, green circle).

Table 4.1: Maximum penetration depth pen_{max} in mbsf (meters below seafloor) and the maximum quasi-static bearing capacity $qsbc_{max}$ in kPa (please note an uncertainty of 15 %) measured with the dynamic free-fall penetrometer *Nimrod* in the un-trawled and the trawled area of the *HE544* site. The mean values pen_{maxM} and $qsbc_{maxM}$ refer to the arithmetic mean of pen_{max} and $qsbc_{max}$, respectively, across each area (un-trawled and trawled).

	pen_{max} [mbsf]			$qsbc_{max}$ [kPa]		
	min.	*max.*	pen_{maxM}	*min.*	*max.*	$qsbc_{maxM}$
un-trawled	0.04	0.39	0.18	58.92	127.3	77.7
trawled	0.02	0.72	0.31	7.89	109.1	58.6

The individual *Nimrod* deployments can be divided into three clusters (I-III) and two isolated deployments (Figure 4.7a). The values pen_{max} and $qsbc_{max}$ were averaged (arithmetic mean) over each cluster (Figure 4.7b-d). In cluster I, the mean pen_{max} of 0.38 mbsf and the mean $qsbc_{max}$ of 63.63 ± 9.54 kPa were the highest (Figure 4.7b). The mean pen_{max} in cluster I is similar to pen_{maxM} of the trawled area (Table 4.1) and the mean $qsbc_{max}$ in cluster I is slightly higher than $qsbc_{maxM}$ in the trawled area (Table 4.1). Cluster II shows a lower mean pen_{max} of 0.22 mbsf and a similar mean $qsbc_{max}$ of 60.15 ± 9.02 kPa like cluster I (Figure 4.7c). The mean pen_{max} of cluster II is rather in the range of pen_{maxM} of the un-trawled area (Table 4.1), but the mean $qsbc_{max}$ observed in cluster II is still comparable to $qsbc_{maxM}$ of the trawled stations (Tabele 4.1). The southern cluster III shows a similar mean pen_{max} of 0.36 mbsf like cluster I, but an even lower mean $qsbc_{max}$ of only 41.86 ± 6.28 kPa (Figure 4.7d). The mud content derived from surface sediment samples is between 6.5 % and 9 % across the clusters (Figure 4.7 b-d).

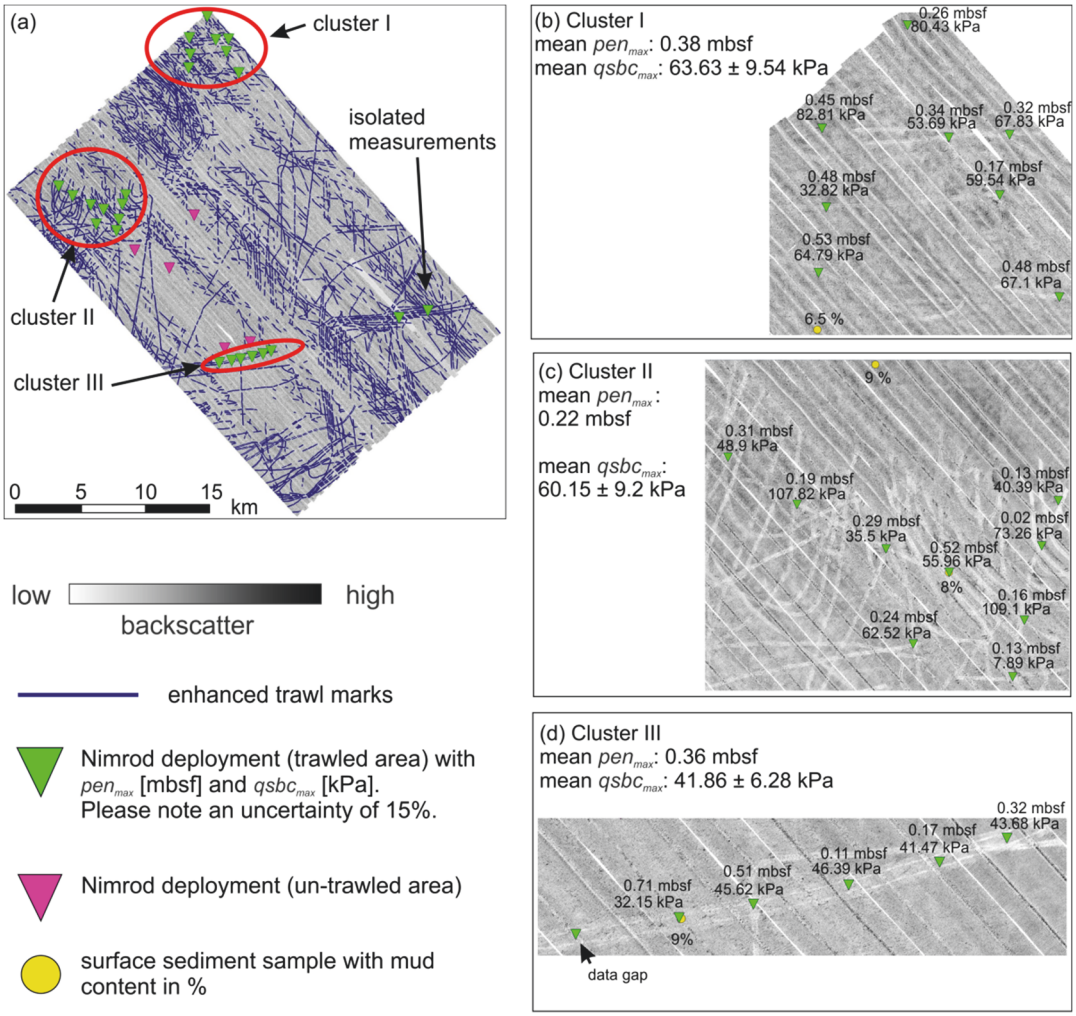

Figure 4.7: (a) The *Nimrod* deployments in the un-trawled (pink triangles) and in the trawled area (green triangles) can be divided into three clusters. (b-d) The values pen_{max} (in meters below seafloor, mbsf) and $qsbc_{max}$ (kPa) of each individual deployment are shown as well as the mean pen_{max} (cluster I: 0.38 mbsf, cluster II: 0.22 mbsf and cluster II: 0.36 mbsf) and mean $qsbc_{max}$ (cluster I: 63.63 ± 9.54 kPa, cluster II: 60.15 ± 9.02 kPa, cluster II: 41.86 ± 6.28 kPa) of each cluster. The mud content is between 6 .5 % and 9 % (yellow circles) throughout the three clusters.

4.5 Discussion

The quasi-static bearing capacity of the sediment denotes the maximum load per unit area that the soil can bear prior to failure and is an expression for sediment strength. In the un-trawled area, $qsbc_{maxM}$ is 77.7 ± 11.67 kPa and pen_{maxM} is 0.18 mbsf, whereas it is 58.6 ± 8.8 kPa and 0.31 mbsf, respectively, in the trawled area (Figure 4.6, Table 4.1). Thus, there is a difference of roughly 20 kPa and 0.2 m between what is assumed to be unaffected sediment (un-trawled) and what is considered as recently mobilized sediment (trawled). Using the *Nimrod* penetrometer, Stark et al. (2009) could identify mobilized sediment in a tidal channel in northern Germany, and

Stark and Kopf (2011) recorded mobile sediment at a wind turbine test site (*Alpha Ventus* site), approx. 40 nautical miles south of *HE544* site. However, in both studies, the authors used a different tip for *Nimrod* (60° opening angle) and thus, only the relative quasi-static bearing capacity values are compared here: They could find a difference of approx. 10-40 kPa between less and more consolidated sediments, which is in agreement with the data presented in this study.

The *HE544* results shown here suggest, that the penetration depth is higher and the quasi-static bearing capacity is lower in areas where bottom trawling took place shortly before and/or parallel to the survey compared to areas where trawl marks were absent, i.e., trawling never happened or took place further in the past. However, reduced sediment strength (= quasi-static bearing capacity) of natural origin such as reworking by currents and waves, lateral changes in sediment type or bioturbation have to be considered: The water depth at the *HE544* site ranges between 39 m and 42 m and morphological change is absent (Figure 4.1). Reworking by waves is therefore evenly distributed across the study area, whereas the influence of tidal currents is small compared to wave driven reworking (Aldridge et al., 2015).

At *HE544* site, modelled mean shear stress by currents is below 0.12 Nm^{-2} and mean shear stress by waves is smaller than 0.25 Nm^{-2} (Bockelmann et al., 2018). Thus, sediment transport and reworking occurs only under heavy weather conditions when the effective wave-base reaches the seabed. According to Son et al. (2012) and Flemming (2005), the effective wave-base reaches a seabed at a few tens of meters water depth only under stormy conditions (e.g., at 28 m during a storm with a significant wave height of 2.4 m and a wave period of T = 6 seconds). The SSS backscatter data presented here (Figure 4.3a) do not indicate bedforms, which agrees with Aldridge et al. (2015), who concluded that a disturbance of the seabed in the upper 5 cm by waves may occur a few days per year in the sea area of *HE544* site. Therefore, it is assumed that re-working by currents and waves has played (and plays) a minor role throughout the *HE544* site.

The analysis of the grain size distribution shows that the main sediment component is fine sand, and that the mud content as a secondary component varies across the study area (Figure 4.5b). However, it is evenly distributed in the trawled areas (6 % - 9 %). In the un-trawled areas, similar quasi-static bearing capacities could be measured at sediment sample stations with different mud content. For example, *Nimrod* stations 34-1 (16 % mud, sediment sample 35-1) and 32-1 (7 % mud, sediment sample 33-1) both show a quasi-static bearing capacity of roughly 65-70 kPa. Therefore, we assume that natural changes in the bulk density and the void ratio, which influence the sediment strength or quasi-static bearing capacity as well (Stark et al., 2011b) play a minor role in determining the quasi-static bearing capacity at the *HE544* study site. Moreover, the

quasi-static bearing capacity depends on particle shape and the friction angle of the sediment (Stark et al., 2011b). It is very unlikely that these factors vary across the *HE544* site, because the sedimentary and current conditions are stable. Stark et al. (2011b) could show that the quasi-static bearing capacity depends also on the material of the individual grains; carbonate sand had higher quasi-static bearing capacities compared to siliciclastic sand. At the *HE544* site, the sediment can be described as siliciclastic sand throughout and thus, a change in material composition as an explanation for the differing quasi-static bearing capacity can be ruled out. Following these assumptions, the differences in quasi-static bearing capacity and penetration depth between the two areas (trawled and un-trawled) are probably not related to lateral changes in sediment type. However, to consider bulk density, void ratio and particle shape as similar across the study site only based on the grain size distribution and the knowledge of the predominant transport mechanisms is just a rough estimation.

The occurrence of benthic organisms may decrease sediment strength due to bioturbation (e.g., Krantzberg, 1985, Dairain et al., 2020). The epibenthic biomass as an indicator for the biological productivity is relatively high at the *HE544* site and common benthic species are, for example, bivalves, brittle stars and amphipods (e.g., Pesch et al., 2008, Neumann et al., 2017). However, Dairain et al. (2020) found that the bivalve *Cerastoderma edule* as well as microphytobenthos have a minor contribution to sediment stability in non-cohesive sediments, which applies to the northern and westernmost parts of the *HE544* site, where the mud content is below 10 % and where the majority of *Nimrod* samples of were taken (Figure 4.5b). Some species may decrease the sediment stability, i.e., the structural fabric, in cohesive sediments by grazing on microflora (Grant and Daborn, 1994) or by moving within the upper centimeters of the sediment (Winterwerp et al., 2012). However, it is difficult to determine the exact contributions of bioturbation to sediment stability (e.g., Winterwerp et al., 2012, Dairain et al., 2020) and to distinguish the influence of bioturbation on sediment disturbance from that of bottom trawling (Oberle et al., 2016b). Thus, it is a rough estimation based on the knowledge of the predominant benthic species that bioturbation plays a minor role in sediment strength at the *HE544* site.

The spatial analysis of the trawled areas shows similar mean $qbsc_{max}$ values in the northern part of the *HE544* site (63.63 ± 9.54 kPa in cluster I and 60.15 ± 9.02 kPa in cluster II (Figure 4.7b,c). The southern cluster III has a lower mean $qbsc_{max}$ of 41.86 ± 6.28 kPa (Figure 4.7d). The mud content in the sediment grab samples of the three clusters ranges between 6.5 % and 9 % and thus, it is considered unlikely that the grain size distribution has a major influence on the quasi-static bearing capacity. Bruns et al. (2020) found that the overall density of 6 - 13 trawl marks per km^2 (beam trawl marks and otter trawl marks cumulated) at cluster I was higher compared to the area of cluster II, which showed a trawl mark density of 6 - 8 marks per km^2 (only beam

trawl marks, otter trawl marks were absent). The area of cluster III has the lowest quasi-static bearing capacity (Figure 4.7d) and lowest trawl mark density of 2 - 3 marks per km^2 (only beam trawl marks, otter trawl marks were absent) as calculated by (Bruns et al., 2020). The deployments of cluster III are orientated along the center of a single, prominent trawl mark (Figure 4.7d). Its good visibility in the SSS data indicates recent trawling activity and thus recent sediment mobilization as well. The deployments of the other clusters are distributed across areas where a mesh-like pattern of trawl marks was observed in SSS data (Figure 4.7b,c), which is reflected by the higher trawl mark density. Here, the variety of trawl marks with good visibility (recent trawling activity) and less good visibility (less recent trawling activity) is higher. Therefore, it is likely that the mean $qbsc_{max}$ and mean pen_{max} values of clusters I and II also reflect this mix of highly impacted sea floor (recent trawling activity) and less impacted seafloor (less recent trawling activity). It is unknown how much time passed between the single, recent trawling event in cluster III and the multiple, less recent trawling events (clusters I and II). However, the results suggest that a single recent trawling event lowers the sediment strength more than multiple events that occurred over time.

Considering all the points discussed above, the data presented in this study unambiguously show that bottom trawling alters the seabed by means of a decreased quasi-static bearing capacity, i.e., sediment strength. A possible explanation may be a decrease in bulk density due to sediment amalgamation after bottom trawling occurred, as described by Aspden et al. (2004). Another explanation for the decreased quasi-static bearing capacity could be an increased accumulation of soft or less dense, silty material as observed by Stark and Kopf (2011) related to scouring at a wind farm test site. The accumulation of fine-grained sediment may be induced by trawling as well. For example, Trimmer et al. (2005) and Gilkinson et al. (2015) showed that in areas where disturbances due to currents and waves are low, chronic trawling causes an increase of the fine fraction because the fine grained material is re-suspended by trawling and settles back directly in the area that was touched by the bottom trawling gear instead of being transported away to settle elsewhere. This is in concordance with the backscatter signature of the trawl marks at *HE544* site (Figure 4.3c) and Bruns et al. (2020) interpreted the backscatter pattern as follows: The center of the trawl mark is characterized by a narrow strip of higher backscatter values due to coarsening and/or increased roughness due to mechanical interactions of the trawl gear with the seabed but it is surrounded by a prominent low backscatter area indicating either finer material or a decreased roughness of the seabed. However, high resolution vertical and lateral sediment sampling would be necessary to investigate selective transport in-depth.

From the change of quasi-static bearing capacity with depth, Stark et al. (2009) and Stark et al. (2011b) could derive that sediment mobilization on the seabed surface is characterized by a less

consolidated layer with a thickness of a few centimeters on top of a more consolidated layer. Within the top layer, the quasi-static bearing capacity increases more slowly with depth compared to the underlying, more consolidated layer (Stark et al., 2009, Stark and Kopf, 2011). Such a layering could not be observed in this study; neither in the quasi-static bearing capacity data nor in the sediment samples. The increase of quasi-static bearing capacity with depth at *HE544* site is rather comparable with the data obtained by Stark et al. (2009) and Stark et al. (2011b) at the *Alpha Ventus* study site, which they classified as homogenous, i.e., absent or very low sediment mobilization. Considering a penetration depth of the trawl gear of ≥ 10 cm in mixed sediments (Bruns et al., 2020, Eigaard et al., 2016), about 90 % of the *Nimrod* samples in the trawled area should have penetrated as far as the trawl gear. Geochemical analyses, however, showed that bottom trawling may alter the sediment structure up to 35 cm deep into the subsurface (e.g., Oberle et al., 2016b, Bunke et al., 2019). Hence, only 8 *Nimrod* samples may have reached the pristine subsurface at the *HE544* site and a sampling setup with higher penetration depths is needed in order to make even more robust statements concerning a possible layering.

4.6 Conclusion

This study strongly suggests a difference in sediment strength comparing a trawled and an un-trawled area of seabed in the German North Sea: The quasi-static bearing capacity and the penetration depth were roughly 20 kPa lower and 0.13 m higher, respectively, in trawled areas compared to un-trawled ones. The changes in sediment strength (i.e., quasi-static bearing capacity) likely reflect sediment, which was re-suspended by bottom trawling and re-settled within the trawl marks or in direct vicinity and thus, also a decrease in bulk density of the surface sediments due to sediment amalgamation within the trawled region. The identification of different layers (less consolidated above more consolidated sediment) indicating mobilized sediment as observed by Stark et al. (2009) and Stark et al. (2011b), was not possible in this study. This is probably related to a limited overall penetration depth of the dynamic penetrometer and therefore the pristine subsurface (i.e., not influenced by bottom trawling) could not be reached.

The differences in sediment strength measured in this study were attributed to trawling. Reworking by currents and waves, lateral changes in sediment type and bioturbation may contribute to changes in sediment strength, but were estimated to be of minor importance at the study site. The stronger impact is inferred from the trawling, as attested by lower strength in the trawl marks, which is most likely a consequence of fluid entrainment when the fishing gear ploughs through the seabed sediment.

If the strength of the surface sediment is decreased due to bottom trawling, as this study suggests, it is more likely to be mobilized, both by recurring bottom trawling as well as natural events such as storm surges. This may alter the general sediment budget in the area (Paradis et al., 2021) and therefore the benthic habitat. The loss of organic carbon induced by bottom trawling and a following loss of fauna may be the consequence (De Borger et al., 2021). Not only nutrients can be remobilized more easily but contaminants as well, which may be taken up by benthic species (Bradshaw et al., 2012). Therefore, it is highly recommended to further assess the decrease of sediment strength as a result of bottom trawling in order to enable sustainable management strategies on bottom trawling.

4.7 Acknowledgements

This research was conducted in the framework of the ASKAWZ project, which is a research and development cooperation between Senckenberg am Meer (SaM) and the German Federal Maritime and Hydrographic Agency (BSH, Bundesamt für Seeschifffahrt und Hydrographie, ASKAWZ III Contract-No. 10038520). ASKAWZ is part of the *SedAWZ* project, which is coordinated by BSH and funded by German Federal Agency for Nature Conservation (BfN, Bundesamt für Naturschutz).

The authors like to thank the Captain and Crew of R/V Heincke for the professional support onboard. We are grateful to our deceased colleague Dr. Peter Holler, who was the chief scientist during the survey HE544 and provided fruitful feedback towards the interpretation of the SSS dataset. Moreover, we appreciate the help of Christian Zöllner (MARUM) when designing and providing the customized tip for the *Nimrod* deployments during HE544, and the outstanding and continued advice by Dr. Robert Roskoden concerning the *Nimrod* data processing. Acknowledgements also go to our lab staff Astrid Raschke (SaM) for supporting the work on the grain size samples as well as to all our student assistants contributing to survey HE544.

4.8 References

Please find the references within the overall reference list of this thesis (chapter 8).

5 Automated mapping of bottom trawling impact

Ines Bruns[1], Alexander Bartholomä[2]

[1]Department of Geosciences, University of Bremen, Klagenfurter Straße 4, 28359 Bremen, Germany

[2]Senckenberg am Meer, Department for Marine Research, Südstrand 40, 26382 Wilhelmshaven, Germany

In preparation for the submission to Remote Sensing

5.1 Abstract

Bottom trawling has a significant impact on marine habitats on a global scale. It displaces compresses and re-suspends seabed sediment, which can disturb sessile and benthic flora and fauna. The monitoring of fishing activity is implemented in strategies that deal with marine spatial planning and nature conservation. However, estimating bottom trawling activity on habitats on a regional scale is challenging because most monitoring approaches focus on highly aggregated data (e.g., fishing effort based on VMS-data). Thus, mapping trawl marks (TM) from hydro-acoustic surveys may be a useful and supporting method, given that enough resources are available for such time and cost extensive mappings. Image classification algorithms were already successfully applied on hydro-acoustic data in numerous studies that demonstrate cost saving approaches for seabed mapping. There are only a few studies that focus on the automated detection of TM and usually, these approaches require skills in programming and image processing. In order to make such approaches more accessible, we are presenting a straightforward procedure for the automated detection of TM in side scan sonar data by using an unsupervised image classification algorithm that is included in the open source geographic information system (GIS) applications GRASS GIS (Geographic Resources Analysis Support System) and QGIS.

5.2 Introduction

The anthropogenic impact on the marine environment is divers and can include pollution due to dense ship traffic, resource extraction such as oil and gas or fishery. Fishery is conducted in various sea regions and concentrates in the shelf seas (Guiet et al., 2019). Different techniques are in use, e.g., gillnets, pelagic trawling and bottom trawling (Guiet et al., 2019). Bottom trawling, in particular, has a significant impact on the marine environment as it directly affects the seabed. This fishing method may be a potential threat to both targeted species and benthic organisms

that are adversely affected by the trawling gear (Lindeboom and de Groot, 1998, Buhl-Mortensen et al., 2016). Moreover, it can alter the seabed by means of erosion (Coughlan et al., 2015), changes in the sediment budget (Paradis et al., 2021) and re-suspension of biogeochemical components (Morys et al., 2021).

Consequently, several approaches have been developed to incorporate the impact of bottom trawling in strategies concerning marine spatial planning and nature conservation (e.g., Stelzenmüller et al., 2015, Buhl-Mortensen and Buhl-Mortensen, 2018). However, monitoring bottom trawling activities can present significant challenges due to the vast sea areas involved and the numerous fishing fleets operating within them. Since 2012 fishing vessels of a certain size (> 12 m length over all) are committed to transmit their geographical positions (EC, 2009) from which, together with log book information, fishing activity maps can be derived (ICES, 2019). Such maps usually have a spatial resolution of 0.05° * 0.05° and the data is often aggregated over one year (ICES, 2019). For particular scientific questions this resolution may be too coarse (Shepperson et al., 2017). Alternatively, evaluating the effects of bottom trawling through the analysis of trawl marks (TM) could be a viable approach to estimate regional and/or seasonal fishing activity, thereby providing insights into its impact on the seabed (Mérillet et al., 2018, Buhl-Mortensen et al., 2016). TM are elongated furrows formed on the seabed as a result of the passage of heavy trawling gear (Mérillet et al., 2018, Krost et al., 1990, Lüdmann et al., 2021). The can be identified through the analysis of backscatter data from side scan sonars (SSS) and bathymetry data from multibeam echo sounders (MBES). (e.g., Friedlander et al., 1999, Lucchetti and Sala, 2012, Bruns et al., 2020, Schönke et al., 2022).

The resolution of SSS and MBES data can be in the cm-range and, thus, enables precise mapping of the seabed while simultaneously covering a relatively large area. (e.g., Harris and Baker, 2012, Mielck, 2015, Bartholomä et al., 2019). These hydro-acoustic techniques have proven to deliver reliable information about seabed characteristics from which sediment and habitat maps can be derived (e.g., Buhl-Mortensen et al., 2015, Galvez et al., 2021). For instance, backscatter data can reveal lateral variations in the roughness of the seabed, which can be attributed to the presence of bedforms or changes in the distribution of grain sizes on the seabed surface (e.g., Goff et al., 2000, Lurton, 2002). Besides these lateral extensive seabed features, also single objects such as pipelines, mines and boulders can be mapped with hydro-acoustic devices (Michaelis et al., 2019, Papenmeier, 2018, Hovland and Indreeide, 1980).

Mapping (TM) in hydro-acoustic data represents a promising method to quantify the impact of bottom trawling. However, the classification of extensive datasets and the extraction of relevant features for further analysis can be time-consuming and costly. Additionally, the interpretation

of various sediment types and features often relies on the expertise of the investigator. As a result, the use of image classification and machine learning algorithms in habitat mapping has gained attention in recent years. (e.g., Lucieer, 2008, Fakiris, 2016, Michaelis et al., 2019). MBES data are highly valuable for automated seabed mapping due to their ability to provide multi-band information. This multi-band data offers a greater amount of information that can be integrated into the classification algorithm, surpassing the capabilities of single-band side scan sonar (e.g., Alevizos et al., 2015, Wan et al., 2022). However, SSS mapping can have advantages over MBES when low grazing angles for e.g., object detection or a water depth independent seabed mapping is needed (Kenny et al., 2003). Due to the beam geometry of MBES systems, the swath width and therefore the coverage of the seabed is strongly reduced (Lurton, 2002). For example, in 100 m water depth the maximum swath width is 200 m, whereas it is only 90 m in 12 m water depth (Grządziel and Wąż, 2016). Thus, in shallow water environments, SSS mapping may be preferred for the sake of a cost and time optimized survey design.

The SSS mosaics are usually gray scale raster images and in order to automatically classify areas according to different gray scale signatures, image statistics can be calculated. First order statistics (grey level histogram) provide information on the reflectivity and second order statistics by means of grey level co-occurrence matrices (GLCMs) allow the analysis of texture (e.g., Haralick et al., 1973, Fakiris and Papatheodorou, 2012). To identify areas with similar characteristics in the SSS mosaic, the classification algorithm employs a clustering approach. It groups together statistical signatures that exhibit similarities and assigns them to classes when using an unsupervised classifier (Zhao et al., 2017). A supervised classification in contrast requires a dataset containing the expected and labeled classes, which are provided by the user, in order to train the classifier. The classifier then uses this training dataset to classify the features in the mosaic based on their characteristics and assigned labels. (Serpetti et al., 2011). The generation of such training datasets requires a good understanding and knowledge of the investigated area as it involves the collection and labeling of representative samples from different classes, which can be a challenging and resource-intensive task (e.g., Pillay et al., 2021, Lin et al., 2023).

The advantages of automated seabed classification based on hydro-acoustic data may be utilized to automatically map TM and, hence, reduce the time and costs for e.g., trawl impact assessment or monitoring trawling activities. However, the number of studies that focus on the automated detection of TM in hydro-acoustic datasets is limited. Schönke et al. (2022) showed that TM can be detected in MBES bathymetry data by applying smoothing algorithms and thresholds using Matlab toolboxes. Inshore MBES datasets, like those Schönke et al. (2022) used, are less biased by limitations in tide correction, however, the accuracy of bathymetric data is significantly

reduced in datasets obtained far offshore due to the lack of measured tide data (Calder and Mayer, 2003). Sams et al. (2004) performed automated image classification on SSS data and they were able to determine trawled seabed areas but the information on individual TM was limited. Gonzales (2004) used an edge detection algorithm by means of a "Canny"-filter that was sensitive to noise with linear shapes. "Haar"-like features were used by Gournia et al. (2019) to detect TM in SSS backscatter data. All methodologies have yielded valuable outcomes; however, they typically necessitate proficiency in programming and image processing, which can be rather challenging for individuals who are new to the field or have limited exposure to such techniques. To our knowledge, no previous studies have addressed automated trawl mark recognition in hydro-acoustic data and outlined workflows that avoid the need for programming skills or extensive knowledge of image processing. As a result, we employed an unsupervised classification algorithm on two distinct SSS datasets obtained from the German North Sea, which exhibit a dense, mesh-like pattern of trawl marks. This analysis was conducted utilizing standard functions and straightforward add-ons within the open-source geographic information system (GIS) application QGIS.

5.3 Materials and Methods

5.3.1 Study sites

The North Sea is a shelf sea and the slope is relatively gentle in the German EEZ. Here, water depths are increasing slightly from <10 m near the coast to >50 m in the north-westernmost part (Figure 5.1). In coastal waters the hydrodynamics are mainly tide driven and more wave driven in the central part of the North Sea (Aldridge et al., 2015), which is reflected by the sediment distribution (Stanev et al., 2009, Sündermann and Pohlmann, 2011). The sedimentary inventory and the morphology of the German North Sea have been mostly influenced by the Pleistocene sequence of glacial and interglacial cycles during the Saalian (300 ka BP – 126 ka BP) and earlier glacials (Zeiler et al., 2008). At the beginning of the Holocene (ca. 10 ka BP), the sea level began to rise and the Saalian (and older) glacial and periglacial sediments were reshaped by waves and currents. This resulted in mobile sand layers and lag deposits, which form the Holocene sediments in the German North Sea (Schwarzer and Diesing, 2006). The process of reworking is still ongoing (Schwarzer et al., 2008).

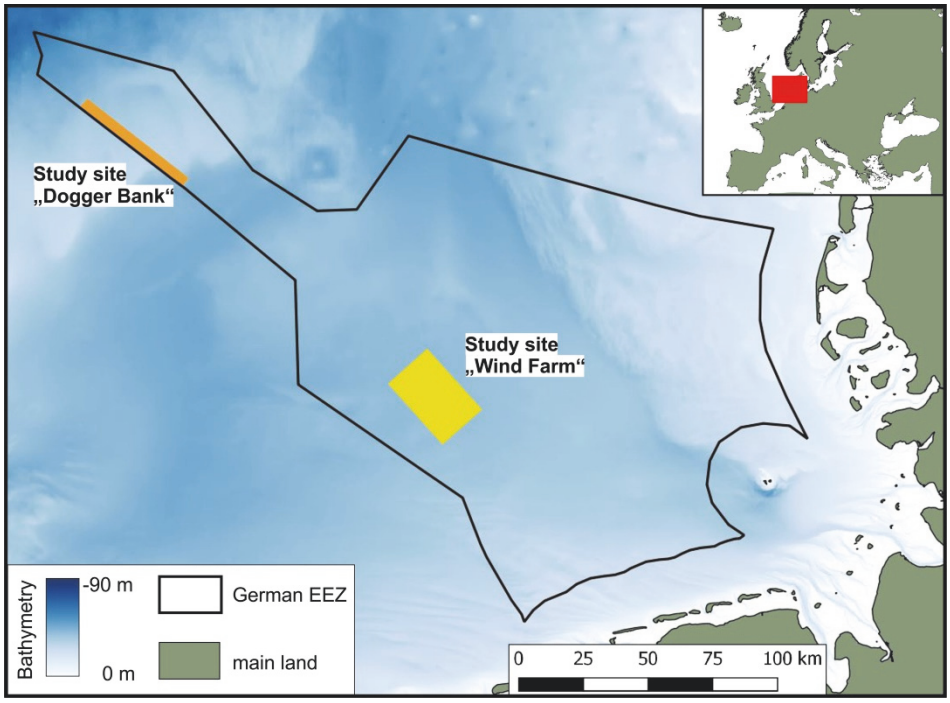

Figure 5.1: The study sites „Dogger Bank” and “Wind Farm” within the German Exclusive Economic Zone (EEZ) in the southern North Sea. Bathymetry is provided by EMODnet-Bathymetry-Consortium (2018).

5.3.1.1 Study site “Wind Farm”

The study site Wind Farm is located in the western German EEZ, approx. 50 nautical miles north of the German coast. The water depths range around 39-42 m (Figure 5.1) and the sediment type was classified as “fine sediment to sand” by Holler et al. (2020). It is homogeneously distributed across the site and bedforms were absent here as well (Holler et al., 2020). The mud content ranged from 3-10 weight % in the northern and western part of the site and up to 20 % in the remaining area and gravel was not observed (Bruns et al., 2020, Holler and Bruns, 2020).

5.3.1.2 Study site “Dogger Bank”

At the study site Dogger Bank in the northern-most part of the German EEZ (approx. 130 nautical miles north of the mainland) the water depths range between 30–40 m (Figure 5.1). This area is associated with the Dogger Bank, which is a topographic height in the central North Sea. Holocene sediments have thicknesses of 1–5 m and in some parts up to 30–40 m (Fitch et al., 2005). Seabed sediments are mainly fine to medium sand with low mud content (< 5%) and no gravel throughout the study site (Laurer et al., 2014, Papenmeier et al., 2019, Holler et al., 2019a). From earlier studies it is known that the sediment type derived from SSS data is homogeneously distributed and bedforms such as dunes and ripples could not identified in SSS data (Papenmeier et al., 2019, Holler et al., 2019a).

5.3.1.3 Trawl marks at the study sites

At both study sites, TM could be identified by Bruns et al. (2020) in the same SSS data sets that were used for this study. They described TM as elongated furrows on the seabed that can intersect each other creating a mesh-like pattern. Common fishing gear types in the southern North Sea are for example beam trawls (TBB) and otter trawls (OTB) (Pedersen et al., 2009, Schulze, 2018). Bruns et al. (2020) found that the majority of TM stem from TBB at the study sites and thus, this study focuses on TBB marks.

Because beam trawls (TBB) are usually towed in pairs, TM that run parallel are common (Figure 5.2a, Bruns et al. (2020). Each TBB generated a mark of approx. 11 m width and the mean total width of a pair is 40 m (Figure 5.2a, Bruns et al. (2020). In the backscatter data, TBB marks appear with increased backscatter intensities in their center, which is bordered by a narrow strip of decreased backscatter intensities compared to the surrounding (Figure 5.2b, Bruns et al. (2020). At the Wind Farm study site, this low backscatter strip is more pronounced (Figure 5.2c) compared to TM at the Dogger Bank study site, which is likely related to the predominant hydrodynamics and sediment type (Bruns et al., 2020).

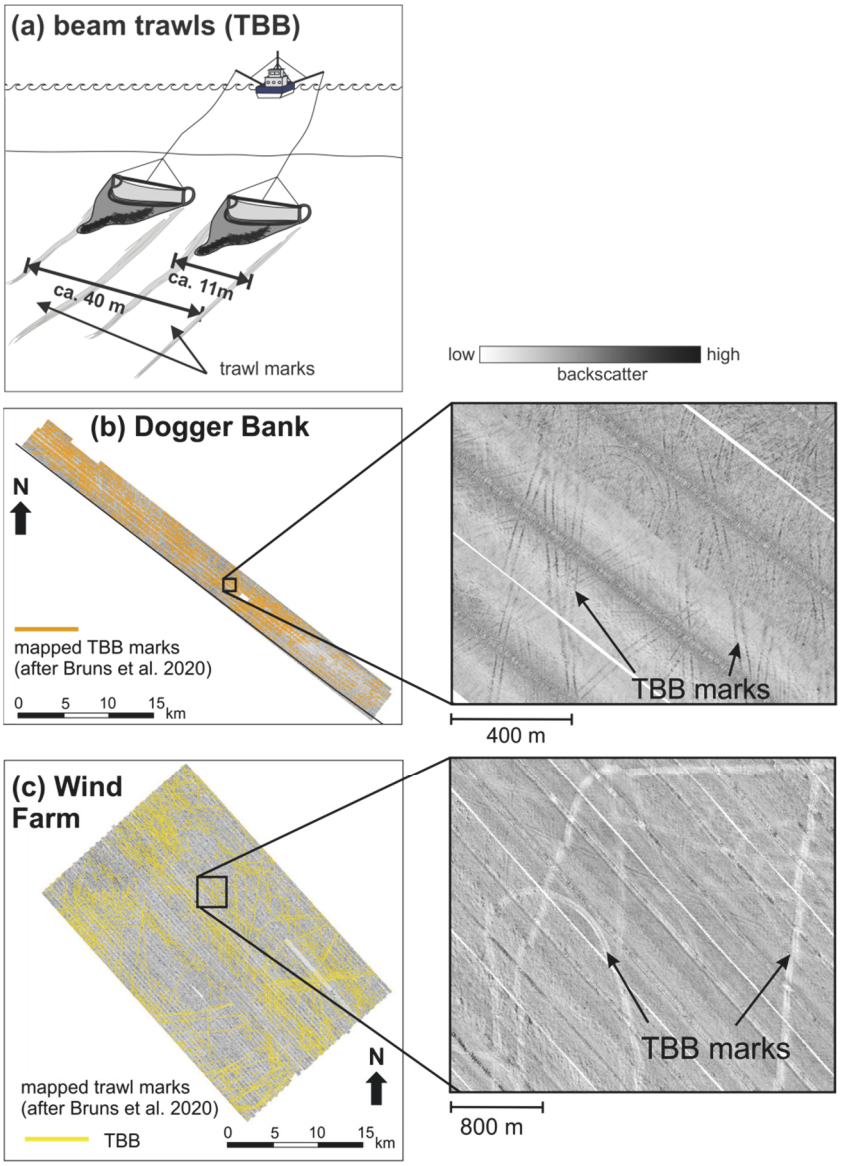

Figure 5.2: (a) Schematic drawing of typical pair-towed beam trawls (TBB) with the dimensions of the corresponding trawl marks (modified after Bruns et al., 2020). (b) Side scan sonar (SSS) mosaic of the Dogger Bank study site. The orange lines represent the trawl marks that were manually mapped by Bruns et al. (2020). The zoom-in shows examples of TBB marks. (C) In the SSS mosaic of the Wind Farm study site, after Bruns et al. (2020) manually mapped TBB marks (yellow lines).

5.3.2 Data acquisition and processing

The SSS dataset that was used in this study consists of two surveys that were conducted in August 2018 (Senckenberg32_2018) and October 2019 (HE544). A prior investigation utilizing the identical SSS datasets demonstrated that trawl marks (TM) exhibit excellent visibility at both study sites, with a calculated spatial density of up to 20 marks per km^2 (Bruns et al., 2020). Thus, the dataset was considered as suitable to perform the automated mapping of TM. The

surveys Senckenberg32_2018 and HE544 were part of the national German seabed mapping program *SedAWZ* (Holler and Bruns, 2020) and the settings for SSS data acquisition followed the guideline for seabed mapping, which was developed in the framework of *SedAWZ* (BSH, 2016). The SSS mosaics were not optimized for the recognition of TM but rather for general sediment type determination.

Table 5.1: List of side scan sonar (SSS) surveys that were carried out in the southern North Sea (German Exclusive Economic Zone) and delivered the SSS datasets for this study.

Survey Name / Vessel	**Study site**	**Date of Survey**	**Survey Area [km2]**	**Water Depth [m]**	**SSS system / Coverage of Survey Area**
Senckenberg 32_2018 / RV Senckenberg	Dogger Bank	22–24 August 2018	230	30–40	KLEIN4000 / 100%
HE544 / RV Heincke	Wind Farm	14–30 October 2019	655	39-42	KLEIN4000 / 100%

During both surveys, a KLEIN4000 two frequency (100 kHz and 400 kHz) SSS system was deployed. The frequencies were operated simultaneously and the beam width is 1° (100 kHz) and 0.3° (400 kHz). The across-track resolution is 9.6 cm and 2.4 m, respectively. The SSS was towed with approx. 5 knots (ca. 2.5 m/s) behind the vessel and the swath (400 m) and survey line spacing (400 m) were planned in order to cover 100% of the seafloor.

For the data acquisition, the software SonarPro14 was used. The automatic gain control (AGC) was turned off and time varying gain (TVG) was active. The post-processing was performed by means of the following procedure using SonarWiz7.01 as described by Bruns et al. (2020): (i) slant-range correction, (ii) an empirical gain normalization was applied in order to correct over- and under-amplified areas, (iii) the build-in de-stripe filter was used to remove artifacts due to tow-fish movements and (iv) the precise positioning within the mosaic was achieved by applying a layback-correction. The resulting mosaics were stored as geoTIFF with a minimum resolution (across and along track) of 1 m in both SSS datasets.

The SSS datasets deliver similar results because the survey settings and post-processing procedure are identical. However, it is important to note that the quality of the SSS data differs between the two surveys due to environmental factors such as weather conditions, sea state, and water turbidity. These variables can vary both within and among surveys, affecting factors

such as signal-to-noise ratio, backscatter absorption, and the potential presence of artifacts. Consequently, the automated identification of trawl marks (TM) in the SSS data may also be influenced by these variables. Additionally, the quality of TM depiction varied between the SSS mosaics at different frequencies. In the high-frequency (400 kHz) image, the trawl marks appeared narrow and less distinct, while they exhibited greater prominence in the low-frequency (100 kHz) image, as previously described by Bruns et al. (2020). Therefore, this study focuses on the low frequency image.

5.3.3 Image preparation and classification algorithm

The objective of this study was to develop an image classification methodology for SSS data that is accessible to a broad range of users. Accordingly, the processing of the SSS mosaics, including automatic classification and image preparation, was conducted using the open source geographic information system (GIS) software QGIS 3.30 (QGIS-Development-Team, 2023), which is a widely used GIS-software. Within QGIS, the GRASS GIS 8.2 (Geographic Resources Analysis Support System) application is integrated (GRASS-Development-Team, 2022). GRASS GIS offers specialized functions that are not available in the standard version of QGIS, including the classification algorithm. While GRASS GIS allows the execution of functions using Python code, many functions are also supported by a graphical user interface (GUI). GRASS GIS also contains a model builder which allows the concatenation of functions and modules to automate the workflow of the desired processing steps. The Python script of the procedure used in this study can be found in the appendix.

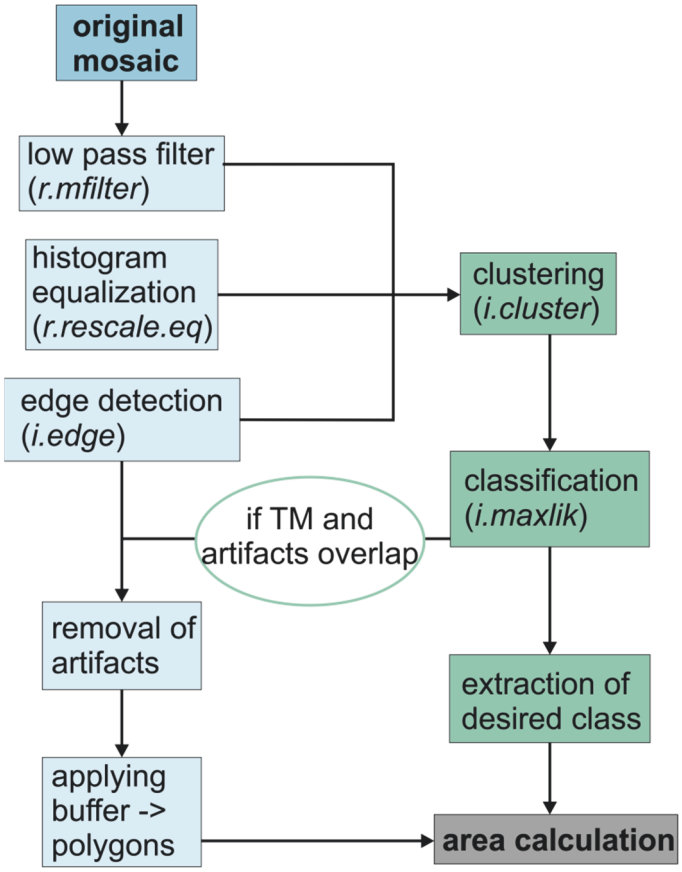

Figure 5.3: Flow chart of the processing steps applied to the original side scan sonar (SSS) mosaics in order to perform the unsupervised classification (clustering) with the used GRASS GIS functions in brackets.

For this study it was decided to focus on an unsupervised classification. In contrast to supervised classification techniques, which need a dataset comprising training data, namely the expected classes with labels, is not required. This bears several advantages: (i) it reduces the time and costs for the classification, (ii) in-depth understanding of the study area (i.e., expected classes) is not necessary, (iii) it can be applied to a variety of SSS datasets without retraining the model. Especially the latter is important in the scope of this study. The backscatter characteristics of the TM differ among the study sites (Figure 5.2). Applying a supervised algorithm would necessitate a distinct training dataset for each survey, which would be contrary to the aim of providing a straightforward, accessible procedure.

Prior to undertaking the unsupervised classification, the SSS mosaics were prepared. Since the surveys had a large geographical extend (Table 5.1), sub-regions of the SSS mosaics (approx. 3 * 6 km and 3.5 * 2 km, Figure 5.4) were extracted. Like the original mosaics, the sub-regions are 8-bit grey scale raster images (geoTIFF), with each individual pixel assigned a value ranging from 0 to 255. To further refine their suitability for analysis the simple GRASS GIS filter

algorithms were used (Figure 5.3, Appendix). With the aim of reducing speckle noise, a low pass filter was employed using the function *r.mfilter*. This particular filter has a soft-focus effect and reduces noise but the general structural elements such as edge are preserved (Figure 5.4, Gonzales (2004). In order to improve the contrast of the mosaics and thus enhancing the clarity of TM (Figure 5.4), a histogram-equalization was executed by applying the function *r.rescale.eq*. The original range of grey values (0-255) remained unaltered, only normalization was applied. The use of both low pass filtering and histogram equalization have previously proven to be beneficial in image classification regarding TM by Gonzales (2004).

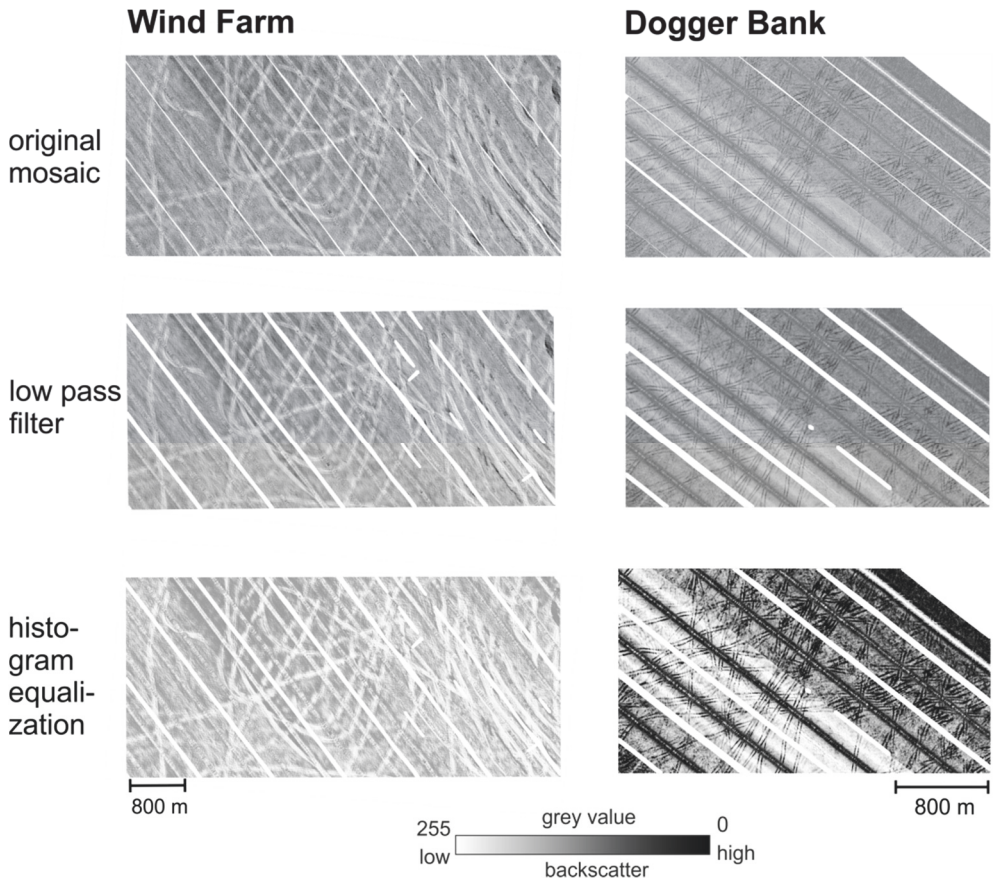

Figure 5.4: Exemplary sub-region from the original side scan sonar mosaics of the Wind Farm and the Dogger Bank study sites (first row). The sub-regions were prepared for the unsupervised classification by applying a low pass filter (second row) and a histogram-equalization (third row).

Further enhancement of the TM was achieved by applying an edge detector based on the Canny filter (Canny, 1986). This is realized by the GRASS add-on *i.edge* (GRASS-Development-Team, 2023). Initially, the image is smoothed with a Gaussian filter and subsequently, the gradient of changes in the grey scale is calculated (GRASS-Development-Team, 2023). By identifying the local maxima, i.e., the edges, these features are enhanced and all non-maximum values are suppressed. Finally, a hysteresis threshold evaluation is performed (GRASS-Development-

Team, 2023). The thresholds are defined by the user and depend on the specific properties of the image. The values that were used in this study can be found in the GRASS GIS model (Appendix). Any values below the lower threshold are designated as weak or no edges while those surpassing the upper threshold, or ranging the thresholds, are identified as true edges (GRASS-Development-Team, 2023). The output is a raster image containing thin lines consisting of the pixels considered as edges.

The raster images derived from the filter outputs (low pass filter, histogram equalization and canny filter) were grouped and regarded as input for the classification (Figure 5.3). The unsupervised classification was performed with the GRASS function *i.cluster,* which is based on k-means clustering (GRASS-Development-Team, 2023). The function identifies clusters (k) based on the means and covariance matrices of the spectral information. Firstly, an initial number of clusters is generated based on the means and standard deviation of the pixels in the mosaic. In this stage, the clusters are all equally separated (measured in Euclidian distance) (GRASS-Development-Team, 2023). During iteration, the pixels are assigned to the closest cluster defined by the minimum separation and new cluster means are calculated forming the basis for another assignment of pixels to the nearest new cluster and this is repeated until the maximum number of iterations or the desired percent convergence is reached (GRASS-Development-Team, 2023). The convergence is the percent of pixels that are stable and do not move anymore between the clusters. The user has to specify the initial number of classes (or clusters), the maximum number of iterations, the convergence and the minimum cluster separation (GRASS-Development-Team, 2023). The number of iterations needs to be sufficiently high so that the desired percent convergence and the minimum separation is achieved or exceeded before the iteration is stopped. A common value for the convergence is 98 % and the cluster separation is typically between 0.5 and 1.5 (Harmon and Shapiro, 2007). The values of these variables are image specific and the values that were used for this study can be found in the GRASS GIS model (Appendix). The outcomes of the clustering are called signatures and are stored in a text file, which also incorporates the class separation matrix. This matrix serves as a graphical representation of the statistical distinctiveness or, in other words, the overlap of the classes. The signature file is the input for the actual classification with the function *i.maxlik*. The function is a maximum-likelihood classifier and assigns the classes to the corresponding pixels by determining the highest probability with which a pixel belongs to a certain class (GRASS-Development-Team, 2023). The classification output is a raster file in which each pixel has the value of its assigned class.

From the classified raster, solely the class containing the targeted TM was extracted from the classified raster and transformed into a vector file and imported to QGIS. The area in m^2 of the

polygon features was determined by using the QGIS field calculator and it represents the area of the seabed that was trawled. This result was then compared with the area of the manually mapped TM (Bruns et al., 2020). The polyline features Bruns et al. (2020) created were buffered by 11 m which is the average width of TBB marks (Bruns et al., 2020). It must be pointed out that the area estimate of the manually mapped TM is only a rough approximation, because the buffer width is based on an average value and, moreover, TM that appear indistinctive in the SSS mosaic may have not been recognized.

In case of the Dogger Bank study site the noise around the nadir was relatively high and the backscatter signatures were comparable to these of the TM. Thus, the class with TM contained a relatively high amount of false positive results. In order to extract the nadir noise, the direction (azimuth) of the polygons was determined. Because the polygons from the classification were too irregular to robustly calculate the azimuth, the output raster of the edge detection was used instead (Figure 5.3). It was converted to vector data and imported to QGIS, which resulted in a polygon file containing linear shapes (edges) around the TM and the nadir. The user-friendly QGIS plugin "Geo Simplification" (Natural-Resources-Canada, 2021) was used to create the centerline of each polygon and for each centerline the direction (azimuth) was calculated. The centerlines representing the nadir were removed by simple filtering for the range of the direction of the nadir, which was 105-135 degrees in this case. After removing these polylines, only the edges of the TM remained and in some areas also edges that were created around roundly shaped artifacts. The centerlines were buffered also by 11 m in order to create a polygon vector file containing the area of the TM for comparison with the manually mapped TM area.

5.4 Results

For the dataset of the Wind Farm study site, the best results in terms of statistical class separation by the k-means clustering algorithm could be achieved by specifying five expected classes (Figure 5.5a). Fewer classes caused the loss of details, i.e., the classes had an insufficient separation. When utilizing six classes, the TM became more fragmented as they were divided into multiple classes. Further increasing the number of classes beyond six did not yield satisfactory results, as the clustering algorithm was unable to identify additional classes with significant statistical separation. As a result, the algorithm automatically provided only six classes, indicating the limitation of achieving distinct separations beyond this point. From a first, subjective visual inspection of the five classes it was determined that class 5 is congruent with the TM, however, small areas of noise are still present (Figure 5.5b). The subsequent

comparison of the calculated area of automatically and manually mapped TM shows that the classification overestimated TM with a deviation from the manually mapped TM of roughly 8.5 % (Figure 5.5c).

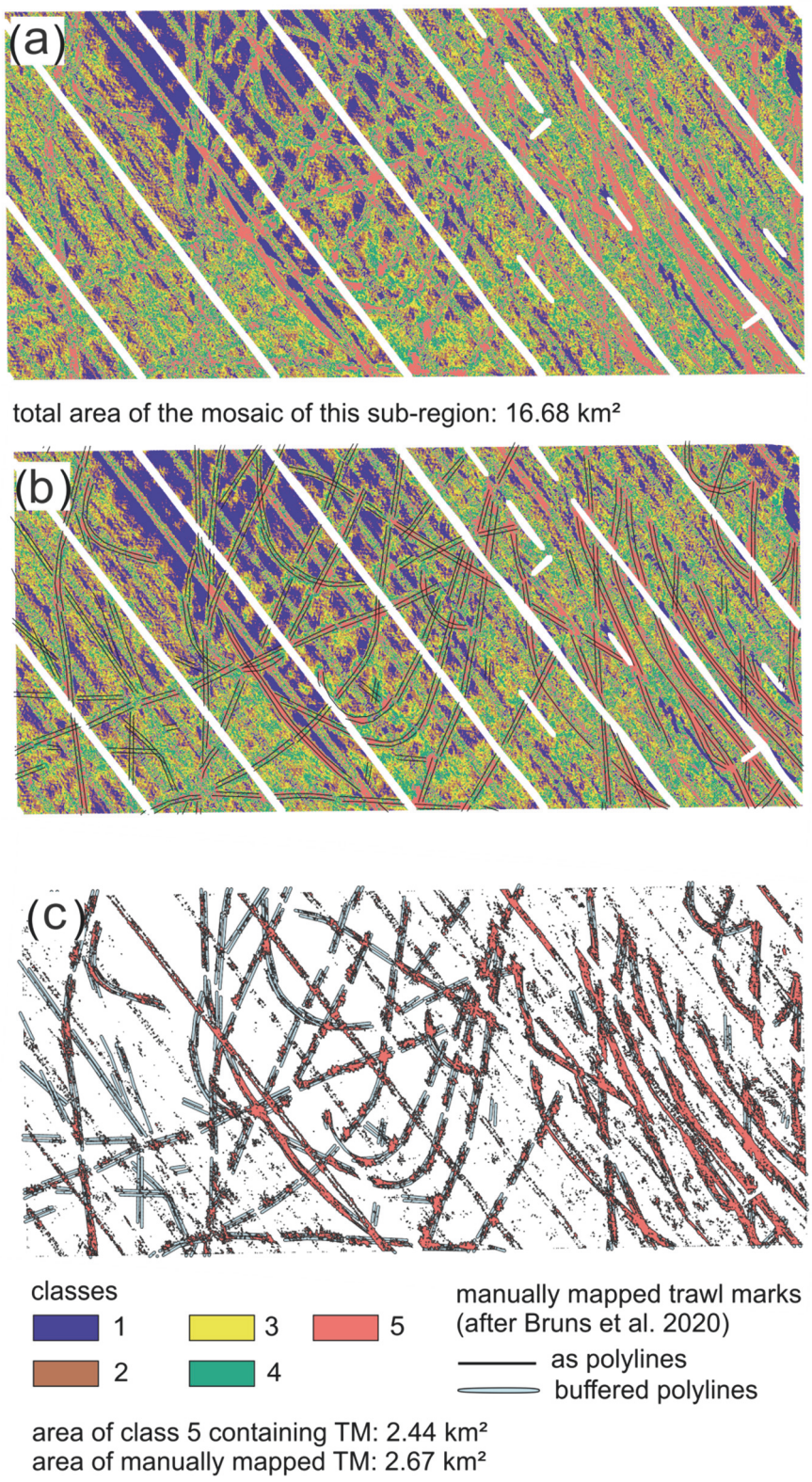

Figure 5.5: (a) The same sub-region mosaic of the Wind Farm study site as in Figure 5.4 was classified with the unsupervised algorithm. The trawl marks (TM) were assigned to class 5. (b) For a first visual inspection, the polylines of the manually mapped TM (Bruns et al., 2020) were compared with the

classification. (c) Class 5 was extracted as polygon vector file from the classification and the area was calculated. In order to perform a comparison with the area of class 5, the polylines of the manually mapped TM (Bruns et al., 2020) were buffered by 11 m (average TM width after Bruns et al. (2020) and the area was calculated.

The class separability matrix (Table 5.2) shows that the minimum class separation (0.6) was exceeded in all cases. The highest separation (3.0) was achieved between classes 1 and 5. The lowest separation (0.9) occurs between classes 1 and 2 and thus, these classes have the highest overlap.

Table 5.3: Class separability matrix of unsupervised classification applied to the mosaic of the Wind Farm study site. The highest separation was achieved between classes 1 and 5 (3.0) while classes 1 and 2 are separated the least (0.9). Class 5 contains the trawl marks.

classes	1	2	3	4	5
1	0				
2	0.9	0			
3	1.9	1.0	0		
4	2.4	1.8	1.0	0	
5	3.0	2.6	2.0	1.0	0

In the case of the Dogger Bank study site dataset, an initial expectation of five classes was set for classification. However, it was found that the best result, in terms of consistency with the TM, was achieved when using four classes. This configuration allowed for a higher degree of congruency (first, subjective visual inspection) between one specific class and the TM observed in the data. (Figure 5.6a,b). Class 1 was assigned to the TM but a large proportion of nadir noise is included in this classification result. Thus, the area estimation was performed based on the edge detection results as described in the methods section. However, the area calculated from the automatically generated TM representations (buffered centerlines of edges) still overestimates the area of TM compared to the manually mapped area by roughly 65 % (Figure 5.6d).

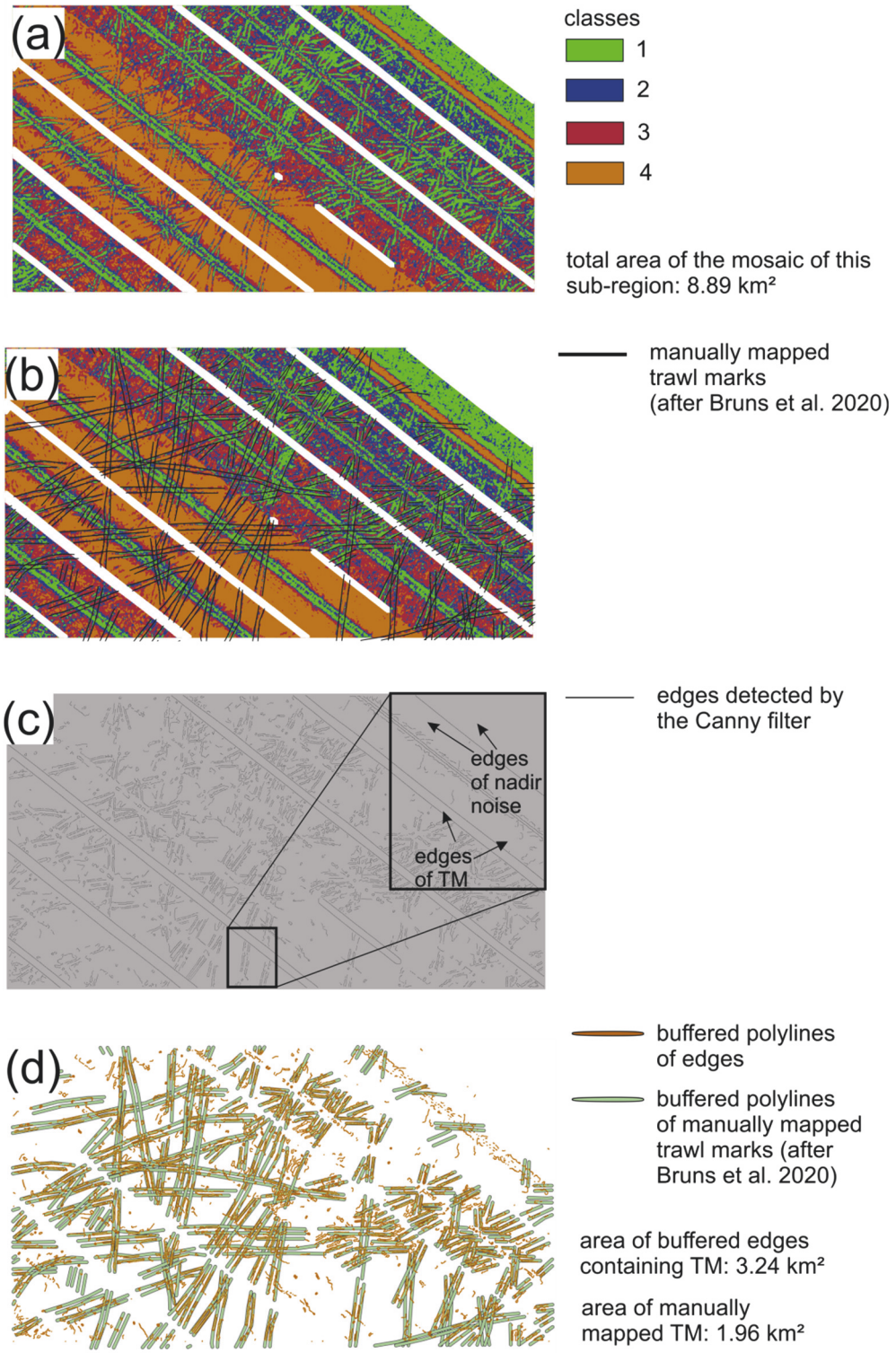

Figure 5.6: (a) The same sub-region mosaic of the Dogger Bank study site as in Figure 5.4 was classified with the unsupervised algorithm. The trawl marks (TM) were assigned to class 1. (b) For a first visual inspection, the polylines of the manually mapped TM (Bruns et al., 2020) were compared with the classification. (c) In order to remove the noise that occurred around the nadir, the edges detected by the Canny filter were used. The direction (azimuth) of the lines was calculated and all polyline features with an azimuth of 103-135 degree were deleted. (d) The polylines representing the edges were buffered by

5.5 m. One TM consists of two edges and 11 m is the approx. TM width (after Bruns et al., 2020). The area of the buffered features was calculated and compared with the area of the TM that were manually mapped by Bruns et al. (2020). The polylines were buffered by 11 m.

Table 5.3 is the class separability matrix for the Dogger Bank mosaic and the minimum class separation (0.6) was exceeded between all classes. The highest separation was achieved between classes 1 and 4. The lowest separation (or highest overlap) appears between classes 1 and 2, 2 and 3 as well as between 3 and 4. This general lower class separation compared to the Wind Farm mosaic is reflected by e.g., the high amount of noise such as the nadir that is included in the class that contains the TM.

Table 5.3: Class separability matrix of unsupervised classification applied to the mosaic of the Dogger Bank study site. Class 1 and 4 have the highest separation (3.1) and the highest overlap, i.e., lowest separation, is between classes 1 and 2, 2 and 3, 3 and 4. Class 1 contains the trawl marks.

classes	**1**	**2**	**3**	**4**
1	0			
2	1.2	0		
3	2.3	1.2	0	
4	3.1	2.3	1.2	0

5.5 Discussion and conclusion

The unsupervised classification successfully identified TM in the SSS mosaics. In the Wind Farm site, the classification provided a reliable initial assessment of the extent of the seabed impacted by trawl gear, estimating an area of 2.44 km^2 (Figure 5.5c). This estimate was comparable to the manually mapped TM area of 2.67 km^2 (Figure 5.5c). In contrast, the classification procedure was very sensitive the noise around the nadir when it was applied to the SSS mosaic at the Dogger Bank study site, impacting the accuracy in that area (Figure 5.6b, Table 5.3). TM at the Dogger Bank site show higher backscatter values compared to the surrounding seabed. In contrast, at the Wind Farm site, the TM are surrounded by an area with lower backscatter values compared to the unaffected seabed. This characteristic has been previously documented by Bruns et al. (2020). Thus, the statistical difference between the TM and the untouched seabed is probably higher at Wind Farm site. Moreover, the nadir noise as well as the noise from disturbances in the water column is represented by higher backscatter compared to the seabed. This is why the majority of the noise is not included in the same class as the TM. At

Dogger Bank site, however, the backscatter signature of TM (high compared to the surrounding) is similar to the noise and thus both features are assigned to the same class.

In contrast, the edge detection method yielded better results at the Dogger Bank study site, which can be attributed to the relatively smooth transition from low backscatter TM to the undisturbed seabed. However, the area calculation based on the edge detection method at the Dogger Bank site did not produce satisfactory results. The deviation from the manually mapped TM is roughly 65 % (Figure 5.6d). This discrepancy is likely attributed to the detection of edges around rounded artifacts, which may have been caused by disturbances in the water column and were not adequately removed during nadir correction. An investigation of the curvature of the detected edges, i.e., potential TM, can improve the results as shown by Gonzales (2004). However, in our dataset round edges may be not unique to noise but also included in TM (Figure 5.6c).

Moreover, the challenge to separate the TM from their background is reflected by the class separability matrices. At Wind Farm study site, class 5 contains the TM and the spatially adjacent class is class 4 (Figure 5.5a). The two classes have the second lowest minimum separation of 1.0 (Table 5.2). As a result, certain portions of class 1 may also encompass sections of TM, making it difficult to determine the extent of spatial overlap between the two. Accordingly, this applies to class 1 (contains TM) and class 2 (lowest separation of 1.2) at Dogger Bank study site (Table 5.3). However, this issue is not unique to automated classification methods. Even when manually classifying TM, different interpreters may have varying interpretations and classifications, particularly when TM are less distinct. As a result, the accuracy measure based on area comparison is not robust. Although the area in km^2 may be the same, the specific features included within the area may differ. For instance, the automated classification may underestimate TM while including more noise in the corresponding class compared to the manually mapped TM area. Therefore, comparing the automatically classified area with the manually classified area provides only a rough estimation of both the accuracy measure and the estimation of bottom trawling impact. However, the visual inspection of the classes containing TM confirms congruency with the manually mapped TM. In case of the Dogger Bank study site, the congruency is less evident as class 1 contains a lot of noise (nadir). The pre-processing of the SSS raw data followed a standard procedure that met the requirements for general seabed mapping in the scope of the *SedAWZ* project (BSH, 2016, Bruns et al., 2020) and applying an additional nadir filter may improve the results. The application of a de-stripe filter that removes stripe-like features related to SSS tow fish movement, however, was part of this standard procedure. With regard to the results of this

study, this is highly recommended because the stripe-like features may be yet another candidate for false positive results of the clustering or edge detection (Gournia et al., 2019).

K-means clustering algorithms (supervised and unsupervised) are often used for the interpretation of multi-band datasets, e.g., satellite imagery (e.g., Ahmed and Akter, 2017, Figliomeni et al., 2023). Such images contain more spectral information that can be used by the algorithm to determine the clusters. The single-band SSS data set poses a significant challenge due to its limited spectral information, which is likely the main limitation of this study. In order to overcome this drawback, multibeam echo sounder data may improve the results as they deliver a set of multiple information (Alevizos et al., 2015, Wan et al., 2022). In addition, the unsupervised classification of SSS images is influenced by the geometric characteristics of the signal, including beam configuration, time-varying gain, and angular responses. These factors can result in over-amplification or under-amplification in the SSS image, which is unrelated to the targeted seabed features (TM in this study). While it is possible to correct the image for such radiometric distortions, this procedure can be time-consuming. (Zhao et al., 2017).

The SSS dataset presented in this study was not specifically optimized for the investigation of TM but rather for a time and cost saving seabed mapping as the *SedAWZ* project aimed on mapping large proportions of the seabed (BSH, 2016). To optimize the survey, it would be beneficial to use a narrower swath width and position the SSS at a lower height above the seabed. This approach would enhance the resolution of the acquired data and increase the visibility of acoustic shadows, which could potentially improve the accuracy of edge detection. The challenge of using a dataset obtained in the scope of general reconnaissance mapping for the automated identification of TM was already mentioned by Gournia et al. (2019). The authors also concluded that a multi-angle view, i.e., implementing different survey directions, may increase TM detection as well. Gournia et al. (2019) found that TM that are aligned with the survey direction appear more distinct in the SSS image than TM that run with increased angles or perpendicular to the survey direction. For the datasets presented in this study a relation between the visibility of TM and the survey direction was not evident, probably because the detection of TM is rather related to changes in sediment properties than morphological changes and, thus, acoustic shadows (Bruns et al., 2020). This may also be an explanation why TM were less evident in the 400 kHz mosaic compared to the 100 kHz mosaic because volume scattering predominantly occurs with the lower frequency (Feldens et al., 2018, Bruns et al., 2020). However, limitations in TM detection in the context of survey design would also apply to a manual interpretation and are not unique to automated classifications.

The approach presented in this study offers a user-friendly experience, as the functions are equipped with a GUI that eliminates the need for writing code. However, the procedure still requires user input in the form of variable entry, such as the minimum class separation, which, which is a dimensionless empirical value (Harmon and Shapiro, 2007). This variable highly depends on the specific imagery data (SSS mosaic in this study) and its spectral information (grey value distribution in case of SSS mosaics) and thus choosing a value that delivers sufficient results needs several trials (Harmon and Shapiro, 2007). The determination of the initial number of classes in the classification algorithm is influenced by the overall characteristics of the seabed. In cases where the seabed shows multiple distinct features such as boulders, bedforms, trawl marks, and acoustically smooth areas, a higher initial number of classes is required compared to a relatively simple seabed scenario, where only trawl marks and evenly distributed fine sediment are present, as in this study. However, a number of classes that is too large may cause several small, isolated pixel groups, each representing an own class (Zhao et al., 2017). Regarding the presented study, further filtering methods such as Gabor filters and image segmentation may improve the results. This approach has proven successful to separate a SSS image in two regions or classes; an acoustically rough ("rocky") and an acoustically smooth (sand and mud) region (Saastamoinen and Penttinen, 2021), which might be comparable with TM ("rough") and no TM ("smooth" background).

The proposed approach proved to be applicable to the SSS datasets of the Wind Farm study site, yielding similar results to those obtained through human interpretation. However, it this approach should by applied carefully, as it is highly sensitive to the backscatter signature of TM and may not be directly transferable to other marine areas. Nevertheless, the technique used in this study employs established methods commonly used in satellite image processing and does not require advanced programming skills, thus increasing its accessibility to users without extensive training. Furthermore, similar algorithms can be found in various GIS applications such as ArcGIS (ESRI) or other software platforms like Matlab, facilitating their implementation in different software environments.

5.6 Acknowledgements

This research was conducted in the framework of the ASKAWZ project, which is a research and development cooperation between Senckenberg am Meer and (SaM) the German Federal Maritime and Hydrographic Agency (BSH, Bundesamt für Seeschifffahrt und Hydrographie, ASKAWZ III Contract-No. 10038520). ASKAWZ is part of the *SedAWZ* project, which is

coordinated by BSH and funded by German Federal Agency for Nature Conservation (BfN, Bundesamt für Naturschutz).

The authors are grateful to the captains and crews of R/V Heincke and R/V Senckenberg for the professional support onboard. We also like to thank the late Dr. Peter Holler, who was the chief scientist on surveys Senckenberg32_2018 and HE544. Thanks go also to our student assistants contributing to survey HE544.

5.7 References

Please find the references within the overall reference list of this thesis (chapter 8).

6 Synthesis

The impact of commercial bottom trawling fleets on the seabed is of global relevance (chapter 1.3) and the examination of such effects by means of physical sediment properties was underrepresented to this date (chapter 1.4). The main objectives as stated in chapter 1.4 are addressed in this thesis and the studies it contains. Thus, it provides new insights into alterations of the seabed that can be related to bottom trawling using trawl marks as an indicator and object of investigation (chapters 3-5). Advances were made by means of quantifying the spatial extend of trawl marks, their persistence (chapter 3) and alterations of the internal sediment integrity (chapter 4) as well as a possibility to accelerate trawl mark mapping and thus, eventually the monitoring of trawl mark generation and hence trawling activity (chapter 5).

6.1 Spatial extend of trawl marks

Chapter 3 of this thesis focuses on the mapping of commercial trawl marks, which served as a key component in addressing research question 1). Furthermore, this mapping provided a foundation for addressing the other research questions presented in chapter 1.4. The techniques employed in habitat mapping (chapter 1.2), were successfully applied to the shallow shelf sea of the southern North Sea (chapters 3 to 5).

The mapping relies on approximately 4,700 km^2 of SSS data, making it the most comprehensive mapping effort of commercial trawl marks to date. This extensive mapping facilitated the classification of these trawl marks based on their backscatter signatures. Although the fishing activity based on VMS-data shows similar intensities for TBB and OTB (ICES, 2018c), OTB marks were exclusively found in the northeastern most part of the “Wind Farm” study site (chapter Identifying trawl marks in North Sea sediments. This was rather unexpected; however, it can be attributed to the different approaches taken in quantifying bottom trawling activity. Mostly, the aggregation in the time domain of VMS-based SAR maps (see chapter 1.3.1 for further explanation) contributes to this difference. SSS images, in contrast, represent only a snap-shot of a relatively short period of time, considering that trawl marks are estimated to persist for a few months at the study sites (chapter 3). Moreover, VMS-based SAR maps are derived from positioning data, which considers trawling events that have a spatial overlap, information that SSS do not provide as it is not necessarily inferable if the gear has passed a certain track once or more often (chapter 3). Therefore the spatial density of trawl marks based on manual mapping is probably underestimated if it is derived only from backscatter data. The

subsequent area estimate derived from the automated trawl mark mapping approach presented in chapter 5 should be considered as a rough estimation. It underlies additional restrictions as the classification algorithm, in comparison with the area estimate based on manually mapped trawl marks, underestimated the trawled area in one case (by approx. 8.5 %) and in the other case, the reduction of unwanted noise in SSS data was insufficient, which lead to a major overestimation (roughly 65 %) of the area that was trawled (chapter 5).

The spatial extent of trawl marks derived from SSS mapping cannot be directly compared with other area estimates, such as SAR-maps, due to the inherent differences in data acquisition and analysis methods. However, trawl mark mapping using SSS data offers advantages. Firstly, it allows for the relative comparison of trawling impact between different sites with a higher spatial resolution. This can be particularly beneficial for assessing trawling impact on highly clustered benthic habitats where finer-scale information is needed. Secondly, trawl mark mapping enables the detection of seasonal changes in trawling patterns, providing valuable insights into seasonal variations in trawling impact, as described in the following chapter.

6.2 Seasonal variability and trawl mark persistence

The extensive SSS dataset presented in this thesis has the additional advantage that surveys were conducted during different times of the year, allowing a relatively comparison of the spatial trawl mark densities between different sites and seasons. The highest densities of up to 20 marks per km^2 were observed in the summer months and in October (chapter 3). In the winter months, the density was approximately one order of magnitude lower, which is most likely related to a lower general fishing activity and higher re-working rates due to frequent storm surges (chapter 3). These findings indicate a seasonal variability in bottom trawling impact on the seabed, highlighting the importance of considering temporal dynamics in the assessment of trawling effects on marine ecosystems.

The German North Sea is characterized by dynamic hydrodynamic processes, such as currents and waves that continuously rework the sediment on the seabed (e.g., Aldridge et al., 2015). Consequently, it was anticipated that trawl marks would be relatively rapidly altered by these natural processes. This expectation was supported by previous studies conducted in the southern North Sea using experimental trawls (Depestele et al., 2016). In line with these findings, the evaluation of time series of mapped commercial trawl marks in this thesis confirmed that these marks undergo changes within hours to a few days and likely disappear after a few months (chapter 3).

The persistence and vertical extend of the disturbances in the shallow subsurface of the seabed resulting from bottom trawling remained unclear (chapter 4). However, it is assumed that a portion of the backscatter signal originates from the subsurface (volume scattering, chapter 3), and therefore, the persistence in the subsurface corresponds, at least approximately, to the persistence observed and derived from backscatter data. Other studies were able to show that chronic bottom trawling eroded the sedimentary record of approximately the last 20 years in the Irish mud belt (Coughlan et al., 2015). Bunke et al. (2019) demonstrated that the biogeochemical composition of the seabed surface and subsurface (up to 35 cm deep) was altered, which may have long-term implications for benthic organisms, e.g., reduced availability of nutrients (Ferguson et al., 2020, De Borger et al., 2021). Indeed, considering and assessing the longevity of subsurface disturbances is an important aspect that requires further research.

Although benthic species in dynamic environments may be adapted to regular disturbances by of means of e.g., storm surges (Jennings and Kaiser, 1998), bottom trawling activity represents an additional disturbance. Especially, if the majority of it takes place in the summer months (chapter 3), where sea conditions usually are rather calm compared to the winter months. In the summer months, the burial depth of benthic species may be lower (Reading and McGrorty, 1978) and the abundance of certain species may be increased (Reiss and Kröncke, 2005), which would make these organisms more vulnerable to trawling impact during that time or increases the likelihood of encountering trawl gear, respectively (van Denderen et al., 2014).

The observation of considerable changes in spatial trawl mark density holds significant value as this aspect is often not resolved in conventional fishing activity maps, where estimates of the trawled area (SAR) are typically aggregated over a full year (ICES, 2018a). The availability of higher resolution SAR-maps (in space and time) is highly limited and the request of raw VMS positioning data is complicated by administrative barriers as the raw datasets delivered by the national fishing fleets are held by the relevant authorities of the respective countries (Lee et al., 2010). Regarding the study sites within the German EEZ, datasets of the German fishing fleet may have been available on request, however, the majority of fishing activity in the German North Sea is related to international fleets e.g., of the Netherlands or Denmark (Schulze, 2018). The limited access to raw VMS data or higher resolution SAR-maps hampers the research on fishing activity and thus bottom trawling impact.

6.3 Altered sediment properties due to bottom trawling

The extensive mapping of trawl marks based on SSS data provides an excellent database for studying the physical alterations of the seabed surface induced to bottom trawling. The high

number of trawl marks (up to 20 marks per km^2) enabled a detailed characterization of trawl marks by means of their acoustic backscatter signature, which is related to changes in micro roughness and lateral grain size distribution. In areas where the sediment type mainly consists of fine sand, changes in the micro roughness was more pronounced compared to areas where the mud content was relatively increased (up to 20%). Here, additional selective transport of the fine fraction takes place (chapter 3), which can have implications for the sediment stability (chapter 4).

In order to quantify changes in the sediment properties (research question 2, chapter 1.4), sediment strength data were obtained using a dynamic free-fall penetrometer. Trawled and un-trawled parts (derived from the mapping presented in chapter 3) of the seabed were compared in order to investigate lateral differences. The study presented in chapter 4, clearly shows that bottom trawling provokes reduced sediment strength (roughly 20 kPa) likely due to an increased water content after the trawl gear ploughed through the seabed. This has the potential to affect the benthic habitat on the long term. The more area is affected by bottom trawling in terms of reduced sediment strength, e.g., during high activity times in summer (chapter 3), the more sediment may eventually be re-mobilized after trawling. Bottom trawling can be considered as chronic rather than as single events in the German North Sea as well as in various other sea regions (Eigaard et al., 2017) and thus, re-trawling would further enhance sediment re-mobilization in previously trawled areas. A quantification of trawling related suspended matter and subsequent sediment transport was not part of this thesis. However, the assumption of potential increased sediment transport due to chronic trawling aligns with the same trajectory of the findings that were made by Paradis et al. (2021), who showed an altered sediment budget due to chronic bottom trawling.

Moreover, the sediment strength data were expected to provide further insights into alterations within the shallow subsurface. It was exemplarily shown that the penetration depth of beam trawl gear on fine sand in the northern German North Sea is approx. 10 cm (chapter 3), which is in accordance with the literature (Eigaard et al., 2016). This was considered as the minimum penetration depth of the dynamic penetrometer needed in order to resolve the vertical boundary between re-worked (trawled) sediment and the underlying, pristine subsurface. Strikingly, the data suggested no such boundary and, instead, exhibited substantial similarities with un-trawled sediment (chapter 4). It was assumed that the penetrometer may have failed to reach the hypothesized boundary, given that existing literature indicates that the perturbation caused by trawling can extend several decimeters below the surface (Bunke et al., 2019). Consequently, the investigation into the vertical impact of bottom trawling remained

unresolved within the scope of this thesis. Nevertheless, this observation underscores the need for additional research concerning this topic.

To which extend bioturbation contributed to the reduced sediment strength was not quantified in this thesis (chapter 4). This uncertainty arises from a limitation in the study design, as it lacked the inclusion of fauna samples, which would have facilitated a more accurate assessment. However, quantifying bioturbation rates is challenging and may lead to the inability to differentiate between bioturbation induced sediment re-working and trawling induced re-working (Oberle et al., 2016b and references therin). In conjunction with the conclusion by Oberle et al. (2016b), the outcome of the study presented in chapter 4 highlights the need for further investigations on the differentiation between bioturbation induced sediment alterations and those caused by bottom trawling.

6.4 Developments in automated seabed mapping

The physical alterations of the seabed and the resulting implications (e.g., potentially increased sediment transport) explained in the previous chapters, stress the need for trawling activity monitoring. This may be realized by monitoring trawl marks, however, it can be challenging as large sea areas have to be considered. Consequently, a time effective, user-friendly way to map trawl marks was developed (addressing research question 3, chapter 1.4).

The methodology outlined in chapter 5 offers a more time-efficient trawl mark mapping compared to manual approaches. The software employed, namely QGIS/GRASS GIS, is a widely accessible and often utilized GIS software, and its non-proprietary nature. This accessibility allows financially constrained institutions, such as small research institutes or non-government organizations, to adopt this approach. Additionally, the functions and add-ons employed in this methodology are relatively straightforward to implement, as they do not require programming skills and are accompanied by a user-friendly graphic interface (GUI).

A shortcoming of the presented approach is that the accuracy highly depends on the particular study site and quality of the SSS dataset. Trawl marks may have different signatures as it was shown in chapter 3, which needs parameter adjustment within the classification process and may lead to poor feature detection (chapter 5). If automated trawl mark mapping is utilized for the purpose of tracking fishing activity, it may be necessary to establish standardized workflows tailored to acoustically comparable locations. The area estimate based on the automated recognition is limited by the quality of the SSS data (chapter 5). If the area estimation provides more robust results, models for potential trawling induced erosion in the

studied areas could be developed in conjunction with data on sediment strength (chapter 4) and further measurements of shear strength, as well as shear stress due to currents and waves.

Chapter 5 showed that automated classification algorithms are well established in the realm of marine habitat mapping and its use is highly recommended as it is time and cost saving compared to investigations made by a human interpreter. This may accelerate also the identification of trawled areas and the monitoring of fishing activity. In order to resolve seasonal variability in the spatial trawl mark density and thus trawling activity, however, re-surveys are needed. Due to expenses by means of time and costs, such datasets may be sparse and probably only available on a regional scale. The automated recognition may further be enhanced by a careful pre-processing of the SSS data by applying additional noise reduction such as Gabor filters (Saastamoinen and Penttinen, 2021) and an advanced k-means clustering (Zhao et al., 2017). In this case, however, it must be ensured that the effort does not contradict the objective of using a low-threshold, time-saving process.

6.5 Application to other shelf seas

Bottom trawling is known to be conducted around the globe but it concentrates in shelf sea areas (Guiet et al., 2019). One prominent example of a shelf sea significantly affected by bottom trawling is the southern North Sea (chapter 1.3.1). Consequently, the techniques employed within the scope of this thesis are adapted to shelf sea research and are potentially applicable to other shelf seas characterized by diverse environmental conditions. While certain implications derived from the main conclusions of this thesis may be specific to particular sites, there are overarching patterns that can be transferred to other shelf seas.

The regional and seasonal variability in trawl mark density mainly depends on factors that are site specific, i.e., the regional and seasonal availability of target fish, weather conditions and, as a result, the behavior of the fishing fleets (chapter 3). However, the presence of seasonal patterns may hold true for other sea regions. While these patterns may vary compared to those observed in the North Sea, e.g., due to a different behavior of target fish, the utilization of higher temporal resolution data by means of trawl mark mapping can reveal previously undetected seasonal patterns due to the availability of only coarse-resolution data such as aggregated SAR-maps. Therefore, it is valuable to consider such regional and seasonal patterns in order to robustly estimate bottom trawling impact.

The use of SSS for trawl mark mapping offers the advantage that it can be deployed across a wide range of water depths with fewer losses in swath width compared to MBES systems. Moreover,

SSS is not solely used in habitat mapping but also in other disciplines such as reconnaissance surveys for cable and pipeline detection (Jing, 2018), wreck detection in archeology (Quinn et al., 2005) and regular surveys conducted by authorities for e.g., shipping route maintenance (Fubara et al., 2020). This bears the advantage that a vast number of datasets may be available, which are potentially applicable to trawl mark research.

When conducting trawl mark mapping in environments characterized by significant bathymetric variations, such as steep slopes, the resolution of trawl marks may be constrained if the slope faces away from the SSS signal. In such cases, a portion of the acoustic energy will be scattered in directions away from the transducer. Even on a horizontal seabed, trawl marks that have already degraded to a certain level may appear indistinct in SSS images (chapter 3). This indistinctness can be amplified by the geometric loss of energy, resulting in unresolved trawl marks. It is crucial to consider these factors during the design of the survey setup (ensuring a heading perpendicular to the slope direction), as well as during SSS data processing (applying geometric corrections, gain control) and data interpretation (acknowledging the inherent limitations). Another interesting observation is, that although UW-video recording is often described as an appropriate way to identify trawl marks on the seabed (Mérillet et al., 2017), the analysis of UW-video footage was not feasible to map trawl marks in the northern German North Sea (chapter 3). For environments predominantly consisting of fine sand, backscatter data may more suitable for trawl mark mapping as changes in the seabed sediment are detectible that cannot be resolved by UW-video, e.g., micro-roughness (chapter 3).

In the scope of this thesis it was found that bottom trawling reduces the sediment strength at the specific site. However, a decrease in sediment strength is expected for other shelf seas, given that the physical properties that contribute to the sediment strength, e.g., particle shape and particle material (chapter 4) are comparable. It is suggested that the decreased sediment strength may enhance erosion (chapter 4), which would be enhanced in environments with strong (tidal) currents (Trimmer et al., 2005) or slope gradients (Paradis et al., 2021). Hence, it is considered valuable to obtain sediment strength data from diverse environments in order to further examine the implications of bottom trawling impact by means of sensitivity to enhanced erosional processes.

The assessment of sediment strength was conducted using the dynamic penetrometer *Nimrod*, as described in chapter 4. *Nimrod* was specifically developed for the application in shallow water environments, with a maximum operational depth of 200 meters (Stark, 2010). In cases where greater water depths are encountered, alternative systems may be employed, although they may possess their own limitations such as sampling resolution or the requirement of lowering them

using winches and cables, which can introduce biases due to ship movements, e.g., instrument tilt (Stoll and Akal, 1999). Another advantage of *Nimrod* lies in its compact size, enabling deployment even from small vessels. This feature contributes to significant cost savings, and its design facilitates operation under adverse sea conditions (Stark, 2010).

The automated recognition of trawl marks holds significant value for any shelf sea that is subject to the research on the impact of bottom trawling, as it expedites the mapping process and can provide estimates of the affected area (chapter 5). However, it is crucial to acknowledge certain limitations. The successful recognition of trawl marks depends on general characteristics of the seabed, as the presence of other elongated seabed features like bedforms may impede accurate classification (Gonzales, 2004). On a rocky seabed, acoustic shadows from trawl marks can overlap with other acoustic shadows or areas of high backscatter, resembling noise. Additionally, the recognition of trawl marks, whether through manual or automated approaches, is influenced by survey parameters such as the height of the SSS above the seabed and the survey heading relative to the orientation of trawl marks (Gournia et al., 2019). However, the availability of optimized datasets specifically dedicated to trawl mark surveys is often limited, as comprehensive spatial mapping programs of shelf seas may prioritize general seabed mapping objectives, as exemplified by *SedAWZ* (BSH, 2016) or MARENO (Buhl-Mortensen et al., 2015). Nonetheless, SSS data obtained within the framework of such broad mapping programs have demonstrated sufficient quality for trawl mark identification and detailed investigations across diverse shelf sea environments, e.g., this thesis.

7 Outlook

This thesis made advances in the spatial and seasonal variability of bottom trawling impact by means of trawl marks in the southern North Sea und could resolve changes of the sediment properties by means of sediment strength. Moreover an easy-access approach to automated trawl mark mapping and thus a time and cost saving possibility towards the monitoring of trawling activity was presented. Besides addressing the research questions (chapter 1.4), the studies identified questions concerning bottom trawl impact that remained unanswered in the scope of this thesis. Needless to say, further research is needed in order to deepen the knowledge regarding bottom trawling impact. This chapter condenses unanswered questions that were identified in this thesis as well as mentions supplementary topics for further research.

The mapping of trawl marks based on SSS data delivered sufficient results to address the research questions. Nevertheless, it would be highly interesting if and to which extend the results can be improved by conducting a survey optimized for trawl mark mapping. This may include (1) the use of different SSS frequencies to increase the resolution and to examine volume scattering in relation to trawl marks and sediment type, (2) operating the SSS closer to the seabed (lower grazing angle to enhance acoustic shadows) and (3) to implement different survey headings in order identify potential directionality of trawl marks relative to the survey heading.

For the automated mapping of trawl marks, it was hindering that the SSS data included increased noise around the nadir in case of the “Dogger Bank” dataset. A follow-up study may overcome this problem by carefully reprocessing this dataset with respect to nadir artifacts and if necessary, by the application of further filtering to also reduce the noise created from water column turbidity.

Another challenge of the presented research was the limitation in seabed samples. It is recommended that future studies focus on the direct sampling of trawled areas. For example, sediment cores and according lab experiments on the sediment strength may resolve the vertical impact of bottom trawling on physical sediment properties. Furthermore, fauna samples by means of, e.g., box coring, would be beneficial to determine the faunal communities and, thus, further approach the question on how bioturbation contributes to differences in sediment strength.

An additional topic that may be the subject of future studies may be to obtain sediment strength data (using *Nimrod*) on trawled seabeds with different sediment properties. For example,

(Stark, 2010) found that carbonate sands show increased sediment strength compared to siliciclastic sands and it would be highly interesting, if such carbonate sands respond similar to trawling impact as siliciclastic North Sea sands or totally different.

An impact of bottom trawling is the reduction of sediment strength, which may enhance sediment transport (chapter 4). Besides the other multiple forms of human impact on marine habitats (chapter 1.1), such long-term and broad-scale implications of bottom trawling may put further pressure on the organisms colonizing these habitats. Thus, more attention should be raised concerning this topic and it should be addressed in future studies. Needless to say, that further comprehensive research similar to this thesis is needed.

8 References

Ahmed, K. R., & Akter, S. (2017). Analysis of landcover change in southwest Bengal delta due to floods by NDVI, NDWI and K-means cluster with landsat multi-spectral surface reflectance satellite data. *Remote Sensing Applications: Society and Environment, 8*, 168-181. https://doi.org/10.1016/j.rsase.2017.08.010

Aldridge, J. N., Parker, E. R., Bricheno, L. M., Green, S. L., & van der Mole, J. (2015). Assessment of the physical disturbance of the northern European Continental shelf seabed by waves and currents. *Continental Shelf Research, 108*, 20. http://dx.doi.org/10.1016/j.csr.2015.03.004

Alevizos, E., Snellen, M., Simons, D. G., Siemes, K., & Greinert, J. (2015). Acoustic discrimination of relatively homogeneous fine sediments using Bayesian classification on MBES data. *Marine Geology, 370*, 31-42. https://doi.org/10.1016/j.margeo.2015.10.007

Amiri-Simkooei, A. R., Koop, L., van der Reijden, K. J., Snellen, M., & Simons, D. G. (2019). Seafloor Characterization Using Multibeam Echosounder Backscatter Data: Methodology and Results in the North Sea. *Geosciences, 9*(7), 292. https://doi.org/10.3390/geosciences9070292

Amoroso, R. O., Pitcher, C. R., Rijnsdorp, A. D., McConnaughey, R. A., Parma, A. M., Suuronen, P. et al. (2018). Bottom trawl fishing footprints on the world's continental shelves. *Proceedings of the National Academy of Sciences, 115*(43), E10275-E10282. doi: 10.1073/pnas.1802379115

Arjona-Camas, M., Puig, P., Palanques, A., Emelianov, M., & Durán, R. (2019). Evidence of trawling-induced resuspension events in the generation of nepheloid layers in the Foix submarine canyon (NW Mediterranean). *Journal of Marine Systems, 196*, 86-96. https://doi.org/10.1016/j.jmarsys.2019.05.003

Aspden, R. J., Vardy, S., Perkins, R. G., Davidson, I. R., Bates, R., & Paterson, D. M. (2004). The effects of clam fishing on the properties of surface sediments in the lagoon of Venice, Italy. *Hydrol. Earth Syst. Sci., 8*(2), 160-169. doi: 10.5194/hess-8-160-2004

Aubeny, C. P., & Shi, H. (2006). Interpretation of Impact Penetration Measurements in Soft Clays. *Journal of Geotechnical and Geoenvironmental Engineering, 132*(6), 770-777. doi:10.1061/(ASCE)1090-0241(2006)132:6(770)

Bartholomä, A., Capperucci, R. M., Becker, L., Coers, S. I. I., & Battershill, C. N. (2019). Hydrodynamics and hydroacoustic mapping of a benthic seafloor in a coarse grain habitat of the German Bight. *Geo-Marine Letters, 40*(2), 183-195. doi: 10.1007/s00367-019-00599-7

Bildstein, T., Schuchardt, B., Kramer, M., Bleich, S., Schückel, S., Huber, A., et al. (2017). *Die Meeresschutzgebiete in der deutschen ausschließlichenWirtschaftszone der Nordsee - Beschreibung und Zustandsbewertung*. Bonn: Bundesamt für Naturschutz.

Blondel, P. (2009). *The Handbook of Side-Scan Sonar*: Springer Verlag.

Blott, S. J., & Pye, K. (2001). GRADISTAT: a grain size distribution and statistics package for the analysis of unconsolidated sediments. *Earth Surface Processes and Landforms, 26*(11), 1237-1248. https://doi.org/10.1002/esp.261

Bockelmann, F.-D., Puls, W., Kleeberg, U., Müller, D., & Emeis, K.-C. (2018). Mapping mud content and median grain-size of North Sea sediments – A geostatistical approach. *Marine Geology, 397*, 60-71. https://doi.org/10.1016/j.margeo.2017.11.003

Boyd, S. E., Coggan, R. A., Birchenough, S. N. R., Limpenny, D. S., Eastwoord, P., Foster-Smith, R. L., . . . Rogers, S. (2005). The role of seabed mapping techniques in environmental monitoring and management. *Sci. Ser. Tech Rep., Cefas Lowestoft, 127*, 166.

Bradshaw, C., Tjensvoll, I., Sköld, M., Allan, I. J., Molvaer, J., Magnusson, J., . . . Nilsson, H. C. (2012). Bottom trawling resuspends sediment and releases bioavailable contaminants in a polluted fjord. *Environmental Pollution, 170*, 232-241. https://doi.org/10.1016/j.envpol.2012.06.019

Brezina, J. (1979). *Particle size and settling rate distributions of sand-sized materials*. Paper presented at the PARTEC 79. Proc 2nd European Symposium on Particle Characterisation, Nürnberg, Germany.

Brown, C. J., Smith, S. J., Lawton, P., & Anderson, J. T. (2011). Benthic habitat mapping: A review of progress towards improved understanding of the spatial ecology of the seafloor using acoustic techniques. *Estuarine, Coastal and Shelf Science, 92*(3), 502-520. https://doi.org/10.1016/j.ecss.2011.02.007

Bruns, I., Holler, P., Capperucci, R. M., Papenmeier, S., & Bartholomä, A. (2020). Identifying Trawl Marks in North Sea Sediments. *Geosciences, 10*(11), 30. doi: 10.3390/geosciences10110422

BSH (2016). Guideline for Seafloor Mapping in German Marine Waters Using High-Resolution Sonars (pp. 147): Federal Maritime and Hydrographic Agency.

BSH (2019). Site Development Plan 2019 for the German North Sea and Baltic Sea (pp. 211): Federal Maritime and Hydrographic Agency.

BSH (2020). FINO Database. Data was made available by the FINO (Forschungsplattformen in Nord- und Ostsee) initiative, which was funded by the German Federal Ministry of Economic Affairs and Energy (BMWi) on the basis of a decision by the German Bundestag, organised by the Projekttraeger Juelich (PTJ) and coordinated by the German Federal Maritime and Hydrographic Agency (BSH). Retrieved 14.09.2020 http://fino.bsh.de/index.cgi?seite=anmeldung_formular

Buhl-Mortensen, L., Buhl-Mortensen, P., Dolan, M. J. F., & Gonzalez-Mirelis, G. (2015). Habitat mapping as a tool for conservation and sustainable use of marine resources: Some perspectives from the MAREANO Programme, Norway. *Journal of Sea Research, 100*, 46-61. https://doi.org/10.1016/j.seares.2014.10.014

Buhl-Mortensen, L., Ellingsen, K. E., Buhl-Mortensen, P., Skaar, K. L., & Gonzales-Mirelis, G. (2016). Trawling disturbance on megabenthos and sediment in the Barents Sea: chronic effects on density, diversity, and composition. *ICES Journal of Marine Science, 73*(Supplement 1), 17. https://doi.org/10.1093/icesjms/fsv200

Buhl-Mortensen, P., & Buhl-Mortensen, L. (2018). Impacts of Bottom Trawling and Litter on the Seabed in Norwegian Waters. *Frontiers in Marine Science, 5*. doi: 10.3389/fmars.2018.00042

Bunke, D., Leipe, T., Moros, M., Morys, C., Tauber, F., Virtasalo, J. J., . . . Arz, H. W. (2019). Natural and Anthropogenic Sediment Mixing Processes in the South-Western Baltic Sea. *Frontiers in Marine Science, 6*. doi: 10.3389/fmars.2019.00677

Burns, C., Bollard, B., & Narayanan, A. (2022). Machine-Learning for Mapping and Monitoring Shallow Coral Reef Habitats. *Remote Sensing, 14*(11), 2666. https://doi.org/10.3390/rs14112666

Caddy, J. F. (1973). Underwater Observations on Tracks of Dredges and Trawls and Some Effects of Dredging on a Scallop Ground. *Journal of the Fisheries Research Board of Canada, 30*(2), 173-180. doi: 10.1139/f73-032

Cai, G., Liu, S., Tong, L., & Du, G. (2009). Assessment of direct CPT and CPTU methods for predicting the ultimate bearing capacity of single piles. *Engineering Geology, 104*(3), 211-222. https://doi.org/10.1016/j.enggeo.2008.10.010

Calder, B. R., & Mayer, L. A. (2003). Automatic processing of high-rate, high-density multibeam echosounder data. *Geochemistry, Geophysics, Geosystems, 4*(6). https://doi.org/10.1029/2002GC000486

Calvert, J., Strong, J. A., Service, M., McGonigle, C., & Quinn, R. (2014). An evaluation of supervised and unsupervised classification techniques for marine benthic habitat mapping using multibeam echosounder data. *ICES Journal of Marine Science, 72*(5), 1498-1513. doi: 10.1093/icesjms/fsu223

Campbell, M. S., Stehfest, K. M., Votier, S. C., & Hall-Spencer, J. M. (2014). Mapping fisheries for marine spatial planning: Gear-specific vessel monitoring system (VMS), marine conservation and offshore renewable energy. *Marine Policy, 45*, 293-300. https://doi.org/10.1016/j.marpol.2013.09.015

Canny, J. (1986). A Computational Approach to Edge Detection. *IEEE Transactions on Pattern Analysis and Machine Intelligence, PAMI-8*(6), 679-698. doi: 10.1109/TPAMI.1986.4767851

Capperucci, R. M. (2013). Marine Habitat Mapping: Stretching the Blue Marble on a Map. In M. Einsporn, Wiedling, J., Schöttener, S., DGM and ICBM (Ed.), *Recent Impulses to Marine Science and Engineering. From coast to deepsea: multiscale approaches to marine sciences*.

Collier, J. S., & Brown, C. J. (2005). Correlation of sidescan backscatter with grain size distribution of surficial sediments. *Marine Geology, 214*, 19. doi: 10.1016/j.margeo.2004.11.011

Commission of the European Communities. (2000). *DIRECTIVE 2000/60/EC OF THE EUROPEAN PARLIAMENT AND OF THE COUNCIL of 23 October 2000 establishing a framework for Community action in the field of water policy*.

Commission of the European Communities (2008). *DIRECTIVE 2008/56/EC OF THE EUROPEAN PARLIAMENT AND OF THE COUNCIL of 17 June 2008 establishing a framework for community action in the field of marine environmental policy (Marine Strategy Framework Directive)*.

Commission of the European Communities. (2005). *Communication from the Commission to the Council and the European Parliament - Review of certain access restrictions in the Common Fisheries Policy (Shetland Box and Plaice Box)*. (52005DC0422).

Coughlan, M., Wheeler, A. J., Dorschel, B., Lordan, C., Boer, W., Gaever, P. v., . . . Mörz, T. (2015). Record of anthropogenic impact on the Western Irish Sea mud belt. *Anthropocene, 9*, 56-69. https://doi.org/10.1016/j.ancene.2015.06.001

Cramp, A., Lee, S. V., Herniman, J., Hiscott, R. N., Manley, L. P., Piper, D. J. W., et al. (1997). Data Report: Interlaboratory comparison of sediment grain-sizing techniques: data from Amazon fan upper levee complex sediments. In R. D. Flood, D. J. W. Piper, A. Klaus & L. C. Peterson (Eds.), *Proceedings of the Ocean Drilling Program, Scientific Results* (Vol. 155, pp. 12).

Dairain, A., Maire, O., Meynard, G., Richard, A., Rodolfo-Damiano, T., & Orvain, F. (2020). Sediment stability: can we disentangle the effect of bioturbating species on sediment erodibility

from their impact on sediment roughness? *Marine Environmental Research, 162*, 105147. https://doi.org/10.1016/j.marenvres.2020.105147

Das, B. M. (1990). *Principles of geotechnical engineering* (Vol. 2nd edn). Boston: PWS-Kent Publishing Company.

Dayal, U. (1980). Free fall penetrometer: a performance evaluation. *Applied Ocean Research, 2*(1), 39-43. https://doi.org/10.1016/0141-1187(80)90046-2

Dayal, U., & Allen, J. H. (1975). The Effect of Penetration Rate on the Strength of Remolded Clay and Sand Samples. *Canadian Geotechnical Journal, 12*(3), 336-348. doi: 10.1139/t75-038

Dayal, U., Allen, J. H., & Jones, J. M. (1973). Marine Impact Cone Penetrometers.

De Borger, E., Tiano, J., Braeckman, U., Rijnsdorp, A. D., & Soetaert, K. (2021). Impact of bottom trawling on sediment biogeochemistry: a modelling approach. *Biogeosciences, 18*(8), 2539-2557. doi: 10.5194/bg-18-2539-2021

de Veen, J. F. (1976). On changes in some biological parameters in the North Sea sole (Solea solea L.). *ICES Journal of Marine Science, 37*(1), 60-90. doi: 10.1093/icesjms/37.1.60

DeAlteris, J., Skrobe, L., & Lipsky, C. (1999). The Significance of Seabed Disturbance by Mobile Fishing Gear Relative to Natural Processes: A Case Study in Narragansett Bay, Rhode Island. *American Fisheries Society Symposium, 22*, 15.

Depestele, J., Degrendele, K., Esmaeili, M., Ivanović, A., Kröger, S., O'Neill, F. G., . . . Rijnsdorp , A. D. (2019). Comparison of mechanical disturbance in soft sediments due to tickler-chain SumWing trawl vs. electro-fitted PulseWing trawl. *ICES Journal of Marine Science, 76*(1), 18. doi: 0.1093/icesjms/fsy124

Depestele, J., Ivanović, A., Degrendele, K., Esmaeili, M., Polet, H., Roche, M., . . . O'Neill, F. G. O. (2016). Measuring and assessing the physical impact of beam trawling. *ICES Journal of Marine Science, 73*(Supplement 1), 12. doi: 10.1093/icesjms/fsv056

Diesing, M., Mitchell, P., & Stephens, D. (2016). Image-based seabed classification: what can we learn from terrestrial remote sensing? *ICES Journal of Marine Science, 73*(10), 2425-2441. doi: 10.1093/icesjms/fsw118

Council Regulation (EC) No 1224/2009 of 20 November 2009 establishing a Union control system for ensuring compliance with the rules of the common fisheries policy, amending Regulations (EC) No 847/96, (EC) No 2371/2002, (EC) No 811/2004, (EC) No 768/2005, (EC) No 2115/2005, (EC) No 2166/2005, (EC) No 388/2006, (EC) No 509/2007, (EC) No 676/2007, (EC) No 1098/2007, (EC) No 1300/2008, (EC) No 1342/2008 and repealing Regulations (EEC) No 2847/93, (EC) No 1627/94 and (EC) No 1966/2006, Official Journal of the European Union Vol. 52 (2009).

Eigaard, O. R., Bastardie, F., Breen, M., Dinesen, G. E., Hintzen , N. T., Laffargue, P., . . . Rijnsdorp , A. D. (2016). Estimating seabed pressure from demersal trawls, seines, and dredges based on gear design and dimensions. *ICES Journal of Marine Science, 73*(Supplement 1), 17. doi: 10.1093/icesjms/fsv099

Eigaard, O. R., Bastardie, F., Hintzen, N. T., Buhl-Mortensen, L., Buhl-Mortensen, P., Catarino, R., et al. (2017). The footprint of bottom trawling in European waters: distribution, intensity, and seabed integrity. *ICES Journal of Marine Science, 74*(3), 847-865. doi: 10.1093/icesjms/fsw194

Eisma, D., Mook, W. G., & Laban, C. (1981). An Early Holocene Tidal Flat in the Southern Bight *Holocene Marine Sedimentation in the North Sea Basin* (pp. 229-237).

Ellis, N., Pantus, F., & Pitcher, C. (2014). Scaling up experimental trawl impact results to fishery management scales — a modelling approach for a “hot time. *Canadian Journal of Fisheries and Aquatic Sciences, 71*, 1–14. doi: 10.1139/cjfas-2013-0426

Emeis, K., Kleeberg, U., Winter, C., Brockmeyer, B., Kröncke, I., Kraus, G., et al. (2019). NOAH - North Sea Observation and Assessment of Habitats - Synthese: BMBF-FONA Verbundvorhaben (03F0670A).

EMODnet-Bathymetry-Consortium (2018). EMODnet Digital Bathymetry (DTM). https://emodnet.ec.europa.eu/en/bathymetry

EMODnet (2019). Kinetic energy at the seabed due to waves - Celtic, North Sea (mean of annual 90th percentile). https://data.europa.eu/data/datasets/kinetic-energy-from-waves-in-the-greater-north-sea-and-celtic-seas-2000-2005-for-the-emodnet-se?locale=de

EUNIS (2019). EUNIS, the European Nature Information System. from https://eunis.eea.europa.eu/index.jsp

Fakiris, E., Blondel, P., Papatheodorou, G., Christodoulou, D., Dimas, X., Georgiou, N., et al. (2019). Multi-Frequency, Multi-Sonar Mapping of Shallow Habitats—Efficacy and Management Implications in the National Marine Park of Zakynthos, Greece. *Remote Sensing, 11*(4), 461. https://doi.org/10.3390/rs11040461

Fakiris, E., & Papatheodorou, G. (2012). Quantification of regions of interest in swath sonar backscatter images using grey-level and shape geometry descriptors: the TargAn software. *Marine Geophysical Research, 33*(2), 169-183. doi: 10.1007/s11001-012-9153-5

Fakiris, E. P., G.; Geraga, M.; ferentinos, G. (2016). An Automatic Target Detection Algorithm for Swath Sonar Backscatter Imagery, Using Image Texture and Independent Component Analysis. *Remote Sensing, 8*(373), 13. https://doi.org/10.3390/rs8050373

Feldens, P., Schulze, I., Papenmeier, S., Schönke, M., & von Deimling, J. S. (2018). Improved Interpretation of Marine Sedimentary Environments Using Multi-Frequency Multibeam Backscatter Data. *Geosciences, 8*(214), 14. doi: 10.3390/geosciences8060214

Ferguson, A. J. P., Oakes, J., & Eyre, B. D. (2020). Bottom trawling reduces benthic denitrification and has the potential to influence the global nitrogen cycle. *Limnology and Oceanography Letters, 5*(3), 237-245. https://doi.org/10.1002/lol2.10150

Figge, K. (1981). Nordsee, Sedimentverteilung in der Deutschen Bucht (Blatt 2900, Maßstab 1:250 000).

Figge, K. (1982). *Begleitheft zur Karte der Seimentverteilung in der Deutschen Bucht*. Deutsches Hydrographisches Insitut, Hamburg.

Figliomeni, F. G., Guastaferro, F., Parente, C., & Vallario, A. (2023). A Proposal for Automatic Coastline Extraction from Landsat 8 OLI Images Combining Modified Optimum Index Factor (MOIF) and K-Means. *Remote Sensing, 15*(12), 3181. https://doi.org/10.3390/rs15123181

Fitch, S., Thomson, K., & Gaffney, V. (2005). Late Pleistocene and Holocene depositional systems and the palaeogeography of the Dogger Bank, North Sea. *Quaternary Research, 64*(2), 185-196. doi: 10.1016/j.yqres.2005.03.007

Flemming, B. W. (2005). *The concept of wave base: fact and fiction*. Paper presented at the Sediment 2005, Gwatt, Lake Thun, Swizerland.

Fliessbach, K. L., Borkenhagen, K., Guse, N., Markones, N., Schwemmer, P., & Garthe, S. (2019). A Ship Traffic Disturbance Vulnerability Index for Northwest European Seabirds as a Tool

for Marine Spatial Planning. *Frontiers in Marine Science, 6*. doi: 10.3389/fmars.2019.00192

Folk, R. L., & Ward, W. C. (1957). A Study in the Significance of Grain-Size Parameters. *Journal of Sedimentary Petrology, 27*, 23. https://doi.org/10.1306/74D70646-2B21-11D7-8648000102C1865D

Friedlander, A. M., Boehlert, G. W., Field, M. E., Mason, J. E., Gardner, J. V., & Dartnell, P. (1999). Sidescan-sonar mapping of benthic trawl marks on the shelf and slope off Eureka, California. *Fishery Bulletin, 97*(4), 15.

Fubara, D., Hart, L., & Otasanya, G. I. (2020). Navigational Hazard Analysis of Part of Bonny River, Rivers State Nigeria. *Journal of Geosciences, 8*(1), 25-34. doi: 10.12691/jgg-8-1-4

Galvez, D. S., Papenmeier, S., Sander, L., Hass, H. C., Fofonova, V., Bartholomä, A., & Wiltshire, K. H. (2021). Ensemble Mapping and Change Analysis of the Seafloor Sediment Distribution in the Sylt Outer Reef, German North Sea from 2016 to 2018. *Water, 13*(16), 2254. https://doi.org/10.3390/w13162254

GEBCO-Compilation-Group (2020). *GEBCO 2020 Grid*. www.gebco.net

Gerritsen, H. D., Minto, C., & Lordan, C. (2013). How much of the seabed is impacted by mobile fishing gear? Absolute estimates from Vessel Monitoring System (VMS) point data. *ICES Journal of Marine Science, 70*(3), 9. https://doi.org/10.1093/icesjms/fst017

Gilkinson, K., King, E. L., Li, M. Z., Roddick, D., Kenchington, E., & Han, G. (2015). Processes of physical change to the seabed and bivalve recruitment over a10-year period following experimental hydraulic clam dredging on Banquereau, Scotian Shelf. *Continental Shelf Research, 92*, 15. http://dx.doi.org/10.1016/j.csr.2014.11.006

Goff, J. A., Olson, H. C., & Duncan, C. S. (2000). Correlation of side-scan backscatter intensity with grain-size distribution of shelf sediments, New Jersey margin. *Geo-Marine Letters, 20*, 7.

Gonzales, B. G. P., Y.; Smith, C. (2004). Detection and classification of trawling marks in side scan sonar images. 9.

Gournia, C., Fakiris, E., Geraga, M., Williams, D. P., & Papatheodorou, G. (2019). Automatic Detection of Trawl-Marks in Sidescan Sonar Images through Spatial Domain Filtering, Employing Haar-Like Features and Morphological Operations. *Geosciences, 9*(214), 23. doi: 10.3390/geosciences9050214

Grant, J., & Daborn, G. (1994). The effects of bioturbation on sediment transport on an intertidal mudflat. *Netherlands Journal of Sea Research, 32*(1), 63-72. https://doi.org/10.1016/0077-7579(94)90028-0

GRASS-Development-Team (2022). Geographic Resources Analysis Support System (GRASS) Software, Version 8.2. *Open Source Geospatial Foundation*. https://grass.osgeo.org/.

GRASS-Development-Team (2023). Geographic Resources Analysis Support System (GRASS 8), reference manual *Open Source Geospatial Foundation Project*. https://grass.osgeo.org/grass82/manuals/.

Grządziel, A., & Wąż, M. (2016). Estimation of effective swath width for dual-head multibeam echosounder. *Annual of Navigation, 23/2016*, 11. doi: 10.1515/aon-2016-0012

Guiet, J., Galbraith, E., Kroodsma, D., & Worm, B. (2019). Seasonal variability in global industrial fishing effort. *PLoS ONE, 14*(5), 17. doi: 10.1371/journal.pone.0216819

Haesler, S., & Lefebvre, C. (2017). Sturmtief HERWART sorgt am 28./29. Oktober 2017 für Orkanböen über Deutschland. In D. Wetterdienst (Ed.), (pp. 6). Offenbach.

Haralick, R. M., Shanmugam, K., & Dinstein, I. (1973). Textural Features for Image Classification. *IEEE Transactions on Systems, Man, and Cybernetics, SMC-3*(6), 610-621. doi: 10.1109/TSMC.1973.4309314

Harmon, V., & Shapiro, M. (2007). GRASS Tutorial: Image Processing. https://grass.osgeo.org/gdp/imagery/grass4_image_processing.pdf: U.S. Army Construction Engineering Research Laboratory.

Harris, P., & Baker, E. (2012). *Seafloor Geomorphology as Benthic Habitat - Geohab Atlas of Seafloor Geomorphic Features and Benthic Habitats*: Elsevier.

Hasan, R. C., Ierodiaconou, D., & Monk, J. (2012). Evaluation of four supervised learning methods for benthic habitat mapping using backscatter from multi-beam sonar. *Remote Sensing, 4*, 3427-3443. https://doi.org/10.3390/rs4113427

Hass, H. C. (2016). Station list and links to master tracks in different resolutions of HEINCKE cruise HE474, Bremerhaven - Bremerhaven, 2016-10-12 - 2016-10-20. PANGAEA: Alfred Wegener Institute, Helmholtz Centre for Polar and Marine Research, Bremerhaven.

Hass, H. C. (2018). Links to master tracks in different resolutions of HEINCKE cruise HE502, Bremerhaven - Bremerhaven, 2017-12-01 - 2017-12-20. PANGAEA: Alfred Wegener Institute, Helmholtz Centre for Polar and Marine Research, Bremerhaven.

Heyer, H., & Schrottke, K. (2013). AufMod (03KIS082-03KIS088) Gemeinsamer Abschlussbericht für das Gesamtprojekt mit Beiträgen aus allen 7 Teilprojekten (pp. 314): Bundesamt für Seeschifffahrt und Hydrographie.

Hiddink, J. G., Jennings, S., Sciberras, M., Szostek, C. L., Hughes, K. M., Ellis, N. et al. (2017). Global analysis of depletion and recovery of seabed biota after bottom trawling disturbance. *Proceedings of the National Academy of Sciences, 114*(31), 6. doi: 10.1073/pnas.1618858114/-/DCSupplemental

Hinz, H., Murray, L. G., Lambert, G. I., Hiddink, J. G., & Kaiser, M. J. (2013). Confidentiality over fishing effort data threatens science and management progress. *Fish and Fisheries, 14*(1), 110-117. https://doi.org/10.1111/j.1467-2979.2012.00475.x

Holler, P. (2016). Station list and links to master tracks in different resolutions of HEINCKE cruise HE456, Bremerhaven - Bremerhaven, 2016-02-08 - 2016-02-22. PANGAEA: Alfred Wegener Institute, Helmholtz Centre for Polar and Marine Research, Bremerhaven.

Holler, P. (2018). Links to master tracks in different resolutions of HEINCKE cruise HE500, Bremerhaven - Bremerhaven, 2017-10-30 - 2017-11-12. PANGAEA: Alfred Wegener Institute, Helmholtz Centre for Polar and Marine Research, Bremerhaven.

Holler, P., Bartholomä, A., Propp, C., Thiesen, M., & Zeiler, M. (2019). Verteilung der Sedimenttypen auf dem Meeresboden in der deutschen AWZ (1:10.000).

Holler, P., Bartholomä, A., Valerius, J., Thiesen, M., & Mulckau, A. (2020). Map of sediment distribution in the German EEZ (1:10.000).

Holler, P., & Bruns, I. (2020). Acoustic Seafloor Classification of the German EEZ- Impact of sediment types, bioturbation, and natural and man-made seabed features on hydroacoustic images, Cruise No. HE544, 14.10.2019 - 30.10.2019, Bremerhaven (Germany) - Bremerhaven (Germany). Bonn: Gutachterpanel Forschungsschiffe. https://doi.org/10.2312/cr_he544

Holler, P., Markert, E., Bartholomä, A., Capperucci, R. M., Hass, H. C., Kröncke, I., . . . Reimers, H. C. (2017). Tools to evaluate seafloor integrity: comparison of multi-device acoustic seafloor classifications for benthic macrofauna-driven patterns in the German Bight, southern North Sea. *Geo-Marine Letters, 37*, 17. doi: 10.1007/s00367-016-0488-9

Holler, P., Neumann, A., & Bruns, I. (2019). Acoustic Seafloor Classification of the German EEZ-Impact of sediment types, bioturbation, and natural and man-made seabed features on hydroacoustic images, Cruise No. AL520-2, 20.03.2019 - 04.04.2019, Cuxhaven (Germany) - Cuxhaven (Germany), ASKAWZ IV. Bonn: Gutachterpanel Forschungsschiffe; URI: https://oceanrep.geomar.de/id/eprint/46772

Hovland, M., & Indreeide, A. (1980). Detailed Sea Bed Mapping for a Pipeline Across the Norwegian Trench. *The International Hydrographic Review, 57*(2).

Hussain, M., Chen, D., Cheng, A., Wei, H., & Stanley, D. (2013). Change detection from remotely sensed images: From pixel-based to object-based approaches. *ISPRS Journal of Photogrammetry and Remote Sensing, 80*, 91-106. https://doi.org/10.1016/j.isprsjprs.2013.03.006

ICES (2008). Interim Report 2007 for the ICES/BfN-project: "Environmentally Sound Fisheries Management in Protected Areas" [EMPAS] (pp. 67).

ICES (2018a). ICES Technical Service: OSPAR request on the production of spatial data layers of fishing intensity/pressure. In Report of the ICES Advisory Committee, 2019, sr.2018.14. https://doi.org/10.17895/ices.pub.4508

ICES (2018b, 12–16 November 2018). *Interim Report of the Working Group on Fisheries Benthic Impact and Trade-offs (WGFBIT)*. (ICES CM 2018/HAPISG:21). ICES Headquarters, Copenhagen, Denmark.

ICES (2018c). OSPAR request 2018 for spatial data layers of fishing intensity/pressure.

ICES (2018d). Report of the Working Group on Spatial Fisheries Data (WGSFD), 11–15 June 2018, Aberdeen, Scotland, UK (Vol. ICES CM 2018/HAPISG:16, pp. 79).

ICES (2018e). Spatial data layers of fishing intensity/ pressure per gear type for surface and subsurface abrasion, for the years 2009 to 2017 in the OSPAR regions II and III (ver. 2, 22 January, 2019).

ICES (2019). Working Group on Spatial Fisheries Data (WGSFD) *ICES Scientific Reports* (pp. 144).

ICES (2020). Working Group on Marine Habitat Mapping (WGMHM) *ICES Scientific Reports*.

Ierodiaconou, D., Schimel, A. C. G., Kennedy, D., Monk, J., Gaylard, G., Young, M., . . . Rattray, A. (2018). Combining pixel and object based image analysis of ultra-high resolution multibeam bathymetry and backscatter for habitat mapping in shallow marine waters. *Marine Geophysical Research, 39*(1), 271-288. doi: 10.1007/s11001-017-9338-z

Ivanović, A., Neilson, R. D., & O'Neill, F. G. (2011). Modelling the physical impact of trawl components on the seabed and comparison with sea trials. *Ocean Engineering, 38*, 9. doi: 10.1016/j.oceaneng.2010.09.011

Ivanović, A., & O'Neill, F. G. O. (2015). Towing cylindrical fishing gear components on cohesive soils. *Computers and Geotechnics, 65*, 8. http://dx.doi.org/10.1016/j.compgeo.2014.12.003

Jennings, S., & Kaiser, M. J. (1998). The effects of fishing on marine ecosystems. *Advances in marine biology, 34*, 151.

Jing, L. (2018). The principle of side scan sonar and its application in the detection of suspended submarine pipeline treatment. *IOP Conference Series: Materials Science and Engineering, 439*(3), 032068. doi: 10.1088/1757-899X/439/3/032068

Joint-Nature-Conservation-Committee. *Kinetic energy from currents in the Greater North Sea and Celtic Seas (2001) for the EMODnet Seabed Habitats project*.

Joint-Nature-Conservation-Committee. *Kinetic energy from waves in the Greater North Sea and Celtic Seas (2000-2005) for the EMODnet Seabed Habitats project*.

Kaiser, M. J., Hill, A. S., Ramsay, K., Spencer, B. E., Brand, A. R., Veale, E. O., . . . Hawkins, S. J. (1996). Benthic disturbance by fishing gear in the Irish Sea: a comparison of beam trawling and scallop dredging. *Aquatic Conservation: Marine and Freshwater Ecosystems, 6*, 17.

Kaiser, M. J., & Spencer, B. E. (1996). The Effects of Beam-Trawl Disturbance on Infaunal Communities in Different Habitats. *Journal of Animal Ecology, 65*(3), 11.

Kampmeier, M., van der Lee, E. M., Wichert, U., & Greinert, J. (2020). Exploration of the munition dumpsite Kolberger Heide in Kiel Bay, Germany: Example for a standardised hydroacoustic and optic monitoring approach. *Continental Shelf Research, 198*, 104108. https://doi.org/10.1016/j.csr.2020.104108

Kenny, A. J., Cato, I., Desprez, M., Fader, G., Schüttenhelm, R. T. E., & Side, J. (2003). An overview of seabed-mapping technologies in the context of marine habitat classification☆. *ICES Journal of Marine Science, 60*(2), 411-418. doi: 10.1016/s1054-3139(03)00006-7

Klaucke, I. (2018). Sidescan Sonar. In A. Micallef, S. Krastel & A. Savini (Eds.), *Submarine Geomorphology* (pp. 554): Springer.

Kopf, A., Stegmann, S., Krastel, S., Förster, A., Straßer, M., & Irving, M. (2007). Marine deep-water free-fall CPT measurements for landslide characterisation off Crete, Greece (Eastern Mediterranean Sea) Part 2: Initial data from the Western Cretan Sea *Submarine Mass Movements and Their Consequences* (pp. 199-208). Netherland: Springer.

Krantzberg, G. (1985). The influence of bioturbation on physical, chemical and biological parameters in aquatic environments: a review. *Environmental Pollution Series A, Ecological and Biological, 39*(2), 23.

Krost, P., Bernhard, M., Werner, F., & Hukriede, W. (1990). Otter trawl tracks in Kiel Bay (Western Baltic) mapped by side-scan sonar. *Meeresforschung, 32*, 10.

Lamarche, G. L., X. (2018). Introduction to the Special Issue "Seafloor backscatter data from swath mapping echosounders: from technological development to novel applications". *Marine Geophysical Research*. https://doi.org/10.1007/s11001-018-9349-4

Lambert, G. I., Jennings, S., Hiddink, J. G., Hintzen , N. T., Hinz, H., Kaiser, M. J., & Murray, L. G. (2012). Implications of using alternative methods of vessel monitoring system (VMS) data analysis to describe fishing activities and impacts. *ICES Journal of Marine Science, 69*(4), 12. doi: 0.1093/icesjms/fss018

Laurer, W.-U., Naumann, M., & Zeiler, M. (2014). Erstellung der Karte zur Sedimentverteilung auf dem Mee-resboden in der deutschen Nordsee nach der Klassifikationvon FIGGE (1981). Retrieved December 2019, from Geopotenzial Deutsche Nordsee http://www.gpdn.de/gpdn/wilma.aspx?pgId=337&WilmaLogonActionBehavior=Default

Lee, J., South, A. B., & Jennings, S. (2010). Developing reliable, repeatable, and accessible methods to provide high-resolution estimates of fishing-effort distributions from vessel monitoring system (VMS) data. *ICES Journal of Marine Science, 67*(6), 1260-1271. doi: 10.1093/icesjms/fsq010

Lin, X., Dong, R., & Lv, Z. (2023). Deep Learning-Based Classification of Raw Hydroacoustic Signal: A Review. *Journal of Marine Science and Engineering, 11*(1), 3.

Lindeboom, H. J., & de Groot, S. J. (1998). The Effects Of Different Types Of Fisheries On The North Sea And Irish Sea Benthic Ecosystem (pp. 412): Netherlands Institute for Sea Research (NOIZ), Netherlands Institute for Fisheries Research (RIVO-DLO).

Lindholm, J., Gleason, M., Kline, D., Clary, L., Rienecke, S., Cramer, A., & Los Huertos, M. (2015). Ecological effects of bottom trawling on the structural attributes of fish habitat in unconsolidated sediments along the central California outer continental shelf. *Fishery Bulletin, 113*, 15. doi: 10.7755/FB.113.1.8

Lucchetti, A., & Sala, A. (2012). Impact and performance of Mediterranean fishing gear by side-scan sonar technology. *Canadian Journal of Fisheries ans Aquatic Sciences, 69*, 11. doi: 10.1139/f2012-107

Lucieer, V. (2008). Object-oriented classification of sidescan sonar data for mapping benthic marine habitats. *International Journal of Remote Sensing, 29*(3), 17.

Lucieer, V. (2012). *Advancing quantitative techniques for the generation of acoustic variables to characterise seabed habitats*. presentation. Institute of Marine and Antarctic Studies University of Tasmania. International workshop on seabed mapping methods and technology, Trondheim.

Lucking, G., Stark, N., Lippmann, T., & Smyth, S. (2017). Variability of in situ sediment strength and pore pressure behavior of tidal estuary surface sediments. *Geo-Marine Letters, 37*(5), 441-456. doi: 10.1007/s00367-017-0494-6

Lüdmann, T., Saitz, Y. M., Metzing, J., & Emeis, K. C. (2021). Acoustic backscatter analysis of ground-fishing activity in the German North Sea sector. *Continental Shelf Research, 212*, 104292. https://doi.org/10.1016/j.csr.2020.104292

Lurton, X. (2002). *An Introduction to Underwater Acoustics*. Chichester, UK: Praxis Publishing Ltd.

Malik, M. A., & Mayer, L. A. (2007). Investigation of seabed fishing impacts on benthic structureusing multi-beam sonar, sidescan sonar, and video. *ICES Journal of Marine Science, 64*, 13. https://doi.org/10.1093/icesjms/fsm056

Manea, E., Bianchelli, S., Fanelli, E., Danovaro, R., & Gissi, E. (2020). Towards an Ecosystem-Based Marine Spatial Planning in the deep Mediterranean Sea. *Science of The Total Environment, 715*, 136884. https://doi.org/10.1016/j.scitotenv.2020.136884

Manley, R. B. (1977). *Drag Marks, A New Tool For Studying Soil Stability Offshore.* Paper presented at the Offshore Technology Conference.

Markert, E. H., P.; Kröncke, I.; Bartholomä, A. (2013). Benthic habitat mapping of sorted bedforms using hydroacoustic and ground-truthing methods in a coastal area of the German Bight/North Sea. *Estuarine, Coastal and Shelf Science, 129*, 12. http://dx.doi.org/10.1016/j.ecss.2013.05.027

McLaverty, C., Eigaard, O. R., Olsen, J., Brooks, M. E., Petersen, J. K., Erichsen, A. C., . . . Dinesen, G. E. (2023). European coastal monitoring programmes may fail to identify impacts on benthic macrofauna caused by bottom trawling. *J Environ Manage, 334*, 117510. doi: 10.1016/j.jenvman.2023.117510

Mengual, B., Cayocca, F., Le Hir, P., Draye, R., Laffargue, P., Vincent, B., & Garlan, T. (2016). Influence of bottom trawling on sediment resuspension in the 'Grande-Vasière' area (Bay of Biscay, France). *Ocean Dynamics, 66*(9), 1181-1207. doi: 10.1007/s10236-016-0974-7

Mérillet, L., Kopp, D., Robert, M., Salaün, M., Méhault, S., Bourillet, J.-F., & Mochet, M. (2018). Are trawl marks a good indicator of trawling pressure in muddy sand fishing grounds? *Ecological Indicators, 85*, 5. https://doi.org/10.1016/j.ecolind.2017.11.016

Mérillet, L., Mouchet, M., Robert, M., Salaün, M., Schuck, L., Vaz, S., & Kopp, D. (2017). Using underwater video to assess megabenthic community vulnerability to trawling in the

Grande Vasière (Bay of Biscay). *Environmental Conservation, 45*(2), 10. doi: 10.1017/S0376892917000480

Methratta, E. T., & Dardick, W. R. (2019). Meta-Analysis of Finfish Abundance at Offshore Wind Farms. *Reviews in Fisheries Science & Aquaculture, 27*(2), 19. doi: 10.1080/23308249.2019.1584601

Meyerhof, G. G. (1953). *The bearing capacity of foundations under eccentric and inclined loads.* Paper presented at the Proceedings, 3rd International Conference on Soil Mechanics and Foundation Engineering.

Michaelis, R., Hass, H. C., Papenmeier, S., & Wiltshire, K. H. (2019). Automated Stone Detection on Side-Scan Sonar Mosaics Using Haar-Like Features. *Geosciences, 9*(5), 216. https://doi.org/10.3390/geosciences9050216

Michałowska, M., & Rapiński, J. (2021). A Review of Tree Species Classification Based on Airborne LiDAR Data and Applied Classifiers. *Remote Sensing, 13*(3), 353. https://doi.org/10.3390/rs13030353

Mielck, F. H., P.; Bürk, D., Hass, H.C. (2015). Interannual variability of sorted bedforms in the coastal German Bight (SE NorthSea). *Continental Shelf Research, 111*(A), 10. http://dx.doi.org/10.1016/j.csr.2015.10.016

Morys, C., Brüchert, V., & Bradshaw, C. (2021). Impacts of bottom trawling on benthic biogeochemistry in muddy sediments: Removal of surface sediment using an experimental field study. *Marine Environmental Research, 169*, 105384. https://doi.org/10.1016/j.marenvres.2021.105384

Natural-Resources-Canada. (2021). QGIS plugin geo_sim_processing. https://github.com/NRCan/geo_sim_processing.

Neumann, H., Diekmann, R., Emeis, K.-C., Kleeberg, U., Moll, A., & Kröncke, I. (2017). Full-coverage spatial distribution of epibenthic communities in the south-eastern North Sea in relation to habitat characteristics and fishing effort. *Marine Environmental Research, 130*, 11. http://dx.doi.org/10.1016/j.marenvres.2017.07.010

O'Neill, F. G., & Ivanović, A. (2015). The physical impact of towed demersal fishing gears on soft sediments. *ICES Journal of Marine Science, 73*(suppl_1), i5-i14. doi: 10.1093/icesjms/fsv125

Oberle, F. K. J., Storlazzi, C. D., & Hanebuth, T. J. J. (2016). What a drag: Quantifying the global impact of chronic bottom trawling on continental shelf sediment. *Journal of Marine Systems, 159*, 11. http://dx.doi.org/10.1016/j.jmarsys.2015.12.007

Oberle, F. K. J., Swarzenski, P. W., Reddy, C. M., Nelson, R. K., Baasch, B., & Hanebuth, T. J. J. (2016). Deciphering the lithological consequences of bottom trawling to sedimentary habitats on the shelf. *Journal of Marine Systems, 159*, 120-131. https://doi.org/10.1016/j.jmarsys.2015.12.008

Palanques, A., Guillén, J., & Piug, P. (2001). Impact of bottom trawling on water turbidity and muddy sediment of an unfished continental shelf. *Limnol. Oceanogr., 46*(5), 11.

Palanques, A., Puig, P., Guillén, J., Demestre, M., & Martín, J. (2014). Effects of bottom trawling on the Ebro continental shelf sedimentary system (NW Mediterranean). *Continental Shelf Research, 72*, 15. http://dx.doi.org/10.1016/j.csr.2013.10.008

Papenmeier, S. (2017). Station list and links to master tracks in different resolutions of HEINCKE cruise HE478, Bremerhaven - Bremerhaven, 2017-03-02 - 2017-03-15. PANGAEA: Alfred Wegener Institute, Helmholtz Centre for Polar and Marine Research, Bremerhaven.

Papenmeier, S., Hass, H. C., Propp, C., Thiesen, M., & Zeiler, M. (Cartographer). (2019). Verteilung der Sedimenttypen auf dem Meeresboden in der deutschen AWZ (1:10.000).

Papenmeier, S. H., C. (2018). Detection of Stones in Marine Habitats Combining Simultaneous Hydroacoustic Surveys. *Geosciences, 8*(279), 14. doi: 10.3390/geosciences8080279

Paradis, S., Lo Iacono, C., Masqué, P., Puig, P., Palanques, A., & Russo, T. (2021). Evidence of large increases in sedimentation rates due to fish trawling in submarine canyons of the Gulf of Palermo (SW Mediterranean). *Marine Pollution Bulletin, 172*, 112861. https://doi.org/10.1016/j.marpolbul.2021.112861

Paschen, M., Richter, U., & Köpnick, W. (2000). Trawl penetration in the seabed (TRAPESE) *Final Report EC-Study Contract* (Vol. Nr. 96-006, pp. 150).

Pedersen, S. A., Fock, H., Krause, J., Pusch, C., Sell, A. L., Böttcher, U., . . . Rice, J. C. (2009). Natura 2000 sites and fisheries in German offshore waters. *ICES Journal of Marine Science, 66*(1), 155-169. doi: 10.1093/icesjms/fsn193

Pesch, R., Pehlke, H., Jerosch, K., Schröder, W., & Schlüter, M. (2008). Using decision trees to predict benthic communities within and near the German Exclusive Economic Zone (EEZ) of the North Sea. *Environmental Monitoring and Assessment, 136*(1), 313-325. doi: 10.1007/s10661-007-9687-1

Phiri, D., & Morgenroth, J. (2017). Developments in Landsat Land Cover Classification Methods: A Review. *Remote Sensing, 9*(9), 967. https://doi.org/10.3390/rs9090967

Pillay, T., Cawthra, H. C., & Lombard, A. T. (2021). Integration of machine learning using hydroacoustic techniques and sediment sampling to refine substrate description in the Western Cape, South Africa. *Marine Geology, 440*, 106599. https://doi.org/10.1016/j.margeo.2021.106599

Populus, J., Vasquez, M., Albrecht, J., Manca, E., Agnesi, S., Al Hamdani, Z., . . . Tunesi, L. (2017). EUSeaMap, a European broad-scale seabed habitat map. 174. http://doi.org/10.13155/49975

QGIS-Development-Team (2023). QGIS Geographic Information System *Open Source Geospatial Foundation Project*. http://qgis.osgeo.org.

Queirós, A. M., Hiddink, J. G., Kaiser, M. J., & Hinz, H. (2006). Effects of chronic bottom trawling disturbance on benthic biomass, production and size spectra in different habitats. *Journal of Experimental Marine Biology and Ecology, 335*(1), 91-103. https://doi.org/10.1016/j.jembe.2006.03.001

Quinn, R., Dean, M., Lawrence, M., Liscoe, S., & Boland, D. (2005). Backscatter responses and resolution considerations in archaeological side-scan sonar surveys: a control experiment. *Journal of Archaeological Science, 32*(8), 1252-1264. https://doi.org/10.1016/j.jas.2005.03.010

Reading, C. J., & McGrorty, S. (1978). Seasonal variations in the burying depth of Macoma balthica (L.) and its accessibility to wading birds. *Estuarine and Coastal Marine Science, 6*(2), 135-144. https://doi.org/10.1016/0302-3524(78)90095-6

Reiss, H., & Kröncke, I. (2005). Seasonal variability of infaunal community structures in three areas of the North Sea under different environmental conditions. *Estuarine, Coastal and Shelf Science, 65*(1), 253-274. https://doi.org/10.1016/j.ecss.2005.06.008

Richardson, M., Valent, P., Briggs, K., Bradley, J., & Griffin, S. (2001). *NRL mine burial experiments.* Paper presented at the NRL report, project no. BE-782-001.

Rijnsdorp, A. D., Buys, A. M., Storbeck, F., & Visser, E. G. (1998). Micro-scale distribution of beam trawl effort in the southern North Sea between 1993 and 1996 in relation to the trawling

frequency of the sea bed and the impact on benthic organisms. *ICES Journal of Marine Science, 55*, 17.

Rijnsdorp, A. D., Depestele, J., Eigaard, O. R., Hintzen, N. T., Ivanovic, A., Molenaar, P., et al. (2020). Mitigating seafloor disturbance of bottom trawl fisheries for North Sea sole Solea solea by replacing mechanical with electrical stimulation. *PLoS ONE, 15*(11), e0228528. doi: 10.1371/journal.pone.0228528

Roskoden, R. R. (2020). *Processing advancements of free fall penetrometer data and their ground proving in regional studies in New Zealand*. Dissertation. Bremen.

Runya, R. M., McGonigle, C., Quinn, R., Howe, J., Collier, J., Fox, C., et al. (2021). Examining the Links between Multi-Frequency Multibeam Backscatter Data and Sediment Grain Size. *Remote Sensing, 13*(8), 1539. https://doi.org/10.3390/rs13081539

Saastamoinen, K., & Penttinen, S. (2021). Visual seabed classification using k-means clustering, CIELAB colors and Gabor-filters. *Procedia Computer Science, Volume 192*, 7. https://doi.org/10.1016/j.procs.2021.09.016

Sala, A., Notti, E., Bonanomi, S., Pulcinella, J., & Colombelli, A. (2019). Trawling in the Mediterranean: An Exploration of Empirical Relations Connecting Fishing Gears, Otterboards and Propulsive Characteristics of Fishing Vessels. *Frontiers in Marine Science, 6*(534). doi: 10.3389/fmars.2019.00534

Sams, T., Hansen, J. L., Thisen, E., & Stage, B. (2004). Segmentation of sidescan sonar images. http://server.oersted.dtu.dk/publications/views/publication_details.php?id=2612: Danish Defence Research Establishment.

Schönke, M., Clemens, D., & Feldens, P. (2022). Quantifying the Physical Impact of Bottom Trawling Based on High-Resolution Bathymetric Data. *Remote Sensing, 14*(12), 2782. https://doi.org/10.3390/rs14122782

Schulze, T. (2018). International fishing activities (2012-2016) in German waters in relation to the designated Natura 2000 areas and proposed management within. Hamburg: Johann Heinrich von Thünen-Institute Federal Research Institute for Rural Areas, Forestry and Fisheries Institute of Sea Fisheries.

Schwarzer, K., & Diesing, M. (2006). Identification of submarine hard-bottom substrates in the German North Sea and Baltic Sea EEZ with high-resolution acoustic seafloor imaging *Progress in Marine Conservation in Europe* (pp. 111-125). Springer Berlin Heidelberg.

Schwarzer, K., Ricklefs, K., Bartholomä, A., & Zeiler, M. (2008). Geological Development of the North Sea ans the Baltic Sea. *Die Küste, 74*, 15.

Schwinghammer, P., Gordon, J., D.C.; , Rowell, T. W., Prena, J., McKeown, D. L., Sonnichsen, G., & Guignés, J. Y. (1998). Effects of Experimental Otter Trawling on Surficial Sediment Properties of a Sandy-Bottom Ecosystem on the Grand Banks of Newfoundland. *Conservation Biology, 12*(6), 8.

Sciberras, M., Hiddink, J. G., Jennings, S., Szostek, C. L., Hughes, K. M., Kneafsey, B., . . . Kaiser, M. J. (2018). Response of benthic fauna to experimental bottom fishing: A global meta-analysis. *Fish and Fisheries, 19*(4), 698-715. https://doi.org/10.1111/faf.12283

Serpetti, N., Heath, M., Armstrong, E., & Witte, U. (2011). Blending single beam RoxAnn and multi-beam swathe QTC hydro-acoustic discrimination techniques for the Stonehaven area, Scotland, UK. *Journal of Sea Research, 65*(4), 442-455. https://doi.org/10.1016/j.seares.2011.04.001

Shepperson, J. L., Hintzen, N. T., Szostek, C. L., Bell, E., Murray, L. G., & Kaiser, M. J. (2017). A comparison of VMS and AIS data: the effect of data coverage and vessel position recording

frequency on estimates of fishing footprints. *ICES Journal of Marine Science, 75*(3), 988-998. doi: 10.1093/icesjms/fsx230

Smith, C. J., Banks, A. C., & Papadopoulou, K.-N. (2007). Improving the quantitative estimation of trawling impacts from sidescan-sonar and underwater-video imagery *ICES Journal of Marine Science, 64*, 9. https://doi.org/10.1093/icesjms/fsm165

Son, C. S., Flemming, B. W., & Chang, T. S. (2012). Sedimentary facies of shoreface-connected sand ridges off the East Frisian barrier-island coast, southern North Sea: climatic controls and preservation potential. *Int. Assoc. Sedimentol. Spec. Publ., 44*, 16. https://doi.org/10.1002/9781118311172.ch7

Stanev, E. V., Dobrynin, M., Pleskachevsky, A., Grayek, S., & Günther, H. (2009). Bed shear stress in the southern North Sea as an important driver for suspended sediment dynamics. *Ocean Dynamics, 59*, 12. doi: 10.1007/s10236-008-0171-4

Stark, N. (2010). *Geotechnical Investigation of Sediment Remobilization Processes using Dynamic Penetrometers.* Dissertation, Bremen University, Bremen.

Stark, N., Coco, G., Bryan, K. R., & Kopf, A. (2012). In-Situ Geotechnical Characterization of Mixed-Grain-Size Bedforms Using A Dynamic Penetrometer. *Journal of Sedimentary Research, 82*(7), 540-544. doi: 10.2110/jsr.2012.45

Stark, N., Hanff, H., Svenson, C., Ernstsen, V., Lefebvre, A., Winter, C., & Kopf, A. (2011). Coupled penetrometer, MBES and ADCP assessments of tidal variations in surface sediment layer characteristics along active subaqueous dunes, Danish Wadden Sea. *Geo-Marine Letters, 31*(4), 249-258. doi: 10.1007/s00367-011-0230-6

Stark, N., & Kopf, A. (2011, 19-22 Sept. 2011). *Detection and quantification of sediment remobilization processes using a dynamic penetrometer.* Paper presented at the OCEANS'11 MTS/IEEE KONA.

Stark, N., Kopf, A., Hanff, H., Stegmann, S., & Wilkens, R. (2009, 26-29 Oct. 2009). *Geotechnical investigations of sandy seafloors using dynamic penetrometers.* Paper presented at the OCEANS 2009.

Stark, N., Wilkens, R., Ernstsen, V. B., Lambers-Huesmann, M., Stegmann, S., & Kopf, A. (2011). Geotechnical Properties of Sandy Seafloors and the Consequences for Dynamic Penetrometer Interpretations: Quartz Sand Versus Carbonate Sand. *Geotechnical and Geological Engineering, 30*(1), 1-14. doi: 10.1007/s10706-011-9444-7

STECF (2019). *Review of Joint Recommendations for Natura 2000 sites at Dogger Bank, Cleaver Bank, Frisian Front and Central Oyster grounds (STECF-19-04)*. Luxembourg: Publications Office of the European Union.

Stein, R. (1985). Rapid grain-size analyses of clay and silt fraction by SediGraph 5000D: Comparison with Coulter Counter and Atterberg methods. *Journal of Sedimentary Petrology, 55*(4), 4.

Stelzenmüller, V., Fock, H. O., Gimpel, A., Rambo, H., Diekmann, R., Probst, W. N., . . . Kröncke, I. (2015). Quantitative environmental risk assessments in the context of marine spatial management: current approaches and some perspectives. *ICES Journal of Marine Science, 72*(3), 21. doi: 10.1093/icesjms/fsu206

Stoll, R. D., & Akal, T. (1999). XBP- Tool for Rapid Assessment of Seabed Sediment Properties. *Sea technology, 40*(2), 47-52.

Stoll, R. D., Sun, Y. F., & Bitte, I. (2007). Seafloor Properties From Penetrometer Tests. *IEEE Journal of Oceanic Engineering, 32*(1), 57-63. doi: 10.1109/JOE.2007.890943

Sündermann, J., & Pohlmann, T. (2011). A brief analysis of North Sea physics. *OCEANOLOGIA, 53*(3), 27. doi: 10.5697/oc.53-3.663

Terzaghi, K. (1943). *Theoretical soil mechanics*. New York: Wiley.

Tiano, J. C., van der Reijden, K. J., O'Flynn, S., Beauchard, O., van der Ree, S., van der Wees, J., et al. (2020). Experimental bottom trawling finds resilience in large-bodied infauna but vulnerability for epifauna and juveniles in the Frisian Front. *Marine Environmental Research, 159*, 104964. https://doi.org/10.1016/j.marenvres.2020.104964

Trimmer, M., Petersen, J., Sivyer, D. B., Mills, C., Young, E., & Parker, E. R. (2005). Impact of long-term benthic trawl disturbance on sediment sorting and biogeochemistry in the southern North Sea. *Marine Ecology Progress Series, 298*, 16.

Turenhout, M. N. J., Zaalmink, B. W., Strietman, W. J., & Hamon, K. G. (2016). Pulse fisheries in the Netherlands; Economic and spatial impact study (Vol. 2016-104, pp. 32). Wageningen: Wageningen Economic Research.

van Denderen, P. D., Hintzen, N. T., van Kooten, T., & Rijnsdorp, A. D. (2014). Temporal aggregation of bottom trawling and its implication for the impact on the benthic ecosystem. *ICES Journal of Marine Science, 72*(3), 952-961. doi: 10.1093/icesjms/fsu183

van der Molen, J., Aldridge, J. N., Coughlan, C., Parker, E. R., Stephens, D., & Ruardij, P. (2013). Modelling marine ecosystem response to climate change and trawling in the North Sea. *Biogeochemistry, 113*(1), 213-236. doi: 10.1007/s10533-012-9763-7

Wan, J., Qin, Z., Cui, X., Yang, F., Yasir, M., Ma, B., & Liu, X. (2022). MBES Seabed Sediment Classification Based on a Decision Fusion Method Using Deep Learning Model. *Remote Sensing, 14*(15), 3708. https://doi.org/10.3390/rs14153708

Weih, R. C., & Riggan, N. D. (2010). Object-based classification vs. pixel-based classification: Comparative importance of multi-resolution imagery. *The International Archives of the Photogrammetry, Remote Sensing and Spatial Information Sciences, 38*(4), C7.

Werner, F., Hoffmann, G., Bernhard, M., Milkert, D., & Vikgren, K. (1990). Sedimentologische Auswirkungen der Grundfischerei in der Kieler Bucht (Westliche Ostsee). *Meyniana, 42*, 29.

Winterwerp, J. C., van Kesteren, W. G. M., van Prooijen, B., & Jacobs, W. (2012). A conceptual framework for shear flow–induced erosion of soft cohesive sediment beds. *Journal of Geophysical Research: Oceans, 117*(C10). https://doi.org/10.1029/2012JC008072

Yan, W. Y., Shaker, A., & El-Ashmawy, N. (2015). Urban land cover classification using airborne LiDAR data: A review. *Remote Sensing of Environment, 158*, 295-310. https://doi.org/10.1016/j.rse.2014.11.001

Zeiler, M., Milbradt, P., Plüß, A., & Valerius, J. (2014). Modelling Large Scale Sediment Transport in the German Bight (North Sea). *Die Küste, 81*, 24.

Zeiler, M., Schwarzer, K., Bartholomä, A., & Ricklefs, K. (2008). Seabed Morphology and Sediment Dynamics. *Die Küste, 74*, 13.

Zhang, W., Wirtz, K., Daewl, U., Wrede, A., Kröncke, I., Kuhn, G., . . . Schrum, C. (2019). The Budget of Macrobenthic Reworked Organic Carbon: A Modeling Case Study of the North Sea. *Journal of Geophysical Research: Biogeosciences, 124*, 26. https://doi.org/10.1029/2019JG005109

Zhao, J., Yan, J., Zhang, H., & Meng, J. (2017). A New Radiometric Correction Method for Side-Scan Sonar Images in Consideration of Seabed Sediment Variation. Remote Sensing, 9(6), 575. https://doi.org/10.3390/rs9060575

Appendix

The source code of the procedure for the automated mapping of trawl marks presented in chapter 5 can be found on the following pages. It was generated using the GRASS GIS model builder (GRASS-Development-Team, 2022). The output vector files of this model are further processed using QGIS as indicated in chapter 5.3.3. Please note that the file names, data paths and directories may differ according to the specific structure and nomenclature that is used.

```
#!/usr/bin/env python3
#
############################################################################
#
# MODULE:       Modell
#
# AUTHOR(S):    IBruns
#
# PURPOSE:      Skript erzeugt durch den wxGUI  Grafischen Modellierer.
#
# DATE:         Tue Jul  4 16:39:07 2023
#
############################################################################

# %module
# % description: Skript erzeugt durch den wxGUI  Grafischen Modellierer.
# %end
# %option
# % key: rimport1_verbose
# % description: Ausführlicher Ausgabemodus
# % required: yes
# % type: string
# % options: True, False
# % guisection: Flags
# % answer: True
# %end
# %option
# % key: rimport1_input
# % description: Name of GDAL dataset to be imported
# % required: yes
# % type: string
# % key_desc: name
# % answer: C:\Users\path\original_raster
# %end
# %option
# % key: rimport1_output
# % description: Name der Ausgabe-Rasterkarte.
# % required: yes
# % type: string
# % key_desc: name
# % answer: original_raster
# %end
# %option
# % key: rimport1_extent
# % description: Output raster map extent
# % required: yes
# % type: string
# % answer: input
# %end
# %option
```

```
# % key: rmfilter2_verbose
# % description: Ausführlicher Ausgabemodus
# % required: yes
# % type: string
# % options: True, False
# % guisection: Flags
# % answer: True
# %end
# %option
# % key: rmfilter2_input
# % description: Name der Eingabe-Rasterkarte
# % required: yes
# % type: string
# % key_desc: name
# % answer: original_raster
# %end
# %option
# % key: rmfilter2_output
# % description: Name der Ausgabe-Rasterkarte
# % required: yes
# % type: string
# % key_desc: name
# % answer: raster_lowpass
# %end
# %option
# % key: rmfilter2_filter
# % description: Pfad zur Datei mit Filterinformationen.
# % required: yes
# % type: string
# % key_desc: name
# % answer: C:\Users\ C:\Users\path\rmfilter_lowpass.txt
# %end
# %option
# % key: rmfilter2_repeat
# % description: Wie oft soll der Filter wiederholt werden?
# % required: yes
# % type: integer
# % answer: 15
# %end
# %option
# % key: rrescaleeq3_verbose
# % description: Ausführlicher Ausgabemodus
# % required: yes
# % type: string
# % options: True, False
# % guisection: Flags
# % answer: True
# %end
# %option
# % key: rrescaleeq3_input
# % description: Name der Rasterkarte, die reskaliert werden soll.
# % required: yes
# % type: string
# % key_desc: name
# % answer: raster_lowpass
# %end
# %option
# % key: rrescaleeq3_output
# % description: Name der resultierenden Rasterkarte.
# % required: yes
# % type: string
# % key_desc: name
# % answer: raster_lowp_histeq
# %end
# %option
# % key: rrescaleeq3_to
# % description: Ausgabe Wertebereich
```

```
# % required: yes
# % type: integer
# % key_desc: min, max
# % answer: 0,255
# %end
# %option
# % key: iedge4_verbose
# % description: Ausführlicher Ausgabemodus
# % required: yes
# % type: string
# % options: True, False
# % guisection: Flags
# % answer: True
# %end
# %option
# % key: iedge4_input
# % description: Name der Eingabe-Rasterkarte
# % required: yes
# % type: string
# % key_desc: name
# % answer: raster_lowp_histeq
# %end
# %option
# % key: iedge4_output
# % description: Name der Ausgabe-Rasterkarte
# % required: yes
# % type: string
# % key_desc: name
# % answer: raster_edge
# %end
# %option
# % key: iedge4_low_threshold
# % description: Low treshold for edges in Canny
# % required: yes
# % type: double
# % answer: 1
# %end
# %option
# % key: iedge4_high_threshold
# % description: High treshold for edges in Canny
# % required: yes
# % type: double
# % answer: 5
# %end
# %option
# % key: iedge4_sigma
# % description: Kernel radius
# % required: yes
# % type: double
# % answer: 3
# %end
# %option
# % key: igroup5_l
# % description: List files from specified (sub)group
# % required: yes
# % type: string
# % options: True, False
# % guisection: Flags
# % answer: True
# %end
# %option
# % key: igroup5_s
# % description: List subgroups from specified group
# % required: yes
# % type: string
# % options: True, False
# % guisection: Flags
```

```
# % answer: True
# %end
# %option
# % key: igroup5_verbose
# % description: Ausführlicher Ausgabemodus
# % required: yes
# % type: string
# % options: True, False
# % guisection: Flags
# % answer: True
# %end
# %option
# % key: igroup5_group
# % description: Name der Bildgruppe.
# % required: yes
# % type: string
# % key_desc: name
# % answer: raster_group
# %end
# %option
# % key: igroup5_subgroup
# % description: Name of imagery subgroup
# % required: yes
# % type: string
# % key_desc: name
# % answer: raster_subgroup
# %end
# %option
# % key: igroup5_input
# % description: Name der Rasterkarte(n), die in die Gruppe eingefügt werden sollen.
# % required: yes
# % type: string
# % key_desc: name
# % answer: raster_lowpass,raster_lowp_histeq,raster_edge
# %end
# %option
# % key: igroup5_file
# % description: Input file with one raster map name per line
# % required: yes
# % type: string
# % key_desc: name
# % answer: C:\Users\\path\original_raster\MAPSET\.tmp
# %end
# %option
# % key: icluster6_overwrite
# % description: Ausgabedateien dürfen bereits existierende Dateien überschreiben.
# % required: yes
# % type: string
# % options: True, False
# % guisection: Flags
# % answer: True
# %end
# %option
# % key: icluster6_verbose
# % description: Ausführlicher Ausgabemodus
# % required: yes
# % type: string
# % options: True, False
# % guisection: Flags
# % answer: True
# %end
# %option
# % key: icluster6_classes
# % description: Initiale Anzahl der Klassen.
# % required: yes
# % type: integer
# % answer: 5
```

```
# %end
# %option
# % key: icluster6_iterations
# % description: Maximale Zahl der Iterationen.
# % required: yes
# % type: integer
# % answer: 300
# %end
# %option
# % key: icluster6_convergence
# % description: Prozent Konvergenz.
# % required: yes
# % type: double
# % answer: 98.0
# %end
# %option
# % key: icluster6_separation
# % description: Cluster-Separation.
# % required: yes
# % type: double
# % answer: 0.6
# %end
# %option
# % key: icluster6_min_size
# % description: Minimale Anzahl von Pixeln in einer Klasse.
# % required: yes
# % type: integer
# % answer: 17
# %end
# %option
# % key: imaxlik7_overwrite
# % description: Ausgabedateien dürfen bereits existierende Dateien überschreiben.
# % required: yes
# % type: string
# % options: True, False
# % guisection: Flags
# % answer: True
# %end
# %option
# % key: imaxlik7_verbose
# % description: Ausführlicher Ausgabemodus
# % required: yes
# % type: string
# % options: True, False
# % guisection: Flags
# % answer: True
# %end
# %option
# % key: imaxlik7_group
# % description: Name der Eingabe-Bildgruppe
# % required: yes
# % type: string
# % key_desc: name
# % answer: raster_group@PERMANENT
# %end
# %option
# % key: imaxlik7_subgroup
# % description: Name der Eingabe-Bild-Untergruppe
# % required: yes
# % type: string
# % key_desc: name
# % answer: raster_subgroup
# %end
# %option
# % key: imaxlik7_signaturefile
# % description: Name of input file containing signatures
# % required: yes
```

```
# % type: string
# % key_desc: name
# % answer: cluster_sig@PERMANENT
# %end
# %option
# % key: imaxlik7_output
# % description: Name for output raster map holding classification results
# % required: yes
# % type: string
# % key_desc: name
# % answer: raster_classif_maxlik
# %end
# %option
# % key: rmapcalcsimple8_q
# % description: Quote the map names
# % required: yes
# % type: string
# % options: True, False
# % guisection: Flags
# % answer: True
# %end
# %option
# % key: rmapcalcsimple8_overwrite
# % description: Ausgabedateien dürfen bereits existierende Dateien überschreiben.
# % required: yes
# % type: string
# % options: True, False
# % guisection: Flags
# % answer: True
# %end
# %option
# % key: rmapcalcsimple8_verbose
# % description: Ausführlicher Ausgabemodus
# % required: yes
# % type: string
# % options: True, False
# % guisection: Flags
# % answer: True
# %end
# %option
# % key: rtovect9_verbose
# % description: Ausführlicher Ausgabemodus
# % required: yes
# % type: string
# % options: True, False
# % guisection: Flags
# % answer: True
# %end
# %option
# % key: rtovect9_input
# % description: Name der Eingabe-Rasterkarte
# % required: yes
# % type: string
# % key_desc: name
# % answer: raster_classif_TM
# %end
# %option
# % key: rtovect9_output
# % description: Name der Ausgabe-Vektorkarte
# % required: yes
# % type: string
# % key_desc: name
# % answer: vect_classif_TM
# %end
# %option
# % key: rtovect9_type
# % description: Output feature type
```

```
# % required: yes
# % type: string
# % answer: area
# %end
# %option
# % key: rtovect10_overwrite
# % description: Ausgabedateien dürfen bereits existierende Dateien überschreiben.
# % required: yes
# % type: string
# % options: True, False
# % guisection: Flags
# % answer: True
# %end
# %option
# % key: rtovect10_verbose
# % description: Ausführlicher Ausgabemodus
# % required: yes
# % type: string
# % options: True, False
# % guisection: Flags
# % answer: True
# %end
# %option
# % key: rtovect10_input
# % description: Name der Eingabe-Rasterkarte
# % required: yes
# % type: string
# % key_desc: name
# % answer: raster_edge
# %end
# %option
# % key: rtovect10_output
# % description: Name der Ausgabe-Vektorkarte
# % required: yes
# % type: string
# % key_desc: name
# % answer: vect_edge
# %end
# %option
# % key: rtovect10_type
# % description: Output feature type
# % required: yes
# % type: string
# % answer: area
# %end

import sys
import os
import atexit

from grass.script import parser, run_command

def cleanup():
    pass

def main(options, flags):
    run_command("r.import",
                verbose = True,
                input=options["rimport1_input"],
                memory=300,
                output=options["rimport1_output"],
                resample="nearest",
                extent=options["rimport1_extent"],
                resolution="estimated")

    run_command("r.mfilter",
                overwrite = True,
```

```
                verbose = True,
                input=options["rmfilter2_input"],
                output=options["rmfilter2_output"],
                filter=options["rmfilter2_filter"],
                repeat=options["rmfilter2_repeat"],
                nprocs=1)

    run_command("r.rescale.eq",
                overwrite = True,
                verbose = True,
                input=options["rrescaleeq3_input"],
                output=options["rrescaleeq3_output"],
                to=options["rrescaleeq3_to"])

    run_command("i.edge",
                overwrite = True,
                verbose = True,
                input=options["iedge4_input"],
                output=options["iedge4_output"],
                angles_map="edge_angles",
                low_threshold=options["iedge4_low_threshold"],
                high_threshold=options["iedge4_high_threshold"],
                sigma=options["iedge4_sigma"])

    run_command("i.group",
                flags='ls'    +    getParameterizedFlags(options,    ["igroup5_l",
"igroup5_s"]),
                verbose = True,
                group=options["igroup5_group"],
                subgroup=options["igroup5_subgroup"],
                input=options["igroup5_input"],
                file=options["igroup5_file"])

    run_command("i.cluster",
                overwrite = True,
                verbose = True,
                group="raster_group@PERMANENT",
                subgroup="raster_subgroup",
                signaturefile="cluster_sig",
                classes=options["icluster6_classes"],
                iterations=options["icluster6_iterations"],
                convergence=options["icluster6_convergence"],
                separation=options["icluster6_separation"],
                min_size=options["icluster6_min_size"])

    run_command("i.maxlik",
                overwrite = True,
                verbose = True,
                group=options["imaxlik7_group"],
                subgroup=options["imaxlik7_subgroup"],
                signaturefile=options["imaxlik7_signaturefile"],
                output=options["imaxlik7_output"])

    run_command("r.mapcalc.simple",
                flags='q' + getParameterizedFlags(options, ["rmapcalcsimple8_q"]),
                overwrite = True,
                verbose = True,
                expression="if("raster_classif_maxlik"                          ==
1,"raster_classif_maxlik", null())",
                a="raster_classif_maxlik",
                output="raster_classif_TM")

    run_command("r.to.vect",
                overwrite = True,
                verbose = True,
                input=options["rtovect9_input"],
                output=options["rtovect9_output"],
```

```
                type=options["rtovect9_type"],
                column="value")

    run_command("r.to.vect",
                overwrite = True,
                verbose = True,
                input=options["rtovect10_input"],
                output=options["rtovect10_output"],
                type=options["rtovect10_type"],
                column="value")

    return 0

def getParameterizedFlags(paramFlags, itemFlags):
    fl = ''
    for i in [key for key, value in paramFlags.items() if value == 'True']:
        if i in itemFlags:
            fl += i[-1]

    return fl

if __name__ == "__main__":
    options, flags = parser()
    atexit.register(cleanup)
    sys.exit(main(options, flags))
```

Acknowledgements

Firstly, I would like to sincerely thank my supervisor Prof. Dr. André Freiwald for giving me the opportunity to accomplish this dissertation as well as for fruitful advices and supporting my ideas. Secondly, I like to express my gratitude to Prof. Dr. Ingrid Kröncke, who kindly agreed to be the second reviewer of my thesis.

Dr. Alexander Bartholomä, head of the Marine Sedimentology working group at Senckenberg am Meer, I would like to genuinely thank for patiently and constantly supporting my thesis with his decades of experience in marine science. Our deceased colleague Dr. Peter Holler (SaM) I like to thank for being an excellent chief scientist on all the expeditions I participated and for answering my millions of questions on hydro-acoustics. The late Dr. H. Christian Hass (AWI Sylt) I like to thank for being part of my thesis committee enriching the discussions with great advices and ideas.

A huge thank you goes to all the seafarers I met during the data acquisition for this thesis. Without you this research would not have been possible! The captains and crews of R/V Senckenberg, R/V Heincke and R/V Alkor made everything possible and maneuvered us safely through rough North Sea weathers. I really enjoyed the friendly and supportive working atmosphere onboard.

Thanks go to Astrid Raschke for her support in the lab (and reminding us of Alex' birthday every year right on time). I also would like to thank Maik Wilsenack for his technical support onboard, using an old piece of wire for 50 Pfennig to reliably repair things I don't even know the name of.

Barbara, Jana, Julia, Neele and Ruggero, my Senckenberg fellows, I like to thank you very much for the nice lunch breaks, hallway-chats and discussions on all sorts of (scientific) subjects. I also like to express my appreciation to Robert, Janine, Conny, Roberto and all L2.4ies from LBEG Hannover for their constant support and asking how it is going with the thesis.

My warmest thanks go to Anna and Wiebke for being there for me anytime, listening to my concerns and dispelling them with lots of hugs, silly jokes, white wine and soul food. Moreover, I like to appreciate the fluffy support by Bonny & Rosalie in their important function as emotional support cats while writing my thesis at Annas place.
Benno, my husband and dearest friend, I deeply thank you for being with me for 16 years now, supporting me in all respects with this distinctive mixture of love, rationality, imagination and a fairly strange sense of humor. From all the weird things I found on the internet you are by far the best <3

Versicherung an Eides Statt / Affirmation in lieu of an oath

gem. § 5 Abs. 5 der Promotionsordnung vom 15.07.2015 / *according to § 5 (5) of the Doctoral Degree Rules and Regulations of 15 July, 2015*

Ich/I,

Ines Bruns

versichere an Eides Statt durch meine Unterschrift, dass ich die vorliegende Dissertation selbständig und ohne fremde Hilfe angefertigt und alle Stellen, die ich wörtlich dem Sinne nach aus Veröffentlichungen entnommen habe, als solche kenntlich gemacht habe, mich auch keiner anderen als der angegebenen Literatur oder sonstiger Hilfsmittel bedient habe und die zu Prüfungszwecken beigelegte elektronische Version (PDF) der Dissertation mit der abgegebenen gedruckten Version identisch ist. / *With my signature I affirm in lieu of an oath that I prepared the submitted dissertation independently and without illicit assistance from third parties, that I appropriately referenced any text or content from other sources, that I used only literature and resources listed in the dissertation, and that the electronic (PDF) and printed versions of the dissertation are identical.*

Ich versichere an Eides Statt, dass ich die vorgenannten Angaben nach bestem Wissen und Gewissen gemacht habe und dass die Angaben der Wahrheit entsprechen und ich nichts verschwiegen habe. / *I affirm in lieu of an oath that the information provided herein to the best of my knowledge is true and complete.*

Die Strafbarkeit einer falschen eidesstattlichen Versicherung ist mir bekannt, namentlich die Strafandrohung gemäß § 156 StGB bis zu drei Jahren Freiheitsstrafe oder Geldstrafe bei vorsätzlicher Begehung der Tat bzw. gemäß §161 Abs. 1 StGB bis zu einem Jahr Freiheitsstrafe oder Geldstrafe bei fahrlässiger Begehung. / *I am aware that a false affidavit is a criminal offence which is punishable by law in accordance with § 156 of the German Criminal Code (StGB) with up to three years imprisonment or a fine in case of intention, or in accordance with § 161 (1) of the German Criminal Code with up to one year imprisonment or a fine in case of negligence.*

_____	_____	_____
Ort/P*lace*	Datum/*Date*	Unterschrift/*Signature*